Comb-Mode-Resolving Broadband Fourier Transform Spectroscopy

Jake M Charsley

A dissertation submitted in partial fulfillment

of the requirements for the degree of

Master of Science by research

of

Heriot Watt University.

Institute of Photonics and Quantum Sciences

Heriot Watt University

May 1, 2018

I, Jake M Charsley, confirm that the work presented in this thesis is my own. Where information has been derived from other sources, I confirm that this has been indicated in the work.

Abstract

This report demonstrates progress made to develop a robust turn-key astrocomb architecture for the calibration package of the HIRES spectrograph planned for installation on the upcoming Extremely-Large Telescope (ELT) which intends to enable novel research across a range of scientific disciplines.

Here, we demonstrate progress towards a laser frequency comb covering optical and infra-red wavelength ranges and made possible by use of nonlinear interactions driven by a single stabilised mode-locked laser source. We also detail a proof-of-concept experiment carried out with a compact broadband Fourier-transform spectrometer to identify the subset of filtered frequency-comb modes, an important ancillary technology for any future broadband Fabry-Pérot-based astrocomb.

ACADEMIC REGISTRY
Research Thesis Submission

Name*:	Jake Charsley		
School:	EPS/IPAQS		
Version: *(i.e. First, Resubmission, Final)*	Final	Degree Sought:	MSc by research in Physics

Declaration

In accordance with the appropriate regulations I hereby submit my thesis and I declare that:

1) the thesis embodies the results of my own work and has been composed by myself
2) where appropriate, I have made acknowledgement of the work of others and have made reference to work carried out in collaboration with other persons
3) the thesis is the correct version of the thesis for submission and is the same version as any electronic versions submitted*.
4) my thesis for the award referred to, deposited in the Heriot-Watt University Library, should be made available for loan or photocopying and be available via the Institutional Repository, subject to such conditions as the Librarian may require
5) I understand that as a student of the University I am required to abide by the Regulations of the University and to conform to its discipline.
6) I confirm that the thesis has been verified against plagiarism via an approved plagiarism detection application e.g. Turnitin.

* *Please note that it is the responsibility of the candidate to ensure that the correct version of the thesis is submitted.*

Signature of Candidate*:	*Charsley*	Date:	26/04/2018

Submission

Submitted By *(name in capitals):*	
Signature of Individual Submitting:	
Date Submitted:	

For Completion in the Student Service Centre (SSC)

Received in the SSC by *(name in capitals):*			
Method of Submission (Handed in to SSC; posted through internal/external mail):			
*E-thesis Submitted (**mandatory for final theses**)*			
Signature:		Date:	

Please note this form should be bound into the submitted thesis.
Academic Registry/Version (1) August 2016

Acknowledgements

Firstly, many thanks to Professor Derryck Reid, my supervisor, for the opportunities and experiences. I cannot thank you enough for your support and understanding in response to my decision to step away from PhD research to better deal with my anxiety and depression.

Thank you to Dr Richard McCracken for your tutelage in the ways of experimental ultrafast optics, for always being available to learn from, and for having me as a guest teacher at Science Club. I wish you and your family all the best in the future.

To the other member of the Ultrafast Optics research group during my time there: Dr Jinghua Sun, Dr Oguzhan Kara, Dr Marius Rutkauskas, Dr Luke Maidment, Toby Mitchell, Hollie Wright, and Lauren Reid. I have been exceptionally privileged to work with you all.

Thank you to Dr Philipp Huke, Professor Piotr Maslowski, and Professor Yohei Kobayashi, and their respective research groups for the valuable collaborations.

I would like to thank my family to whom I will spend the rest of my life repeatedly trying to explain what I did here.

Lastly, thank you to my kindred spirit Amy whose support has made this work possible.

Contents

List of Figures

List of Publications

[1] J. M. Charsley, R. A. McCracken, L. Reid, and D. T. Reid, "Broadband Fourier-transform spectrometer enabling modal subset identification in Fabry-Pérot-based astrocombs," Opt. Express **25**, 19251-19262 (2017).

This paper appeared in the Optics Express special edition on *Recent advances in astrophotonics* and demonstrated a novel ancillary technology in broadband Fabry-Pérot-based astrocombs which can identify the filtered subset over a broad bandwidth by use of a compact Fourier-transform spectrometer (FTS).

My contribution to this paper was substantial as I was the first and corresponding author, sharing the majority of writing responsibilities with R. A. McCracken. I performed the underpinning laboratory work, building the latest embodiment of the FTS capable of balanced detection. I carried out all experimental work alongside R. A. McCracken. I wrote the FTS code for the data retrieval of the interferograms, which included compensation for air dispersion through discussions with D. T. Reid and R. A. McCracken. I performed the inital FTS retrieval for all data which included a novel cross-correlation approach proposed by D. T. Reid to ascertain mode positions using the unresolved lineshape of the spectrometer. I performed modal-subset analysis, including the creation of Figures 3, 4 & 5.

[2] R. A. McCracken, J. M. Charsley, and D. T. Reid, "A decade of astrocombs: recent advances in frequency combs for astronomy," Opt. Express **25**, 15058-15078 (2017).

An invited paper for the Optics Express special edition that overviewed progress

made over the past 10 years of the astrocomb field and outlines future challenges in realising an on-site astrocomb.

My contribution to this paper was to construct and provide the figures as well as being a part of regular discussions where I had input on content and structure.

[3] J. M. Charsley, R. A. McCracken, D. T. Reid, G. Kowzan, P. Maslowski, A. Reiners, and P. Huke, "Comparison of astrophysical laser frequency combs with respect to the requirements of HIRES," in "Optical Measurement Systems for Industrial Inspection X," (2017), pp. 10329-12.

A proceedings manuscript for the SPIE Optical Metrology 2017 conference that proposed an astrocomb calibration architecture for the high-resolution spectrograph ELT HIRES as well as including a review of the success of deployed astrocombs on telescopes thus far.

My contribution to this paper was considerable as I was first- and corresponding author. I provided the majority of the paper's content as well as generating all the figures and tables.

[4] P. Huke, L. Origlia, M. Riva, F. Pepe, A. Reiners, J. M. Charsley, R. A. McCracken, D. T. Reid, G. Kowzan, P. Maslowski, H. Korhonen, C. Broeg, F. Dolon, I. Boisse, K. Disseau, S. Perruchot, S. Ottogalli, and T. Bandy, "Phase A: Calibration concepts for HIRES," in "Optical Measurement Systems for Industrial Inspection X," (2017), pp. 10329-91.

A consortium publication from the calibration team for work ongoing on the ELT HIRES published at the SPIE Optical Metrology 2017 conference. The paper displayed a variety of calibration concepts from white-light interferometers to astrocombs. I contributed to the astrocomb sections of the manuscript by result of consortium discussions as well as providing input in the review process.

Chapter 1

Introduction

1.1 Stellar radial-velocity measurements

One of the more fruitful ways of testing fundamental physics is to look out into the distant cosmos. In the far-UV to mid-infrared spectrum, the cosmos is illuminated so strongly by starlight that light from other astronomical bodies (planets, comets, moons, etc.) is washed out. Therefore when looking into this spectral band, it is most profitable to fully make use of all information contained within starlight. So, other than the first-order notion of the characterisation of a star's chemical make-up (by matching observed frequencies to known atomic energy transitions) what further information can be extracted from stellar observations?

The answer turns out to be plenty. The key to this is in measuring the radial velocity of stars. Stars with orbiting bodies will themselves orbit around the centre of mass of this system (the barycentre). In effect these stars wobble with respect to Earth and, with a high-enough resolution spectrometer, this can open up a series of potentially-seminal scientific enquiries. A star experiences a gravitational force related to the mass and distance of the neighbouring planet and as this planet orbits the star, the star itself moves towards the planet and orbits the centre of gravity. From the perspective of an observer on Earth, the star will be seen as moving towards and away from them. The Doppler effect causes the frequencies of light from the star to appear higher as the star is moving towards the observer (blue shifted) and the light frequencies appear lower as the star moves away from the observer

- red shifted. This process is in agreement with the illustration of Figure 1.1 (a),
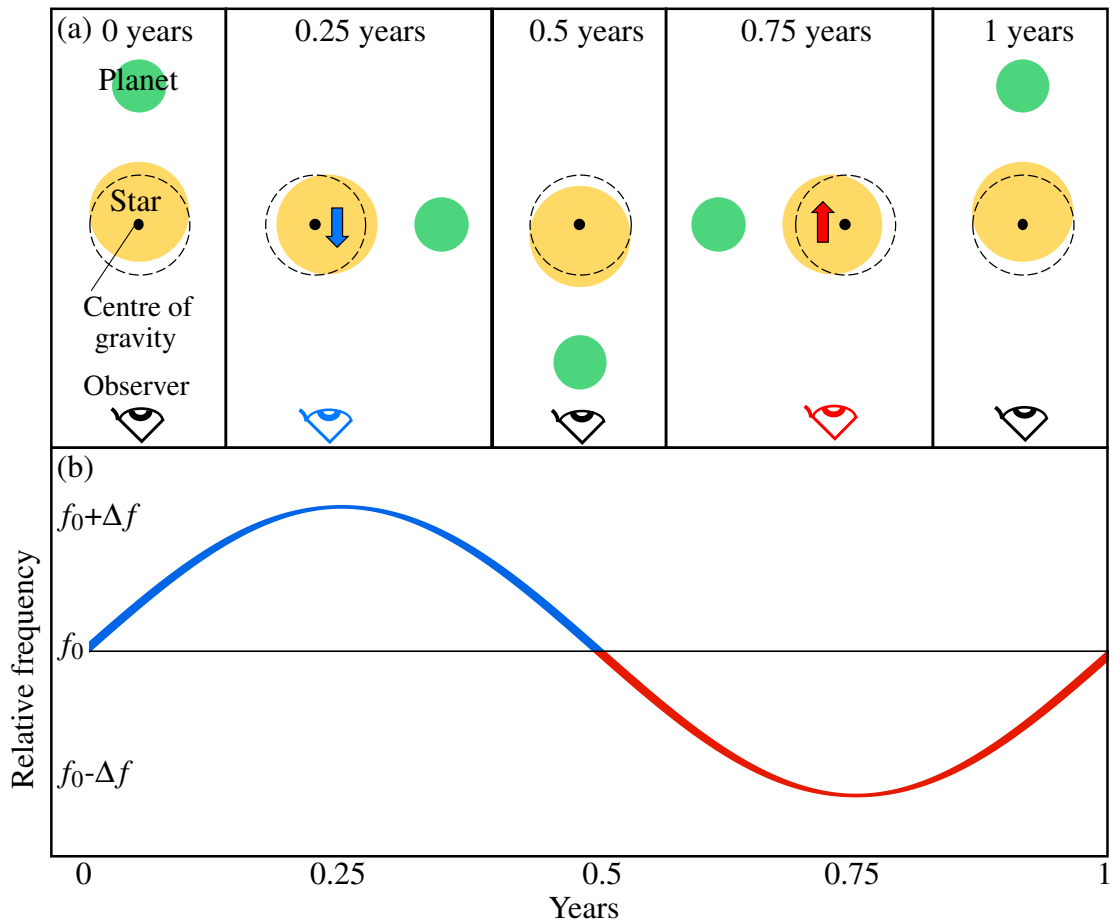
Figure 1.1: The radial-velocity principle. Shifts of a star from gravitational influence of orbiting planet over a year cycle. Illustrated by a 2-D sketch in part (a), and in part (b) as a single-frequency-measurement plot carried out by the observer.

which displays a simple example of a single planet as it orbits a relatively-massive star over the planet's year cycle. The observer (symbolised by an eye) is positioned in the negative *y*-direction, the observer colour corresponding to when the observer sees a red-shift (in red), a blue-shift (in blue), or the rest frequency (in black). Further still, Figure 1.1 Part (b) gives an insight into the analysis an astronomer can start to construct after observing the star for a single planetary orbit. The figure demonstrates the sinusoidal relation over time of a single frequency observed from the star develops due to the planet's orbit. In Figure 1.1 the measurements begin with the star at zero radial velocity in the direction of the observer before accelerating towards the observer, before finding another potential well and beginning its

acceleration away from the observer.

If made with sufficient precision, stellar observations could empirically confirm the acceleration of the expansion of the Universe; delve into the atmospheres of exoplanets; give insight to the mechanisms involved in the evolution of galaxies; and much besides. The discussion of the various science cases is expanded later in Section 1.3.1. These listed science investigations are proposed to be performed via measurements of the radial velocity of distant stars with respect to large telescopes on Earth.

1.2 Frequency comb as a spectrograph calibrator - the 'astrocomb'

The concept of utilising a frequency comb, with its extremely-high precision and stability, for use as a calibrator for astronomical spectrographs was immediately recognised as a promising technique for further increasing precision in extreme-precision radial velocity (RV) measurements on its inception in 2007 [5]. The frequency-comb spectrograph calibrator ('astrocomb') has the potential to enable precision and accuracy enough to explore some truly novel science cases, to help answer profound questions such as 'Are the fundamental constants time-varying?'. The near-immediate recognition of the astronomy community was supported by the proof-of-concept experiment carried out by Steinmetz *et al.* within a year of the former's publication [6].

To date, the predominant resident calibration source on high-resolution astronomical spectrographs are either emission lamps, typically hollow-cathode Thorium-Argon (Th-Ar) lamps, or absorption cells, typically iodine reference cells. These calibration sources produce spectral lines associated with well-mapped atomic transitions and have contributed to the discovery of over 700 exoplanets through the radial velocity method alone [7]. The motivation behind a new calibration source arises partly out of necessity, as the manufacturing of Th-Ar lamps with metallic cathodes, the type of Th-Ar lamp best suited for spectrograph calibration, has ceased worldwide [8], and in part due to scientific motivation from the astron-

omy community for RV precision on the ~ 1 cm s^{-1} scale. Atomic-transition-based sources have spectral lines sparsely positioned across the coverage of a spectrograph, and are entirely absent in the near-IR. Accurate modeling of the instrument profile with these calibration sources has seen their maximum RV precision limits realised at the ~ 1 m s^{-1} level [9, 10].

1.2.1 The frequency comb

1.2.1.1 Modelocking

Laser frequency combs produce thousands of extremely-narrow equally-spaced frequency modes with stability demonstrated to the 10^{-18} level [11], achieved by referencing optical frequencies to microwave standards to exploit highly-accurate microwave frequency measurement techniques [12]. Modelocking is the frequency-domain concept that underpins the frequency comb structure.

An ultrashort pulse is permitted to form inside the laser cavity when the modelocking condition is fulfilled, namely when a multitude of longitudinal modes is permitted to see gain simultaneously and are related by a fixed phase and frequency interval. The active or passive mode-locking technique deployed imposes sidebands on the active laser modes that injection lock neighbouring modes. Kerr-lens modelocking (KLM) is the pervasive technique for modelocking a titanium-sapphire laser. After its initial demonstration [13], KLM was soon characterised as a self-focusing mechanism that occurs inside any gain medium with a nonlinear refractive index [14, 15, 16]. Self focusing can affect the spatial properties of the laser beam in such a way as to make modelocking result in a lower loss compared with CW operation, and therefore preferable [17, 18]. At the output coupler a fraction of the pulse power is emitted once per cavity round trip (subsequently restored by the gain media) and this results in a train of identical ultrashort pulses propagating outside of the laser cavity, each separated by the cavity round trip time T. Due to the pulses emitted from the mode-locked laser being replicas of the intracavity pulse, the electric field representation of this pulse train has a periodic envelope function. The

electric field can be expressed as the Fourier series: [19, 20]

$$E(t) = \sum_m A_m \exp(-2\pi i(f_{car} + f_{CEO} + mf_{rep})t) + \text{c.c.} \tag{1.1}$$

where f_{car} is the frequency of the optical carrier wave, f_{rep} is the repetition rate frequency of the pulses defined as $f_{rep} = 1/T$, and A_m are coefficients containing information on the spectral intensity and relative phases. Fourier analysis of Equation (1.1) into the frequency domain produces the aforestated frequency comb structure, with the set of equally-spaced comb lines centred about the carrier frequency f_{car}.
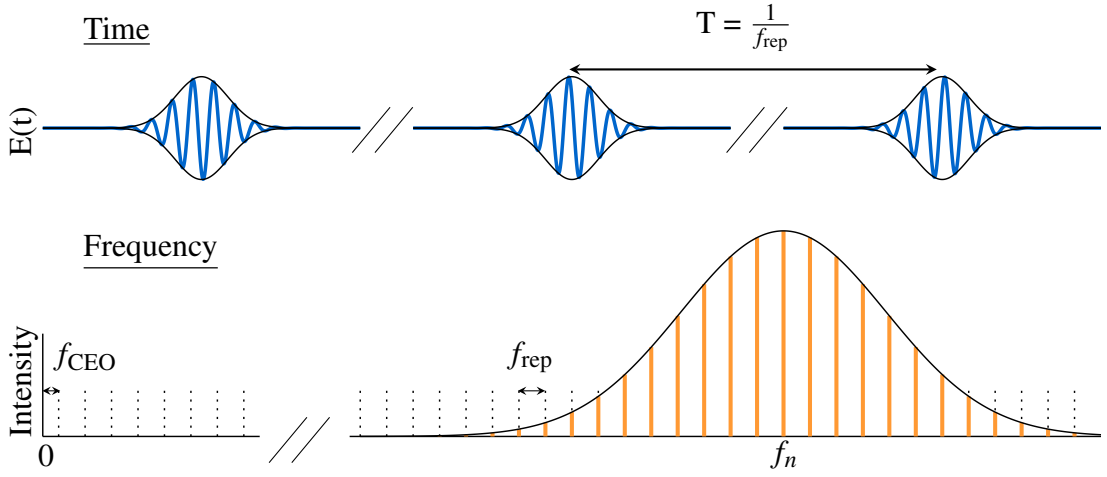
Figure 1.2: The principle of a frequency comb

There is an additional intricacy before getting a full picture of the frequency comb structure which arises from the difference in the phase velocity of the carrier wave to the group velocity of the envelope wave. The origin of this offset is not itself remarkable as there is no reason for the two waves to travel around the cavity at the same speed due to the frequency-dependent dispersion within the cavity. Considering the difference in phase between the carrier and envelope waves between each subsequent pulse stay constant, this phase difference in the time domain manifests itself in the frequency picture as an offset in frequency, known as the carrier-envelope offset frequency f_{CEO}. This can be viewed, as in Figure 1.2, as the offset from zero of the first comb line (n=0) if hypothetically the optical-domain comb structure were to extend to zero, and is given by $f_{CEO} = \Delta\phi/2\pi T$.

The resultant spectrum is a set of equally-spaced exceptionally-narrow comb modes that can be stabilised to traceable microwave standards and is described by the simple relation:

$$f_n = n f_{\text{rep}} + f_{\text{CEO}}, \tag{1.2}$$

where f_n is the frequency of the nth comb mode. The spacing between comb modes throughout the spectrum has so far been demonstrated to agree to the 10^{-19} level [21].

1.2.1.2   Repetition-rate stabilisation

The instantaneous mode spacing will fluctuate due to changes in the length of the laser cavity. Similarly, the offset frequency will fluctuate with changes in the intracavity dispersion. Fixing the cavity length is typically achieved by detecting a high-harmonic of f_{rep} on a fast photodiode and then comparing this frequency with a local oscillator. The resulting difference frequency acts as an error signal which is used to stabilise the cavity length with one or several piezoelectric actuators inside the cavity. The mth harmonic of f_{rep} is used as it allows for increased locking accuracy, albeit with a smaller effective locking range.

1.2.1.3   Carrier-envelope-offset stabilisation

The self-referencing technique was a revelation in frequency metrology when it was first demonstrated in 1999 [22, 23]. The technique, initially made possible by advances in nonlinear optics [24, 25], enables direct translation of microwave frequencies to the optical domain, negating the previously-required complicated frequency chains [26]. Self referencing is available for modelocked laser pulses that have an octave-spanning frequency bandwidth. This can be engineered either directly from the laser cavity [27], or after supercontinuum generation in photonic crystal fibre [24, 28].

For an octave-spanning frequency bandwidth, there exists longitudinal frequency modes at both frequencies f_n and f_{2n}. The mode f_n at the low-frequency 'red' end and the mode f_{2n} at the high-frequency 'blue' end of an octave-spanning

bandwidth are given by equations $f_n = nf_{\text{rep}} + f_{\text{CEO}}$ and $f_{2n} = 2nf_{\text{rep}} + f_{\text{CEO}}$, respectively. If f_n is frequency doubled the equation of the resultant frequency will be $2f_n = 2nf_{\text{rep}} + 2f_{\text{CEO}}$. Heterodyne mixing between the frequency-doubled mode $2f_n$ and the fundamental mode f_{2n} on a fast photodiode will yield a beat frequency at $\pm f_{\text{CEO}}$.

Stabilisation of f_{CEO} can be achieved by modulation of the intracavity dispersion as a result of introducing an optical element such as a prism [29], band-pass filter [30] or SESAM [31], or by means of varying the nonlinear refractive index of the gain medium by constant feedback adjustments to the power of the pump laser [32]. Alternative stabilisation methods such as the feed-forward technique are outside the scope of this discussion [33].

1.2.2 Techniques to achieve a wide-mode-spacing frequency comb

The motivation for obtaining a wide-mode-spacing frequency comb is fundamentally to enable neighbouring comb modes, with their extreme accuracy and precision, to be sufficiently spaced apart in frequency - such that they can be individually identified on a high-resolution spectrograph - to be utilised as a near-optimum calibration tool. Though wavelength-dependent, the optimum spacing of a spectrograph calibrator is of the order of 10-50 GHz which is traditionally challenging from the frequency-comb perspective, where mode spacing is inversely proportional to the size of the laser cavity. A 30-GHz mode spacing, for example, would entail a c/f_{rep}=1 cm optical cavity which is currently ahead of any engineering capability.

1.2.2.1 Modal selection

The principle of modal selection of a multimode laser through a Fabry-Pérot interferometer, or filter cavity, was first proposed in 1989 by Theodore Sizer II [34].

For our purposes, the Fabry-Pérot interferometer, or cavity, is an optical resonator comprising two mirrors with the same reflectivities, aligned parallel with respect to one another, spaced a distance l apart, immersed by a medium with refractive index n. A Fabry-Pérot cavity has transmission modes that can be described

by Equation (1.3), a plane-wave equation for the transmitted complex electric field, E_T, in relation to the incident complex electric field, E_I, and the normalised reflected and transmitted ratios at each mirror surface, R and T, respectively.

$$E_T = \frac{T E_I}{1 - Re^{i\delta}},$$
(1.3)

where δ is the round-trip cavity phase given by

$$\delta = \frac{4\pi nl \cos(\theta)}{\lambda},$$
(1.4)

and θ is the angle of incidence into the Fabry-Pérot cavity.

The incident electric field E_I has no imaginary part and is solely real in the instance of a collimated beam at the normal angle of incidence. In this case the amplitude of the transmitted field, A_T, is given as

$$A_T = \left| \frac{E_T}{E_I} \right| = \sqrt{\frac{T^2}{1 - 2R\cos(\delta) + R^2}}$$
(1.5)

Note that maximum amplitude occurs when $\delta = 2\pi N$, where N is an integer, and this sets the frequency separation of neighbouring transmission peaks at $\Delta f = c/2nl$ [34, 35].

In the case of modal filtering for a frequency comb, the distance between the two Fabry-Pérot mirrors l is adjusted so that the frequency spacing of the transmission profile is precisely matched to an integer multiple M of the frequency-comb repetition rate such that $f_{\text{rep}} = c/2nl$, as displayed in Figure 1.3. When this condition is met, the comb modes transmitted through the cavity will be one of the M subsets of the comb modes, filtered such that the output spectrum has a mode spacing

$$f_{\text{rep-astro}} = M f_{\text{rep}}.$$
(1.6)

The frequency-comb equation which represents a frequency comb filtered by a
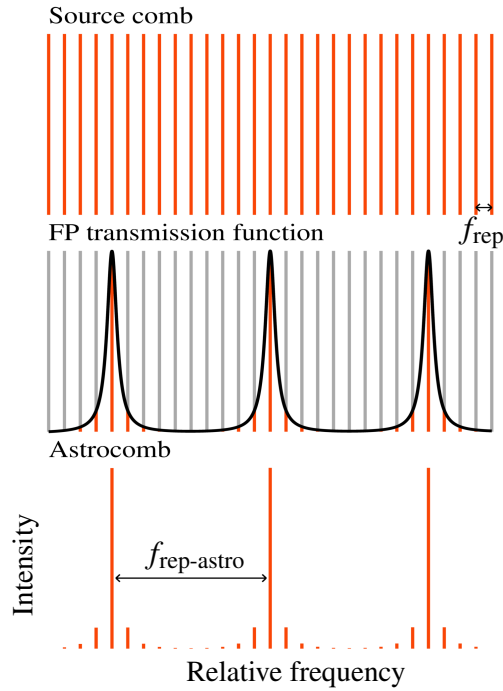
Figure 1.3: The principle of a modal selection with M=10 subsets.

Fabry-Pérot cavity, known as a Fabry-Pérot-based astrocomb in spectrograph calibration, becomes

$$f_{M,\kappa,m} = \left(m + \frac{\kappa - 1}{M} \right) f_{\text{rep-astro}} + f_{\text{CEO}}, \tag{1.7}$$

where m is an integer to number the filtered comb modes analogous to n in Equation 1.2. Notice the introduction of two degrees of freedom not present in the typical comb equation, the filter integer M and the modal subset index κ. This index, defined here as an integer from 1 to M, is used to distinguish between the M-possible subsets. Identification of κ is vital to establish an absolute frequency measurement, as exemplified in Figure 1.4.

The average power of the transmitted beam is M times less than the incident beam's average power as in the frequency domain only one mode out of every M^{th} mode is transmitted. The peak power of the transmitted beam sees a reduction by a factor of M^2 as compared to the peak power of the incident beam. This further reduction by a factor of M is due to the increase in the number of temporal pulses in a given time window by a factor M when compared to the initial repetition rate.
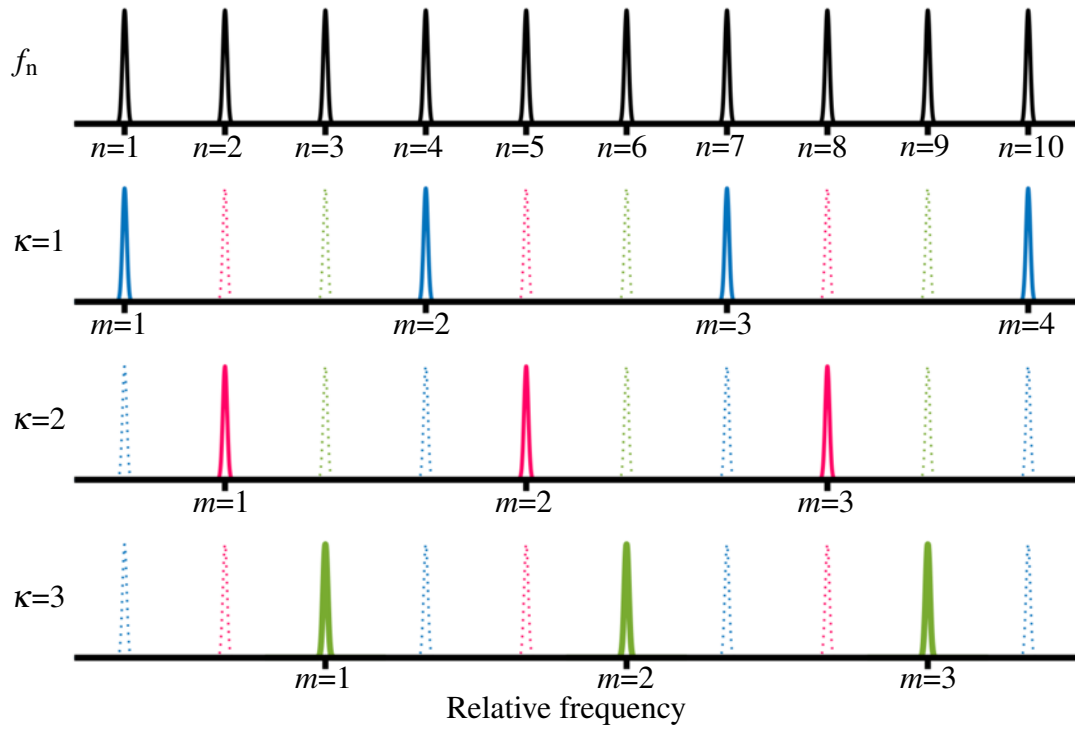
Figure 1.4: Illustration of modal filtering ambiguity with $f(M=3,\kappa,m)$.

In practice, to precisely match the Fabry-Pérot cavity's transmission profile to a subset of frequency-comb modes requires active stabilisation of the Fabry-Pérot cavity by a series of locking electronics (see Section 2.11).

For a more in-depth look at the principle of modal selection, notably the subtleties which arise due to dispersion within the filter cavity, please see Section 2.1 'Principles of Astrocombs' of the 'Astrocomb Proposal for ELT HIRES' paper in Appendix C.

1.2.2.2   Other spectrograph calibrator technologies

As well as Fabry-Pérot-based solid-state and fibre frequency combs, there are a number of alternative calibrator technologies such as multi-GHz solid-state lasers [36, 37, 38, 39, 40, 41], microcavities [42, 43], electro-optically modulated lasers (EOMs) [44], and white-light Fabry-Pérot etalons [45, 46, 47].

For detail of the recent advances in these alternative calibrator technologies, please see Section 2.2 in Paper 2 - Astrocomb Review in Appendix B.

1.3 Astrocomb architecture proposal for calibration of ELT HIRES

1.3.1 Next-generation spectrograph science cases

This section outlines what the scientific community intends to achieve with the next-generation of extremely-large telescopes equipped with high-resolution spectrographs, and highlights among them chief science cases only achievable with the use of an astrocomb calibrator. The science cases for next-generation high-resolution spectrographs can be broadly categorised into four areas: exoplanet cases, stellar cases, galaxy evolution and the intergalactic medium, and fundamental physics and cosmology. Table 1.1 lists a selection of the proposed science cases for investigation with HIRES on the upcoming ELT, adapted from Reference 48. Below are descriptions of specific science experiments that can only be enabled through the wavelength accuracy and stability provided by a laser frequency comb (denoted by * in Table 1.1).

Since the detection of the first exosolar planet in 1995 [49], research interest has amassed about the formation and possible habitability of exoplanets. Current spectral resolution limitations only detect comparably-large radial velocity swings for exoplanet identification and, as such, result in detection of 'hot Jupiters' - Jupiter-mass planets with fortnightly orbits. Further density measurements of some of these hot Jupiters reveal unexpected inflated radii and have opened up research into their formation as the mechanism enabling the apparent migration towards the host star is currently unidentified [50]. Detection of Earth analogues (exo-Earths) to investigate the likelihood of habitability requires RV precision at around 10 cm s^{-1} which corresponds to an optical frequency shift of 100 kHz and is only achievable with a calibration source referenced to microwave standards. The radial velocity signature of an exoplanet is more prominent the smaller the star, and so M dwarfs are prime candidates for detection of low-mass planets within the habitable zone [51].

Table 1.1: Science case calibration requirements of next-generation spectrographs

Science case	Spectral range (μm)	Spectral resolution ($\lambda/\Delta\lambda$)	Wavelength accuracy (m/s)	Stability ($\frac{m}{s}$/night)
Exoplanet cases				
Exoplanet atmospheres	0.38 – 2.4 *	100,000	10	0.1 *
	0.38 – 2.4 *	150,000	1 *	0.05 *
Planetary debris on White Dwarfs	0.37 – 0.5	100,000	not critical	not critical
	0.33 – 0.5	100,000	not critical	not critical
Orbital elements	0.40 – 0.9	100,000	0.1 *	0.1 *
	0.40 – 0.9	150,000	0.1 *	0.1 *
Stellar cases				
Stellar atmospheres	0.37 – 2.4 *	100,000	300	not critical
	0.31 – 2.4 *	150,000	100	not critical
Proto-planetary disks & protostellar jets	0.38 – 2.5 *	100,000	1,000	not critical
	0.33 – 2.5 *	150,000	500	not critical
Stellar populations	0.48 – 2.4 *	30,000	100	not critical
	0.31 – 2.4 *	100,000	500	not critical
Extragalactic star clusters	0.40 – 2.4 *	15,000	100	not critical
	0.37 – 2.4 *	30,000	500	not critical
Galaxy evolution and intergalactic medium cases				
Near pristine gas & reionisation	0.60 – 1.8 *	50,000	not critical	not critical
	0.60 – 2.4 *	100,000	not critical	not critical
3D mapping of IGM & metallicity	0.40 – 1.3 *	5,000	not critical	not critical
	0.37 – 1.3 *	20,000	not critical	not critical
Galaxy evolution	0.40 – 2.4 *	10,000	not critical	not critical
	0.40 – 2.4 *	15,000	not critical	not critical
Low-mass black holes	1.00 – 2.4 *	100,000	not critical	not critical
	0.50 – 2.4 *	100,000	not critical	not critical
Fundamental physics and cosmology cases				
Fundamental constants & CMB temperature	0.37 – 0.67	80,000	2 *	2 *
	0.33 – 0.8	100,000	1 *	1 *
Deuterium abundance	0.37 – 0.7	50,000	50	not critical
	0.33 – 1.0	100,000	50	not critical
Sandage test	0.37 – 0.67	100,000	0.02 *	0.02 *
	0.33 – 0.8	150,000	0.01 *	0.01 *

The Sandage test [52] proposes the challenge of watching the Universe expand in real time from red-shift-drift observations of cosmologically distant objects. Such a direct measurement of the Universe expansion would provide the first model-independent results [48]. The expected drift-rate is on the scale of 6cm s^{-1} decade^{-1} [53] which will require a stability and wavelength accuracy from the spectrograph calibrator unique to laser frequency combs. The proposed target for

this test are Lyα forests of absorption lines from quasars as the lines are numerous and relatively-narrow [54]. It has been estimated that with the 39-m-diameter ELT, the detection of a red-shift drift in these Lyα forests would require 4,000 hours of observation over a 23-year time span [48].

Extreme-precision radial velocity measurements, as well as investigating astronomy and cosmology cases, will be able to probe fundamental physics too. For instance, these measurements could test whether fundamental constants are seen to vary within the limits of the experiment. The expected rate of variation is around 10^{-10} year^{-1}. If variations in a fundamental coupling were found it would imply a violation of the equivalence principle, and as is the case with these kinds of experiments a null result is also highly valuable. To enable such a measurement would require a highly-accurate wavelength calibration to reduce noisy systematic effects present in current instruments.

1.3.2 Astrocomb design

This section provides an overview of the astrocomb design proposed by the Ultrafast Optics group as part of the Phase A calibration package for ELT HIRES. For full context and a broader justification of the design, please refer to Paper 3 - Astrocomb Proposal for ELT HIRES in Appendix C [3, 4].

Figure 1.5 illustrates the design concept proposed to calibrate the ELT HIRES spectrograph. A fully-stabilised 1-GHz Ti:sapphire frequency comb is used as the source comb in this design to provide 1.2 W average power for efficient frequency conversion by a range of nonlinear processes to fulfill the demanding spectral bandwidth of the spectrograph. The supercontinuum coverage from the f-to-$2f$ interferometer is intended to be used to calibrate the spectrograph from 0.52–1.15 μm. The high efficiency of the coupling into the PCF permits a portion of the supercontinuum beam to be directed out of the inteferometer while maintaining stabilisation of the carrier-envelope offset frequency [55, 56].

The spectral bandwidth from 1.15–2.0 μm is proposed to be covered by broadening a synchronous degenerate optical parametric oscillator (OPO) in a highly-
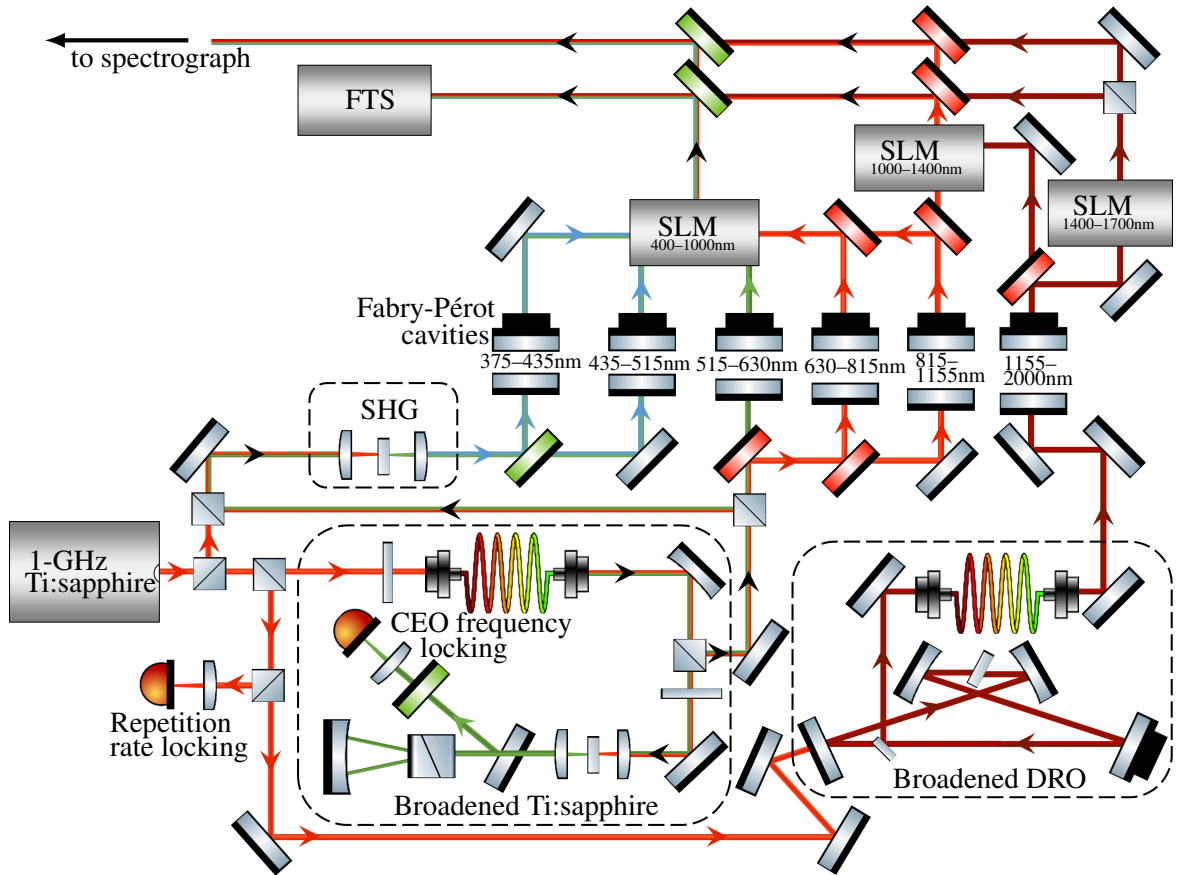
Figure 1.5: Proposed architecture of the LFC calibrator for HIRES.

nonlinear fibre (HNLF). An OPO at degeneracy has been demonstrated to maintain the comb structure of the pump [57, 58]. The broadening of a 1-GHz degenerate OPO with a central wavelength of 1.6 μm has been modelled to fulfill the near-IR bandwidth [59, 60], given high oscillation efficiency, transform-limited OPO pulses, as well as efficient coupling into the HNLF.

The UV coverage of 0.37–0.52 μm for the astrocomb design is intended to be fulfilled by frequency doubling [61]. A portion of the 1-GHz Ti:sapphire comb beam as well as a portion of the 1-GHz Ti:sapphire supercontinuum beam will be sent into two SHG modules (depicted as a single module in Figure 1.5).

A series of Fabry-Pérot cavities is required in this design as the preferred frequency spacings from modal selection differ significantly across the wide bandwidth of the astrocomb from ∼5–40 GHz, due to the spectral resolution of the spectrograph being linear in wavelength. The filter cavities also have to provide minimal

dispersion over the transmitted wavelength region (see Section 2.3.1) which is much more realisable with this modular approach of separating the spectral regions evenly in frequency across the whole astrocomb coverage.

The design has to account for the dispersion provided by the mirror coatings and by the air in the cavity that limit its effective bandwidth, as well as the cavity finesse $\mathscr{F}$ that defines the width of the frequency filter transmission window [62, 63, 64]. These considerations have to be well understood to prevent 'walk off' between the transmission profile of the Fabry-Pérot cavity and the frequency-comb modes which can cause unwanted neighbouring modes to be transmitted as well as, or instead, of the modes from the selected subset [65, 66, 67].

Spectral flatness across the whole astrocomb bandwidth is useful to reduce saturation effects and photon noise when exposed to the CCD. Spatial-light modulators (SLMs) have been demonstrated to provide intensity shaping over a broad range of wavelengths [68, 69]. Here, three commercially-available SLMs are proposed to achieve spectral flatness across most of the spectrograph wavelength coverage from 0.4 μm to 1.7 μm. Suitable spectral flattening outside of this wavelength region will be provided by custom-designed dielectric mirror coatings.

The transmitted modal subsets from the series of Fabry-Pérot cavities will be identified on a broadband compact Fourier-transform spectrometer (FTS) to enable absolute spectral calibration for spectrograph measurements [1, 3]. The FTS is based on a Michelson interferometer whereby a modelocked laser beam is sent into two arms of the interferometer such that on recombination the beams interfere and can be detected as interferograms. With calibration of the optical path length by an atomically-referenced diode laser, the Fourier-transform analysis of the interferogram signals reveals the input beam's spectral content [70, 71]. Previous astrocombs filtered by a single Fabry-Pérot cavity have used laser diodes as optical references to ascertain the transmitted modal subset [63, 72], however this technique is unavailable for ultra-broadband astrocombs due to insufficient optical-reference sources distributed over the HIRES coverage goal of 0.37–2.4 μm [73, 74].

1.4 Roadmap

The following chapters serve as an account of progress made towards achieving the specifications outlined in the astrocomb architecture.

Chapter 2 details the modelocked laser source, the stabilisation of its repetition rate frequency and carrier-offset frequency, and the filtering of its comb modes by modal selection.

Chapter 3 describes the construction of the synchronous degenerate optical parametric oscillator pumped by the 1-GHz Ti:sapphire laser. The chapter begins with the cavity design and then follows closely the alignment process in obtaining oscillation. The stabilisation of the OPO cavity by dither locking is explained before the stabilised cavity's characteristics are fully assessed. Conclusion of the chapter includes plans to engineer broadband infrared coverage from 1 μm to 2 μm by focusing the degenerate OPO beam into a highly nonlinear fibre.

Chapter 4 tells of the build of a compact Fourier-transform spectrometer with broadband capability for the purpose of identifying modal subsets from a Fabry-Pérot-based astrocomb. The chapter starts with a justification of the instrument design along with an account of the data-collection process. A characterisation of the spectrometer's performance is then given with analysis of its limitations. An experiment to prove the concept of using the instrument for identifying modal subsets is examined. Exciting planned developments based off this work are then discussed which include using an FTS with a frequency comb set up to conduct swift on-site air-dispersion measurements, as well as extending the scan length to increase the instrument's resolution to enable characterisation of side-mode suppression in Fabry-Pérot-based astrocombs.

The final section, Chapter 5, summarises the current state of the work to investigate frequency combs designed for calibration systems of high-resolution spectrographs.

Chapter 2

Stabilisation of a 1-GHz Titanium-Sapphire Femtosecond Laser

The 1-GHz Ti:sapphire laser used as the laser source in the proceeding-chapters' experiments was the turn-key Gigajet laser system by Laser Quantum that delivered an average power of ~1.1 W and ~30 fs pulses. The laser is arranged as a ~30 cm folded ring cavity and was pumped by a tuneable green-diode pump laser at 532 nm (Finesse Pure, Laser Quantum).

The spectrum of the 1-GHz Ti:sapphire laser was centred at 807 nm and covered a 24 nm bandwidth. The spectrum recorded on a spectrometer (Ocean Optics USB4000-VIS-NIR) with a wavelength coverage of 660—930 nm and an optical resolution of 1.5—2.3 nm is displayed in Figure 2.1. The laser system allowed adjustment of the repetition rate through two BNC connections on the laser's electronics control box (TL-1000, Laser Quantum) which sent signals to two piezoelectric actuators (one fast, one slow) attached to mirrors in the cavity to effect cavity length. Carrier-envelope offset stabilisation in this laser system was possible by implementing slight changes of the diode power of the pump laser through a feedback signal sent to the laser's control box.
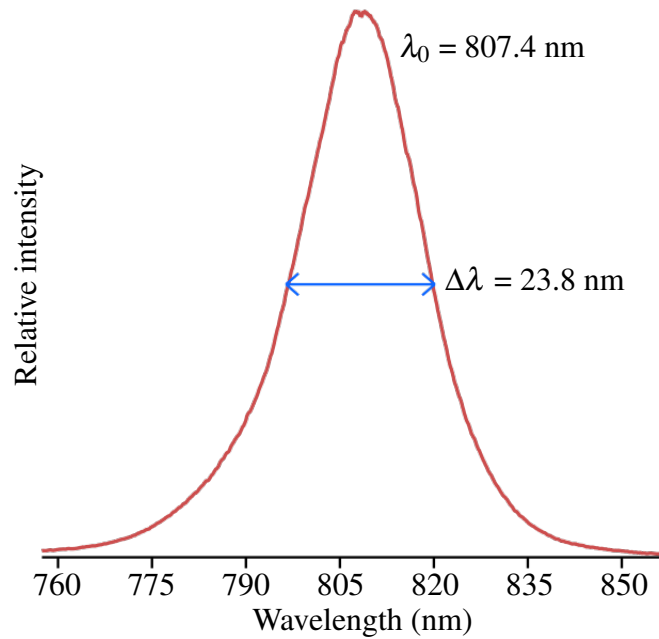
Figure 2.1: Spectrum from the 1-GHz Ti:sapphire laser.

2.1 Repetition-rate stabilisation procedure

The stabilisation procedure of the repetition rate is straightforward relative to the carrier-envelope offset frequency stabilisation procedure as the repetition-rate beat frequency is directly observable on a photodiode as a result of beating between the many thousands of frequency-comb modes spaced f_{rep} apart. As mentioned in Section 1.2.1.2, the repetition-rate frequency is inversely proportional to the cavity length and therefore drifts in cavity length are observable as changes to the repetition rate. Hence stabilisation of the repetition-rate frequency is equivalent to locking the cavity length.

Figure 2.2 illustrates the electronics configuration for repetition-rate locking. The following description of the locking electronics details the procedure undertaken for a 1-GHz Ti:sapphire laser. The repetition-rate signal from the beating comb modes as well as its harmonics were detected by focusing a portion of the Ti:sapphire beam from a beamsplitter into a fast GaAs photodiode (ET-3500 Electro-Optics Technology). The signals were then amplified and a band-pass filter (7.9–8.1 GHz) was used to isolate the eighth harmonic of the repetition rate. The frequency synthesiser (Rb-stabilised microwave synthesiser - FSL-0010 QuickSyn
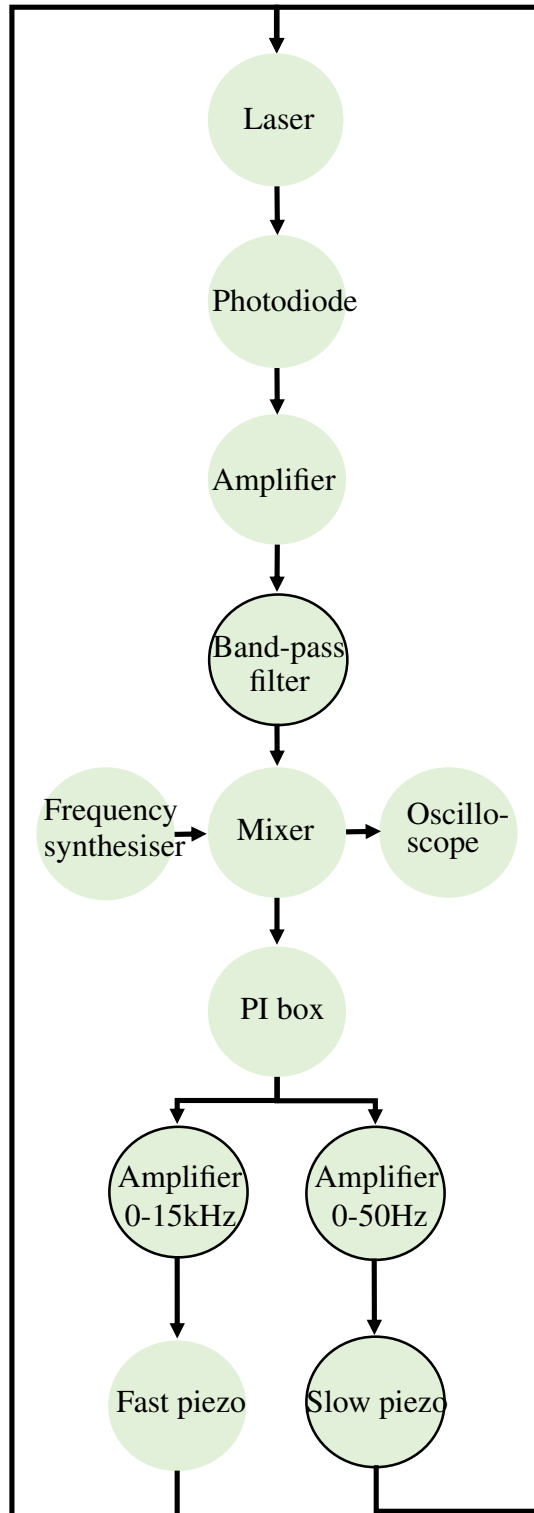
Figure 2.2: Feedback loop block diagram for repetition-rate stabilisation

Lite) was set to a frequency suitably near to the eighth harmonic of the observed repetition rate to be within the catchment range of the piezoelectric actuators. The

synthesised signal and the eighth-harmonic signal were sent into a mixer which provides both sum and difference signals. Stabilising to the eighth harmonic of f_{rep} has the same locking accuracy as the first harmonic as the electronics work with the difference between the synthetic frequency and the beat frequency, not the beat frequency directly. The relative locking accuracy is eight times higher for the eighth harmonic as compared to the first harmonic and was chosen for this reason. On tuning the synthetic frequency towards the beat frequency, the difference signal was viewed on an oscilloscope until the difference frequency was minimal.

The difference signal was sent to the PI lock box (New Focus LB1005 PI server controller), with the sum-frequency signal suppressed by connecting a low-pass filter at the mixer output. The PI lock box uses the difference-frequency signal as an error signal and this is minimised by sending voltage signals to the slow and fast piezoelectric actuators in the 1-GHz Ti:sapphire cavity to actively stabilise the eighth harmonic of the repetition rate to match the synthetic frequency.

2.2 Carrier-envelope-offset stabilisation procedure

2.2.1 Self-referencing by supercontinuum generation

The carrier-envelope-offset frequency, f_{CEO}, of the 1-GHz Ti:sapphire laser was stabilised via the self-referencing technique by using a common-mode-rejection f-to-$2f$ interferometer, as first demonstrated in Ref. 75. Ideally the incoming train of pulses to the interferometer would be transform limited (and therefore have the highest-possible peak power) as this will generate the maximum-frequency-bandwidth supercontinuum possible as the pulse propagates through the photonic crystal fibre (PCF). This is due to the nonlinear processes that occur in supercontinuum generation which scale with peak power. To minimise the chirp on the Ti:sapphire pulses at the entrance of the fibre, two complementary investigations were undertaken.

2.2.1.1 Pulse compression investigations

The first was an autocorrelation experiment to understand the dispersion added to the pulses due to the Ti:sapphire cavity, including the exit window of the laser's

casing. The second investigation analyses the resultant bandwidth of the supercon-
tinuum for a number of different input compression conditions to find the condition
which leads to the broadest frequency range, as this is characteristic of a temporally-
short input pulse.
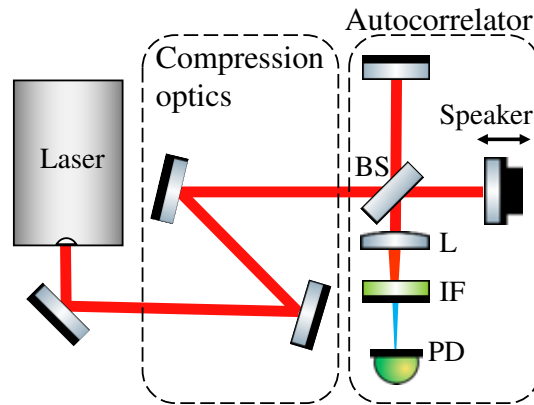
Figure 2.3: Schematic of autocorrelation pulse-compression experiment.

The set up for the autocorrelation experiment is shown in Figure 2.3. The
Ti:sapphire beam from the cavity window was sent toward different combinations
of compression optics (GTIs, windows, chirped-mirror pairs) which distinctly mod-
ified the chirp of the pulses, and aligned into an autocorrelator (Time Warp) based on
two-photon absorption [76]. The dispersion of the resultant pulse was inferred from
the pulse width in time from the autocorrelation reading. The combination of com-
pression optics that was found to attain the shortest pulses at the PCF interface of
$\sim$30 fs was a set of two -500 fs^2 GTI mirrors which added a group-delay-dispersion
(GDD) compensation value of -1000 fs^2.
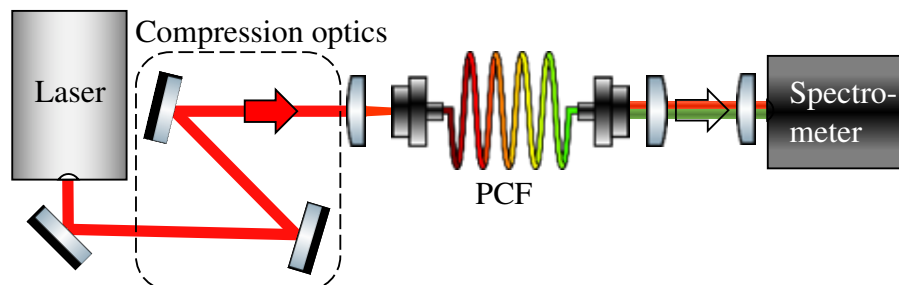
Figure 2.4: Schematic of supercontinuum-coverage pulse-compression experiment.

Figure 2.4 depicts the experimental configuration for the second investigation.

The frequency bandwidth of the supercontinuum is inversely proportional to the temporal width of the input pulse and so this technique can be used in compliment to the autocorrelation investigation to provide an accurate representation of the GDD compensation required to obtain transform-limited Ti:sapphire pulses. The Ti:sapphire beam was focused into the PCF and coupled by optimising the supercontinuum beam's average power through micrometer adjustments of the PCF stage for a number of compression configurations. The fibre output beam has strong divergence and therefore requires collimation at around 2 cm from the fibre end. For this test, collimation was achieved using a doublet lens and the collimated beam was directed into a visible-to-NIR spectrometer (Ocean Optics USB4000-VIS-NIR) capable of capturing the lower-wavelength region of the supercontinuum. Direct
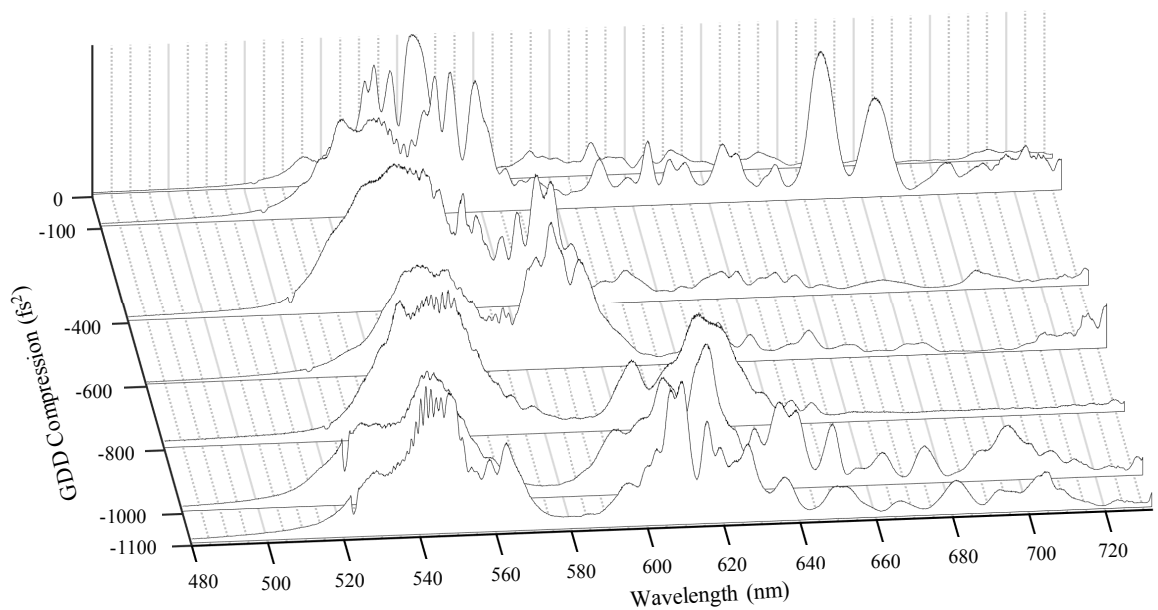
Figure 2.5: The lower-wavelength range of the supercontinuum to investigate various GDD compensation values effect on pulse-compression.

comparison of the range of supercontinuum wavelength coverage between different compression configurations, displayed in Figure 2.5, corroborated with the auto-correlation results showing the widest supercontinuum at the GDD compensation estimate of -1000 fs^2.
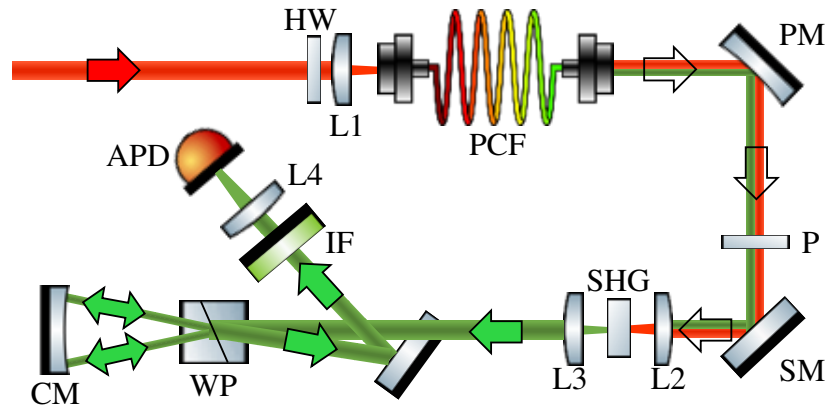
Figure 2.6: Design of common-mode-rejection f-to-$2f$ interferometer.

2.2.1.2 f-to-$2f$ interferometer design

The f-to-$2f$ interferometer design, as illustrated in Figure 2.6, sees the light from a transform-limited horizontally-polarised Ti:sapphire beam tightly focused by a lens (L1) into the 1.8-μm-diameter core of the 12-cm photonic crystal fibre (PCF, NKT Photonics FemtoWHITE 800) to obtain an octave-spanning supercontinuum through four-wave mixing and soliton evolution. A coupling efficiency of 70% was achieved by focusing the $\sim$500 mW Ti:sapphire beam into the PCF.
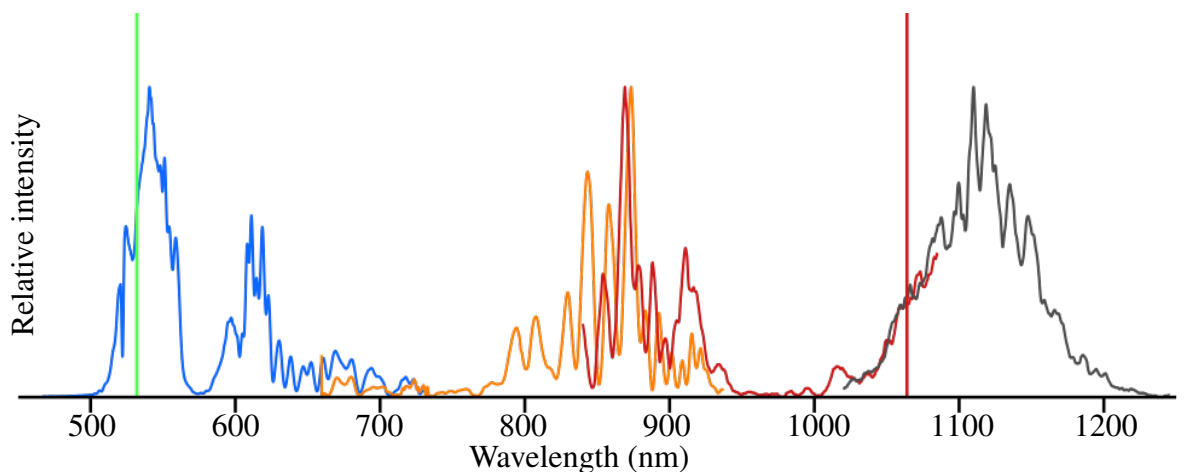
Figure 2.7: Octave-spanning coverage of 1-GHz Ti:sapphire supercontinuum.

Figure 2.7 demonstrates the full achieved octave-spanning supercontinuum by stitching together individually-normalised spectral measurements from four separate spectrometers taken over four different wavelength regions (each region distinctly coloured in the plot). The wavelengths at 532 nm and 1064 nm (marked by

vertical lines on Figure 2.7) span an octave and were chosen as the fundamental-green and fundamental-IR wavelengths for the f-to-$2f$ process because of the ample intensity available at these wavelengths for beating, as well as there being suitable optics at 532 nm.

The PCF was attached in a V-groove holder for high stability and mounted on an *xyz* micrometer stage for high-precision coupling of the Ti:sapphire beam into the fibre core. The phase-coherent supercontinuum beam was collimated soon after the fibre exit by a parabolic mirror (PM) mounted on an *xy* stage. The reflected beam shape was collimated by precision movements of the parabolic mirror stage and was inspected in the near-field, just after the parabolic mirror, and far-field, some metres away, to confirm full collimation.

The collimated supercontinuum beam was then transmitted through a half-wave plate (P) at 532 nm. The half-wave plate allows the horizontal polarisation of the 532 nm wavelength to be rotated to a vertical polarisation without changing the horizontal polarisation at 1064 nm. The opposite polarisations of the fundamental green and the near-infrared regions is the crux to how this interferometer functions with common-mode noise rejection. It enables a birefringent technique using a Wollaston prism to temporally overlap the frequency-doubled-green beam and the fundamental-green beam to be able to record a beat between their respective frequencies, $2f_\mathrm{n}$ and f_2n. The 532 nm and 1064 nm wavelengths were originally separated in time due to group delay in the PCF. Given the assumption that the octave-spanning supercontinuum wavelengths are generated instantaneously on coupling into the PCF and proceed to propagate the full 12 cm fibre length, it was estimated that the temporal difference between the 532 nm and 1064 nm spectral components was Δt=1.2 ps. This calculation used the formula

$$\Delta t = L \int_{\lambda_1}^{\lambda_2} D(\lambda) d\lambda, \tag{2.1}$$

where L is the length of the fibre (12 cm), λ_1 and λ_2 are the 532 nm and 1064 nm wavelengths, respectively, and $D(\lambda)$ is the dispersion as a function of wavelength (estimated from the fibre dispersion profile [77]).

Frequency doubling of the NIR region of the supercontinuum was performed by focusing the beam (L2) into a polarisation-maintaining 2-mm long Type-I SHG crystal (LiB_3O_5). The SHG crystal was chosen as it is polarisation maintaining such that the frequency-doubled green kept the opposite polarisation to the fundamental green. The crystal was placed in a circular-rotation mount to optimise the phase-matching conditions.

The beam was collimated after the crystal (L3) and sent to a Wollaston prism (WP). A Wollaston prism is made of a birefringent crystal whereby the vertically-polarised light will see the ordinary refractive index expected for glass from Snell's law, whereas the horizontally-polarised light will have an extraordinary response and take a different path through the prism. The prism was mounted on a one-dimensional stage aligned to the 5° separation angle of the prism so that the different optical paths of oppositely-polarised beams could be adjusted until they overlapped in time on recombination after two trips through the birefringent material from being reflected back along their respective paths by a curved mirror (CM).

A slight angle was given to the reflected beam from the curved mirror in the *y*-direction such that the returning beam from the Wollaston prism was lower than the flat input beam. This enabled the recombined beam to be picked off by a D-shaped mirror (DSM). The D-shaped mirror sent the recombined beam through a 10-nm bandwidth interference filter at 530 nm (IF), angled in the *x*-direction to transmit the most-intense green wavelengths. A polariser was used to balance the optical power between the fundamental and frequency-doubled beams. The green beam was then focused (L4) into an avalanche photodiode (APD - APD430A2, Thorlabs) which was connected to an RF spectrum analyser (RFSA).

This set up was continually tweaked, taking great care with alignment into the PCF, conditioning the correct beam polarisations, optimising SHG efficiency, finding ideal displacement of the Wollaston prism for temporal overlap, and focusing into the APD, until a beat was observed on the RFSA. Once observed, the beat signal intensity was maximised through further manipulation of the set up to be a sufficiently-strong signal to undergo the locking procedure. Figure 2.8 shows the
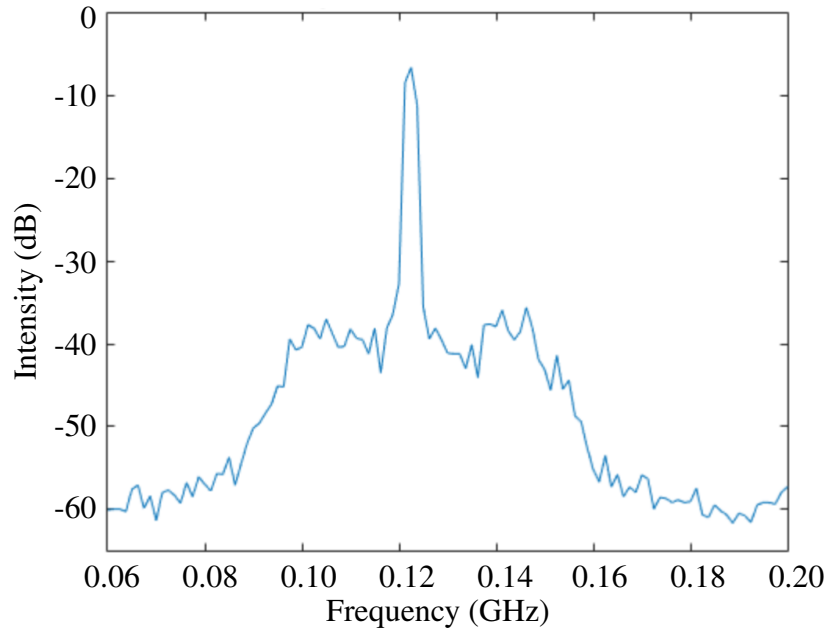
Figure 2.8: The 1-GHz gigajet Ti:sapphire laser carrier-envelope-offset beat frequency taken from the f-to-$2f$ interferometer.

optimised beat signal for the 1-GHz Ti:sapphire laser as measured on the RFSA. The beat intensity was >40 dB above the noise floor which is a signal ideal for the locking electronics and comparable with industry standards (see Appendix D [78]).

2.2.2 Carrier-envelope-offset stabilisation electronics

The electronics set up to achieve active CEO stabilisation is displayed in Figure 2.9. The 1-GHz Ti:sapphire laser beam is aligned into the f-to-$2f$ interferometer which creates an octave-spanning supercontinuum. The frequency-doubled 'red' section and the 'blue' section of the supercontinuum when temporally overlapped create a beat signal equal to f_{CEO} or $f_{\text{rep}} - f_{\text{CEO}}$. The beat frequency is detected on an avalanche photodiode and monitored on an RF spectrum analyser. The photodiode response is sent to a low-pass filter to isolate the single beat frequency below half f_{rep}.

A Rb-stabilised microwave frequency synthesiser was used as the local oscillator to atomically reference the beat frequency, and was initially tuned to a frequency that was sufficiently close to the beat frequency to be within the catch range of the locking mechanism. The isolated beat signal was sent through an amplifier
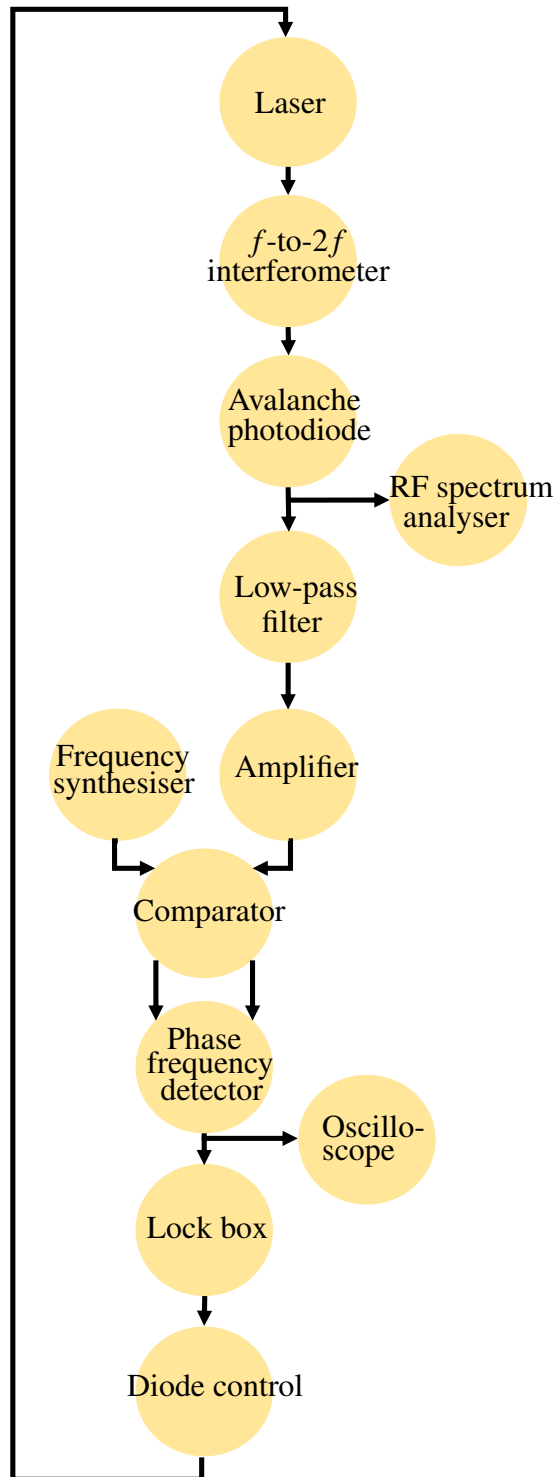
Figure 2.9: Feedback loop block diagram for carrier-envelope stabilisation through self referencing.

to closely match the peak-to-peak voltage of the frequency synthesiser for effective comparison with the phase frequency detector (PFD) downstream. A comparator

was used to condition the signals from sinusoids to square waves for input to the PFD. The PFD was utilised in generating a signal of the difference in frequency between the isolated beat signal and the reference signal.

A lock box (New Focus LB1005 PI server controller) takes the difference frequency as an input and derives an error signal. The lock box sends information to the diode control system to actively control the pump-laser power which through changing the nonlinear refractive index within the Ti:sapphire crystal, alters the cavity dispersion and therefore adjusts the carrier-envelope offset frequency.

The lock box works to minimise the error signal between the beat signal and the synthetic-frequency signal, and by so doing stabilises the carrier-offset frequency to the synthetic frequency referenced to the local oscillator.

2.3 Wide mode spacing by modal selection

2.3.1 Design of Fabry-Pérot cavity for modal selection

The 1-GHz Ti:sapphire laser was filtered by a Fabry-Pérot cavity based on the design in Reference [56]. The design has to account for the dispersion provided by the mirror coatings and by the air in the cavity that limit its effective bandwidth, as well as the cavity finesse $\mathscr{F}$ that defines the width of the frequency filter transmission window [62, 63, 64]. These considerations have to be well understood to prevent 'walk off' between the transmission profile of the Fabry-Pérot cavity and the frequency-comb modes which can cause unwanted neighbouring modes to be transmitted as well as, or instead, of the modes from the selected subset [65, 66, 67]. Please see Paper 3 - Astrocomb Proposal for ELT HIRES, Section 2.1 in Appendix C for further discussion of the considerations for filtering a frequency comb with a Fabry-Pérot cavity.

The mirrors for the cavity were a dispersion-compensating pair (Laseroptik), with the dispersive effects of one mirror coating designed to cancel the others to provide zero group delay and zero GDD across the 550–900 nm bandwidth, as displayed in Figure 2.10 (b) and (c) [65, 56]. The reflectivity of the mirrors was 98% across the intended bandwidth (Figure 2.10(a)) to give the cavity a finesse of
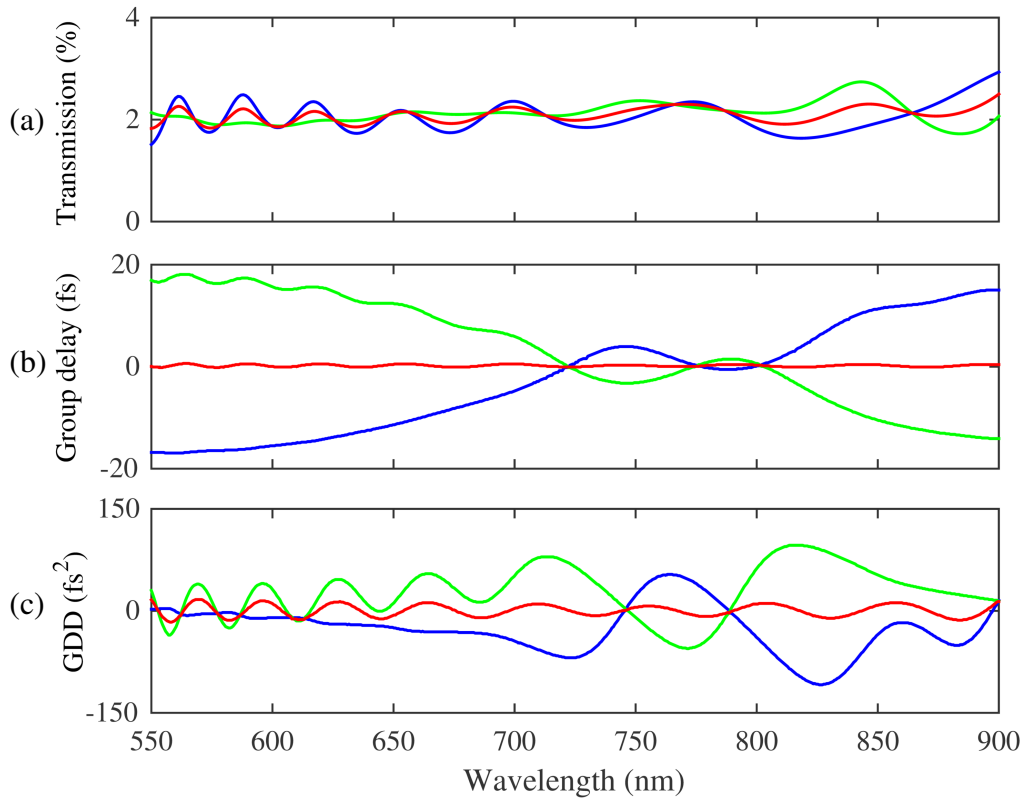
Figure 2.10: The (a) transmission, (b) group delay, and (c) GDD of the chirped-mirror pair
of the Fabry-Pérot cavity design. Key: mirror 1 - green line, mirror 2 - blue
line, and the combined mirror pair - red line.

$\mathscr{F}$=155, chosen to suppress unwanted sidemodes in this region.

2.3.2 Stabilisation of Fabry-Pérot cavity

The electronics configuration to lock a subset of the frequency comb modes to the
transmission profile of the Fabry-Pérot cavity is described by Figure 2.11.

A portion of the transmitted beam from the Fabry-Pérot cavity was directed
onto a photodiode. The photodiode signal was utilised to scan through the possible transmission peaks which correspond to the separate frequency-comb subsets.
A Matlab programme commanded the Red Pitaya to produce two frequencies for
dither locking. The translational stage of one cavity mirror was scanned by a 1 V
peak-to-peak 10-Hz triangle wave signal sent to the servo controller (New Focus
LB1005 PI server controller). Another higher-frequency 3 V peak-to-peak 10-kHz
triangle-wave signal was sent to both the mixer and the piezoelectric actuator con-
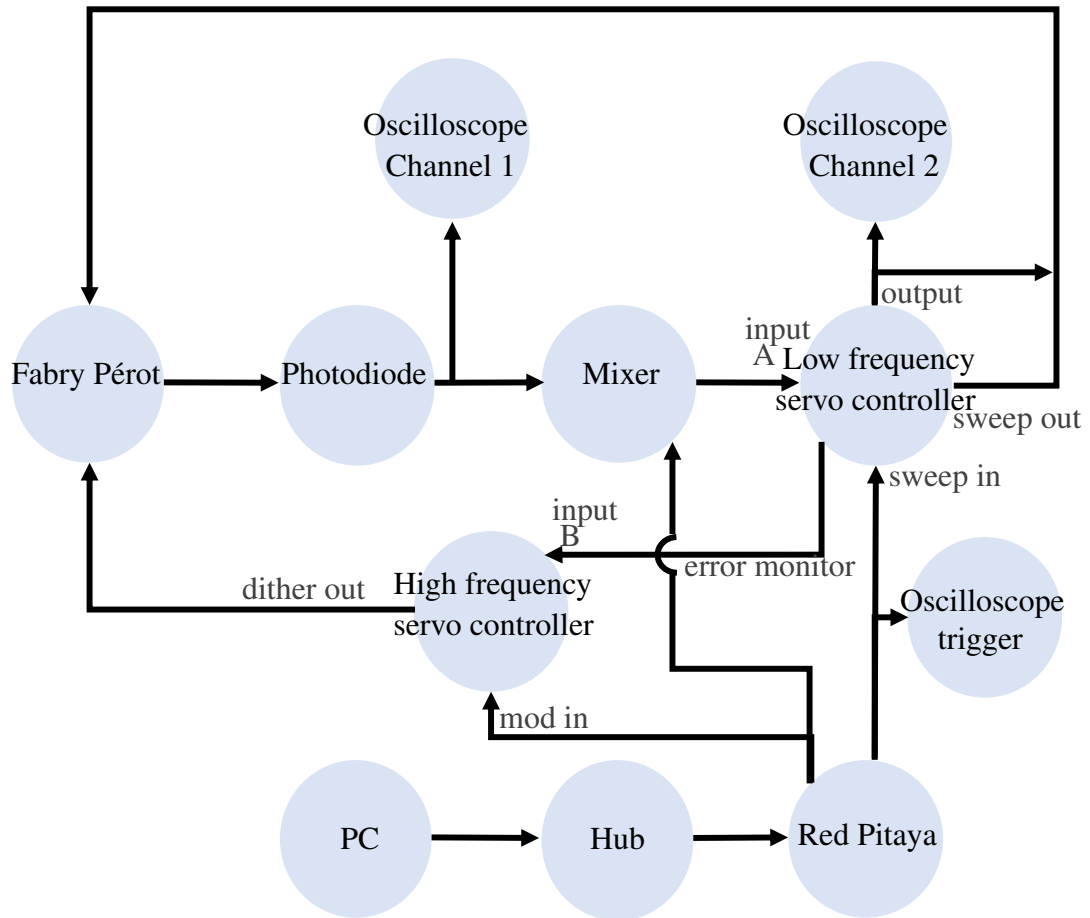
Figure 2.11: Feedback loop block diagram for Fabry-Pérot stabilisation.

nected to the same cavity mirror. The piezoelectric actuator (PZT NPM140, Newport) allowed for 100 μm of travel for cavity-length correction. Dither locking stabilised the Fabry-Pérot spacing to the chosen transmission peak within a 1-MHz accuracy.

2.4 Conclusions

The work discussed in this chapter concludes the build of a fully-stabilised 1-GHz Fabry-Pérot-based Ti:sapphire astrocomb with $\sim$30 fs pulses and access to a portion of the beam with $\sim$600 mW average power. The $\sim$600 mW stabilised Ti:sapphire beam was available as the pump beam for a broadened synchronous degenerate OPO intended to cover the wavelength region of 1–2 μm while maintaining the comb structure of the pump beam [60]. The experimental progress made in this pursuit is described in Chapter 3.

Furthermore, the high efficiency of the supercontinuum generation process from the PCF of the f-to-$2f$ interferometer set up enabled additional use of the supercontinuum beam. Access to the supercontinuum beam was provided by a 550–900 nm dichroic mirror placed just after the interferometer's collimation parabolic mirror. The filtered 1-GHz Ti:sapphire supercontinuum was utilised to demonstrate the broadband capability of the Fourier-transform spectrometer to discriminate between Fabry-Pérot modal subsets detailed in Chapter 4.

Chapter 3

Design and Characterisation of a Titanium-Sapphire-Pumped Degenerate 1-GHz Optical Parametric Oscillator

One of the most daunting hurdles to overcome in the realisation of an astrocomb calibraton source is in meeting the demanding spectral coverage of next-generation astronomical spectrograph, such as the broad wavelength coverage goal of 0.37–2.4 μm for ELT HIRES. Such a broad range is not met by any calibration source demonstrated to date. One unsatisfying solution could be to stitch together the spectra from a number of frequency combs with different gain media. This would not cover the full demanded coverage and would also be a highly-complicated and expensive system. Another solution could be the use of a white-light source filtered to resemble a comb-like structure by a number of broadband Fabry-Pérot etalons. However it is currently unclear how this calibration source would be traceable to microwave standards and therefore at present is not suitable as an absolute wavelength calibrator necessary for a number of science cases (see Table 1.1).

Our proposal is to exploit the rich field of nonlinear optics to create a degenerate optical parametric oscillator (OPO) frequency comb (same design as in Reference 60) and then send the generated $\sim$ 30-fs pulses through a highly nonlinear fibre

(HNLF). This is valid as an OPO at degeneracy has been demonstrated to maintain the comb structure of the pump source [57, 58].

3.1 Cavity design, construction, and stabilisation
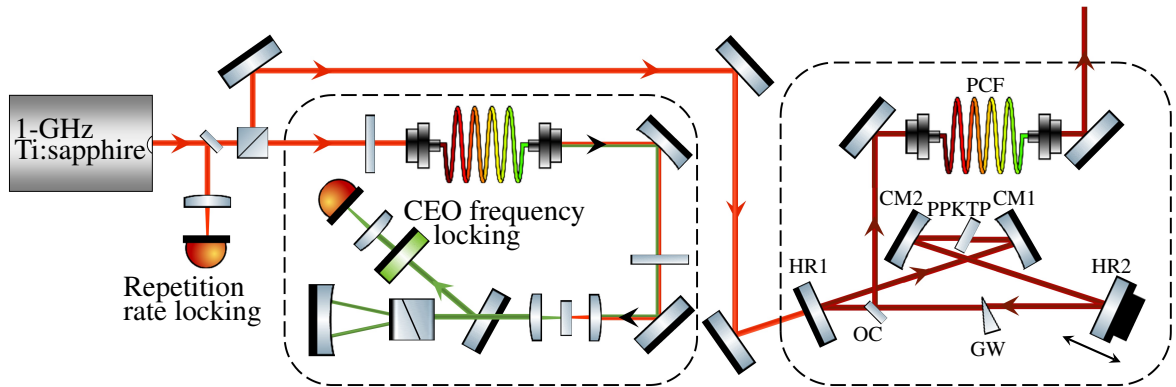
Figure 3.1: Schematic of experimental setup for a fully-stabilised 1-GHz synchronous degenerate OPO frequency comb.

The experimental setup for the 1-GHz broadband Ti:sapphire degenerate OPO is illustrated in Figure 3.1. The ∼600 mW average-power pump beam from the fully-stabilised 1-GHz Ti:sapphire frequency comb (Gigajet, Laser Quantum) is sent through a highly-reflective flat mirror, HR1, at an angle of ϕ=11° and reflected off of the curved-mirror, CM1, to best compensate for the astigmatism originating from the Brewster-angled PPKTP crystal. The curved mirror has a 15-mm focal length estimated to produce an extremely-narrow waist ∼10μm within the PPKTP crystal for efficient mode matching to the ∼14 μm spot size of the 1.6 μm OPO beam which was estimated by Gaussian beam ABCD matrix analysis to be the spot size for the most stable 1-GHz cavity to support a 1.6 μm beam. Oscillation of the OPO cavity was initially found by spatially overlapping the small portion of reflected Ti:sapphire light from HR1 with the low-power beam transmitted from the cavity at HR1 with use of a beam profiler (CCD Camera Beam Profiler, Thorlabs), in complement to looking at interference in time through the observation of fringe effects in the spectrum from an optical spectrum analyser (Ocean Optics USB4000-VIS-NIR).

3.1.1 Cavity assembly

The input Ti:sapphire beam into the system described below is conditioned to be Fourier-limited; focused such that its minimum waist occurs in the centre of the nonlinear crystal; at a chosen fixed height from the optical bench; and at the angle most optimal for cavity stability with respect to the optical bench.

As the OPO is synchronous, the OPO cavity length must precisely match the Ti:sapphire cavity length. The modelling provided boundary conditions for the spacing between the focusing curved mirrors and the crystal (a=10.3 mm, b=76.8 mm), as well as the optimal angle for a stable cavity (ϕ=11°). These conditions are accounted for by attaining the position of each optical component from a simple geometrical calculation.

Figure 3.2 illustrates the steps involved in the degenerate OPO assembly process to be viewed in compliment with the listed description of the assembly process below.

1. Start with placing the highly-reflective flat mirror, HR1, in the centre of the beam. Align the portion of the beam that is reflected from the back of the highly-reflective side to be parallel with the optical bench. Ensure the reflected beam height remains flat by checking at a long distance from the mirror.

2. Position the first curved mirror, CM1, such that the portion of the beam transmitted through HR1 is centred. Similar to step 1, ensure the reflected beam is parallel with the optical bench and that the beam height remains constant. Note as CM1 tightly focuses the beam, it is more involved to align the beam at a far distance due to significant divergence.

3. The next step sees the crystal placed at Brewster's angle into the beam path. The crystal is mounted on an *xyz*-stage which allows for fine tuning of the crystal position as well as the vertical displacement which allows access between the many different poling periods. Once the crystal face is aligned in the beam path, a blue beam will be visible due to second harmonic genera-
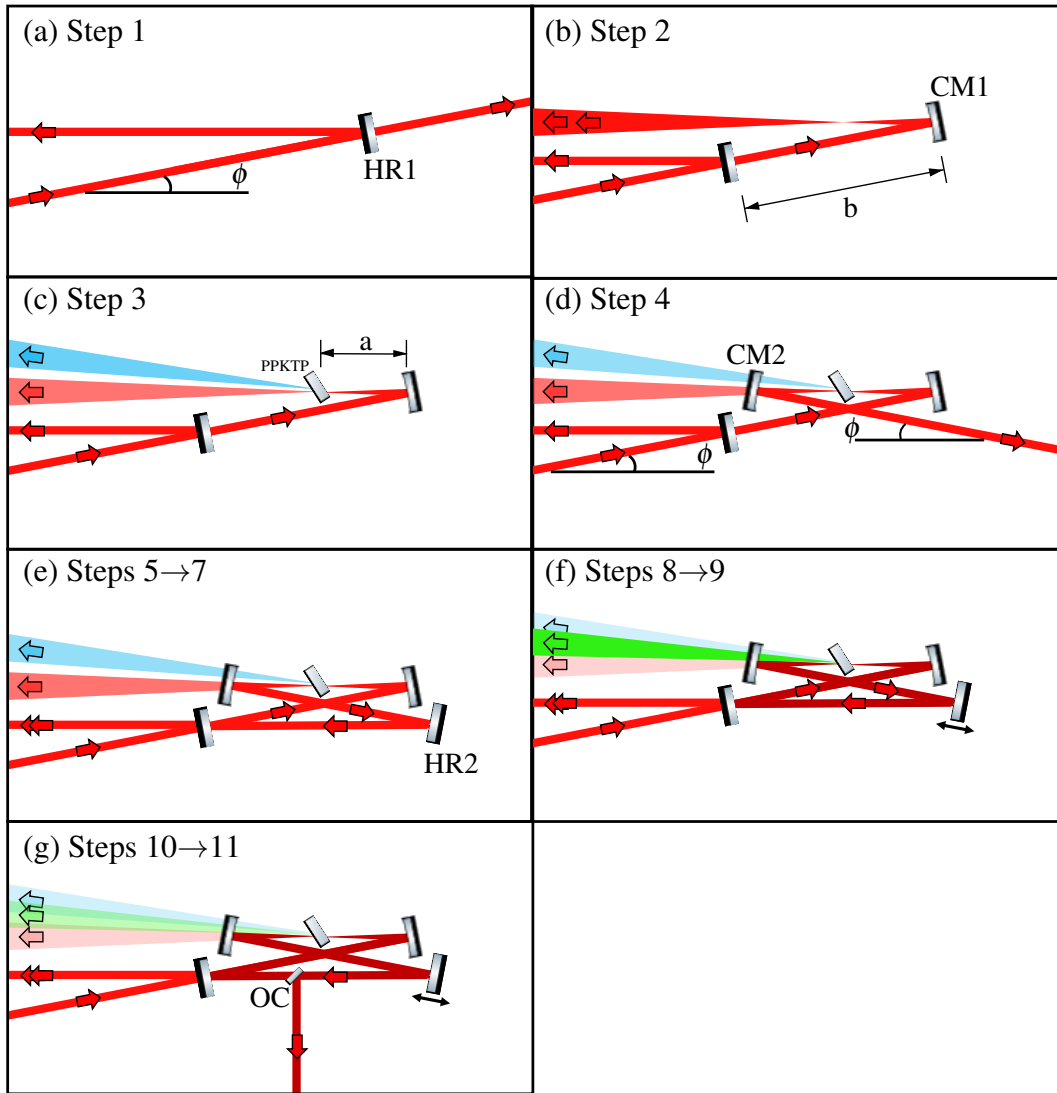
Figure 3.2: The synchronous degenerate OPO assembly process

tion. Note to make sure it is the polished face of the crystal in the beam path, and not the adjacent unpolished side as the crystal is then set at the correct angle for oscillation.

4. Position the second curved mirror, CM2, after the crystal, again checking the long-distance height is consistent. To align the reflected beam to the ideal angle, I temporarily marked the bench at a number of distances from CM2 and adjusted the beam to align with these markers.

5. Precise and accurate alignment and placement of the second high-reflective flat mirror, HR2, is critical to achieving resonance. This mirror sits atop a

one-dimensional translation stage to enable fine tuning of the cavity length to exactly match the pump laser cavity length. Firstly, align HR2 such that the beam reflected off of HR2 is directed to the centre of HR1, parallel to the optical bench.

6. The portion of the beam coming from HR2 that is transmitted through HR1 must be colinear with the portion of the input beam that is back-reflected from HR1 to obtain spatial overlap within the cavity. To achieve spatial overlap, *xy* adjustments are carried out on the HR2 mount while observing the spatial overlap of the two beams by using silver steering mirrors to direct the beams at a beam profiler alternately placed at two distances from HR1.

7. The cavity length is tuned by adjusting the HR2 stage. To enable synchronous oscillation there must exist a single pulse oscillating in the cavity and so the returning pulse from HR2 must exactly temporally overlap the incoming pulse through HR1. In carrying this out the two Ti:sapphire beams (the portion of the beam coming from HR2 that is transmitted through HR1 and the portion of the input beam that is back-reflected from HR1) were shone into a near-IR spectrometer (Ocean Optics) with care not to saturate the spectrometer's detector. Temporally overlap was observed on the spectrometer as fringes in the Ti:sapphire spectrum.

8. Iteration of steps 6 and 7 is necessary to obtain oscillation as it will occur only when the beams are both temporally and spatially overlapped. On oscillation a bright green light will be emitted due to sum frequency generation (SFG) between the Ti:sapphire beam at wavelength $\lambda_1 \sim$0.8 μm and the degerenate OPO beam at wavelength $\lambda_2 \sim$1.6 μm. The sum frequency generation process will give light at wavelength λ_3:

$$\frac{1}{\lambda_3} = \frac{1}{\lambda_1} + \frac{1}{\lambda_2} \quad \Rightarrow \quad \lambda_3 \sim 0.53 \, \mu m \tag{3.1}$$

9. Initially improve alignment by eye by increasing the rate of the SFG process

which occurs in the PPKTP crystal when the optical parametric generation conversion is more efficient. This is performed by carefully adjusting the HR1 and HR2 mirror mounts *x* and *y* positions and optimising the intensity of the green light.

10. Once sufficient OPO beam power is built up in the cavity, place an output coupler with low reflectance at 1.6 μm into the beam path between flat mirrors HR1 and HR2. Direct the reflected light from the output coupler toward a power meter to help further optimise the cavity alignment by minor adjustments of the HR1 and HR2 mirror mounts.

11. Replace the low-reflectance output coupler with a higher-reflectance output coupler and redo steps 9 and 10 to obtain optimum alignment.

12. The next step in building a degenerate OPO involves active stabilisation of the cavity.

3.1.2 Stabilisation procedure

The degenerate OPO beam from the output coupler is sent through an interference filter at $\sim$1.6 μm and then a beam splitter such that a small fraction of the light is focused onto a photodiode. The signal from the photodiode when the OPO cavity length was tuned by adjustment of HR2 (from a 20 V peak-to-peak triangle-wave signal sent to the HR2 stage) was viewed on an oscilloscope and showed a number of available oscillation regions. The different oscillation regions relate to an integer number of signal/idler wavelengths resonating within the OPO cavity. A typical oscilloscope trace of the available oscillation regions over the half the time period of the triangle-wave signal is displayed in Figure 3.3.

Figure 3.4 details the arrangement of the locking electronics. A Red Pitaya was programmed in MatLab to produce two output signals, one a a 1 V peak-to-peak 10-Hz triangle wave, and the other a 3 V peak-to-peak 10-kHz sine wave. The lower-frequency triangle-wave signal was sent to the servo controller (New Focus LB1005 PI server controller) to scan the HR2 translational stage. The higher-frequency sine-
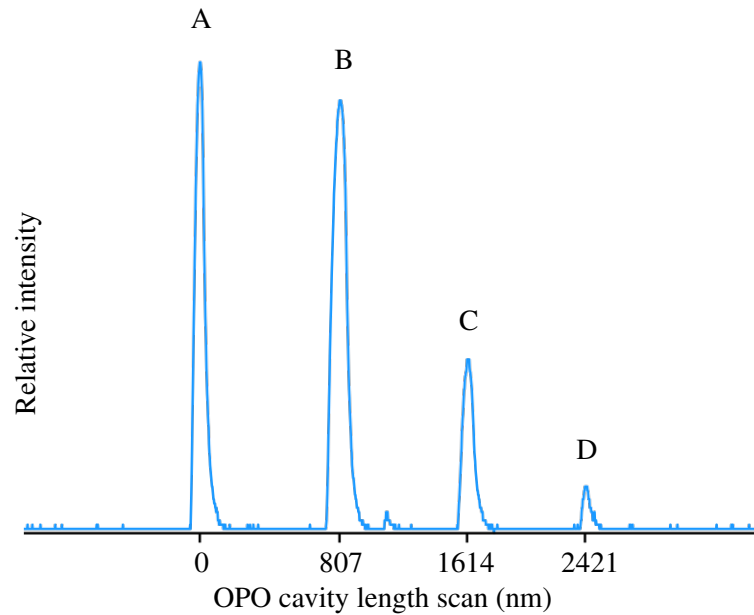
Figure 3.3: Optical-parametric-oscillation regions. Peak labels in line with text.

wave signal was sent to both the piezoelectric actuator (attached to the HR2 mirror) and also sent toward the mixer box for dither locking.

3.2 Characterisation of degenerate optical parametric oscillator

The stabilised degenerate OPO was optimised to achieve a threshold power of $\sim$220 mW, which translates to an efficiency of $\sim$35% (calculated as the signal-beam average power as a fraction of the pump-beam average power).

As part of this ongoing experiment I performed the alignment of the OPO cavity and dither-locked the cavity to each oscillation region peak in turn to scrutinise each spectrum over degeneracy and spectral bandwidth. The results of this investigation so far are viewed in Figure 3.5. Oscillation regions Peak A and Peak B (named in line with Figure 3.3) both suggest degeneracy while Peak C and Peak D do not as the signal and idler comb intensity profiles are clearly separated in frequency. Degeneracy in Peak A and Peak B were independently confirmed as degenerate by sending the OPO beam into a fast photodiode and not observing any sidebands on the photodetector. In the case of non-degeneracy the
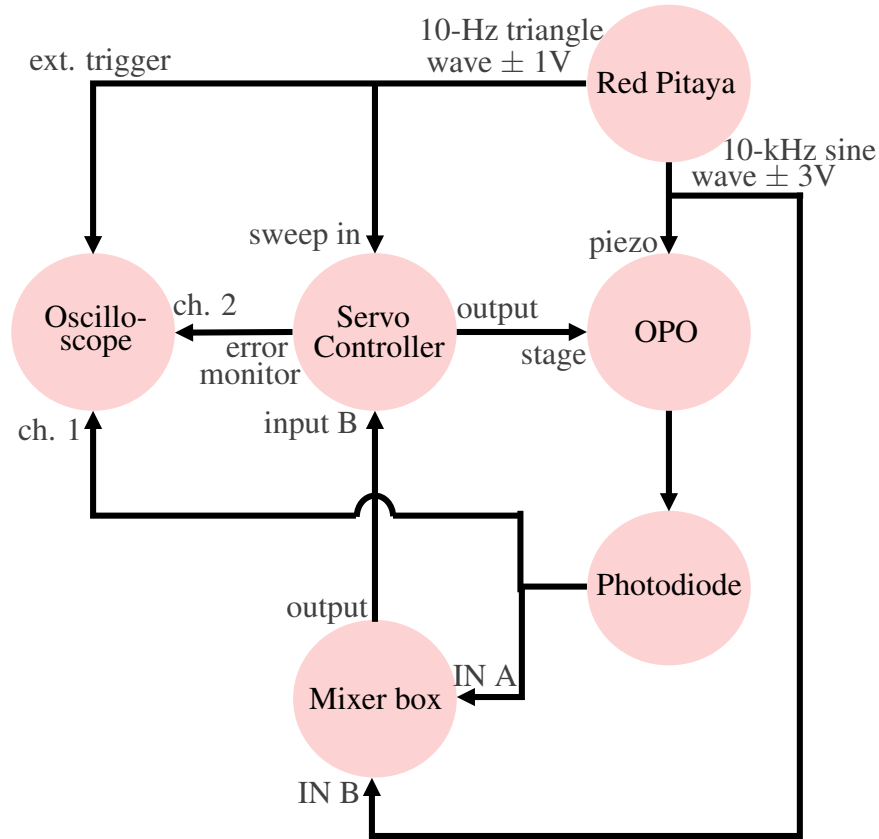
Figure 3.4: Feedback loop block diagram for OPO stabilisation

frequency-comb modes would not be fully overlapped and the observer witnesses the beating of sidebands around the repetition-rate frequency. The degenerate OPO spectrum from locking to Peak A had a central wavelength λ_A=1614 nm with a FHWM $\Delta\lambda_A$=99.6 nm, whereas the degenerate OPO spectrum from locking to Peak B had again a central wavelength λ_B=1614 nm but with a narrower FHWM of $\Delta\lambda_B$=82.0 nm.

3.3 Conclusions

The initial results demonstrated an unbroadened degenerate OPO spectrum with a $\sim$100-nm FWHM and centred at 1.6 μm. The next stage of this experiment is to couple the degenerate signal beam from the OPO into the HNLF and compare the resultant spectrum against a model based on the nonlinear Schrödinger equation [59]. Previous modeling results for broadening an earlier embodiment of the 1-GHz degenerate OPO from our group predicted a promising bandwidth of 1–2 μm (first
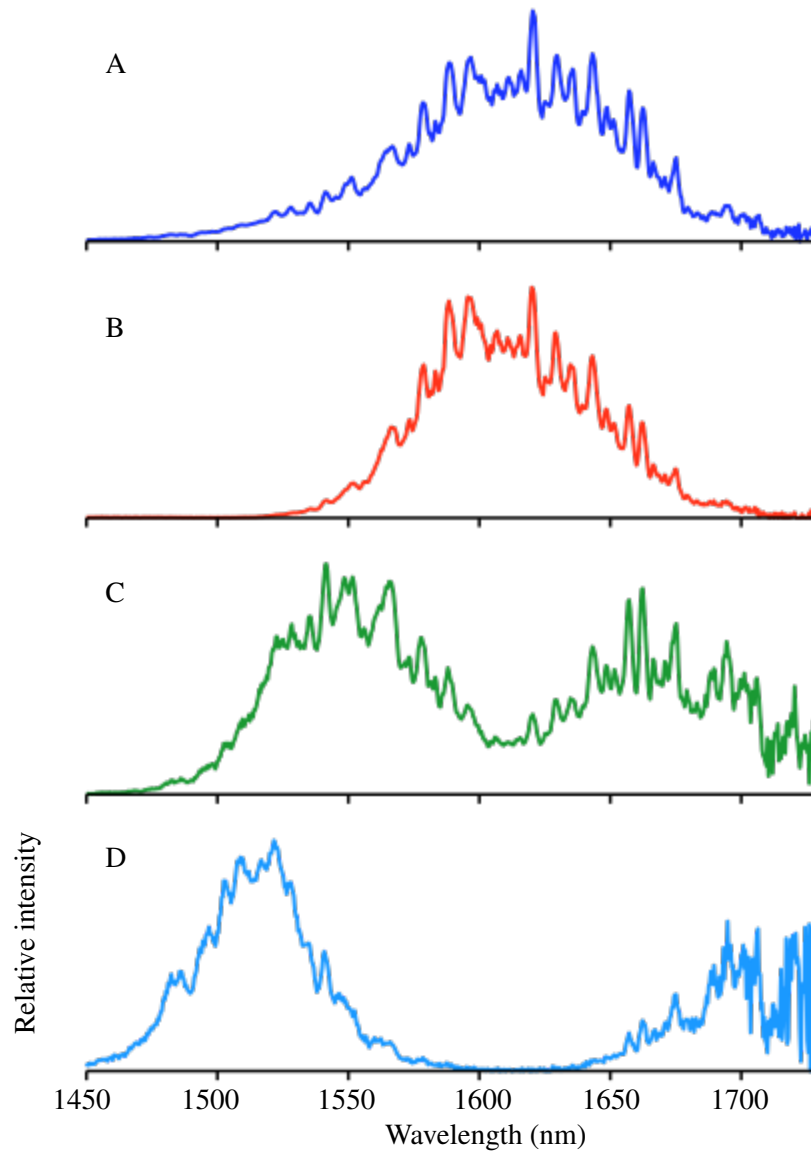
Figure 3.5: Spectral results from locking to different OPO oscillation peaks. Peaks A and B demonstrate degeneracy.

proposed in Reference 60). This investigation was a step towards confirming the ambitious approach of creating a single ultra-broadband astrocomb for spectrograph calibration based on a 1-GHz Ti:sapphire frequency comb.

Chapter 4

Design, Assembly, and Analysis of a Broadband Fourier-Transform Spectrometer

The identification of the transmitted modal subset in a Fabry-Pérot-based astro-comb is essential for resolving absolute wavelength measurements on a high-resolution spectrograph. In this chapter we demonstrate a compact broadband Fourier-transform spectrometer (FTS) for this purpose, with the accompaniment of Appendix A: Paper 1 - Compact Fourier-Transform Spectrometer for Comb-Mode Identification.

The data-retrieval work for the experimental analysis process resulted in the development of a Fourier-analysis software programme with a general user interface (GUI) in Matlab for ease of use as well as speed of analysis. A detailed user guide to the GUI is provided in Appendix E.

4.1 Design and assembly of Fourier transform spectrometer

The optical design of the compact FTS was based on the FTIR design in Reference 79 and is displayed in Figure 4.1. The FTS achieves a compact footprint-to-resolution ratio due to the use of two back-to-back silver retroreflectors mounted on a 10-cm travel stage. As the stage moves along the direction of beam propaga-
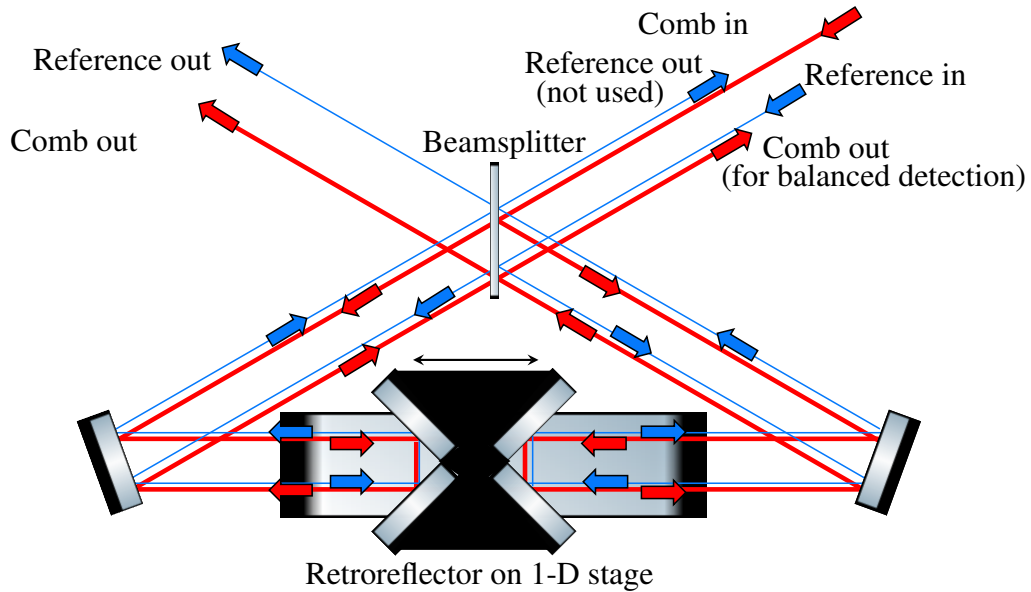
Figure 4.1: Schematic of optical paths in the Fourier-transform spectrometer design with balanced detection.

tion the optical path of one side is reduced by twice the displacement of the stage whereas the optical path of the other side is increased by twice the displacement. As a result the optical path difference (OPD) between the two arms of the interferometer is four times the physical scan length of the stage which, in this case, sets the instrument-limited spectral resolution at $c/40$ cm = 750 MHz [71]. The spectrometer used all metallic optics and a partially-silvered polka-dot beam splitter to obtain a bandwidth capability across the ultraviolet to mid-infrared wavelengths (in line with the optical range proposed for next-generation high-resolution spectrographs).

A photograph of the FTS can be seen in Figure 4.2. Initially, the 10-cm stage (DDSM100, Thorlabs) was centrally secured along the long edge of an optical breadboard (dimensions 45 cm×30 cm). Two flat silver mirrors were then positioned in the corners of the breadboard closest to the stage. The beamsplitter was set centrally on the breadboard with its faces orthogonal to the stage displacement direction. This ensemble of optics comprise the essential elements of the spectrometer, as shown in Figure 4.1. The remaining assembly process involves optimising the overlap of the two recombined comb beams from the two interferometer arms through precision steering; the addition of the reference beam aligned colinearly
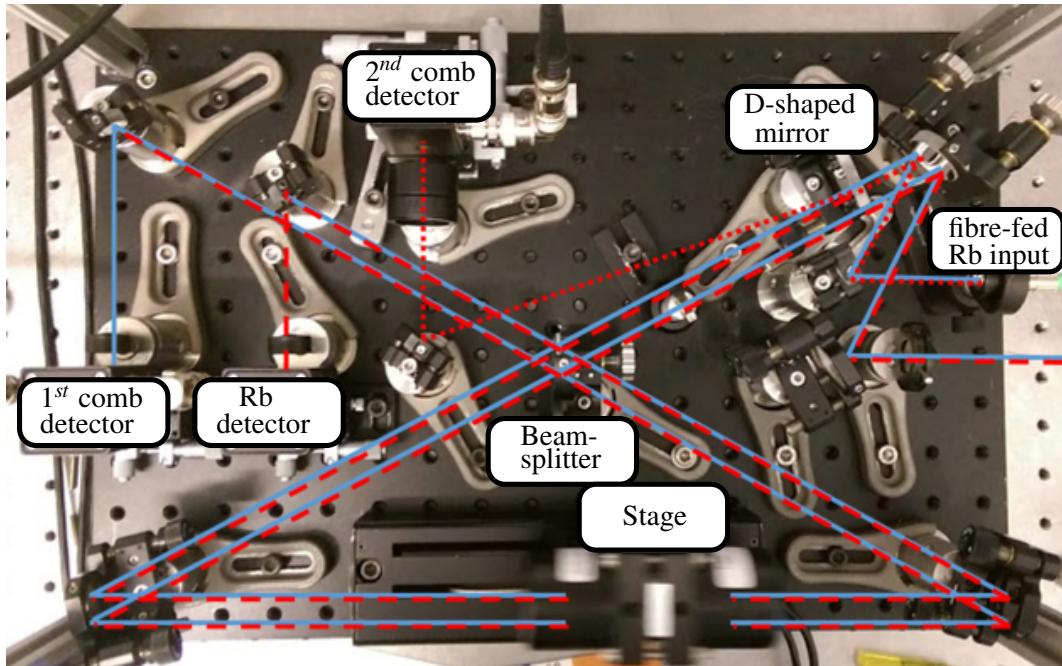
Figure 4.2: Photograph of Fourier-transform spectrometer with balanced detection overlaid with beam path sketch. Beam paths: blue line - Rb reference, red dashed - comb, red dotted - comb for balanced detection.

(near co-propogating) with the comb beam; and the observation of interferogram bursts by focusing the output beams onto detectors.

The FTS was first aligned using the 1-GHz Ti:sapphire beam because the lower red wavelengths of the Ti:sapphire spectrum are visible to the eye. The Ti:sapphire beam was sent into the instrument parallel to the displacement direction of the stage where two silver flat mirrors then aligned the beam into the interferometer path. These two steering mirrors (with the use of pinholes) would allow easier transition between different input laser sources, or indeed realignment of the same input laser source, once instrument alignment is achieved as the source beam is only required to be at the working height and parallel to the FTS. Half the beam is transmitted and half reflected by the beamsplitter into the two arms of the spectrometer. The comb beams propagate their separate paths - each reflected by a flat silver mirror onto a retroreflector where the beam is offset before returning to the mirror and the beamsplitter.

On perfect alignment the two separated trains of pulses are fully-overlapped on recombination at the beamsplitter (as illustrated in Figure 4.1) such that interfer-

ence occurs as the moving stage changes the OPD. Beam overlap was achieved by iteratively centring one beam's cross-section on a USB beam profiler (CCD Camera Beam Profiler, Thorlabs) viewed at two positions (one in the near field, one in the far field) while blocking the beam path of the other arm, and then switching the profiled beam with the blocked beam and repeating the process.

Once the instrument was aligned with the comb beam, the reference beam was sent into the cavity colinear to the comb beam such that the reference beam was also aligned into the interferometer. The reference beam source was provided by a single-frequency diode laser (D2-100-DBR, Vescent Photonics) traceable to an absolute frequency by dither locking to the Rubidium-87 transition F=2$\rightarrow F'$=2,3 [80].

After both the reference and comb beams were aligned in the interferometer the beams were focused into amplified silicon detectors (PDA36A-EC, Thorlabs) placed on xy stages for precise alignment. Note that the detectors could be swapped for other types to investigate different wavelength regions available to the broadband spectrometer. Here the amplified silicon detectors were chosen for characterisation of a supercontinuum Ti:sapphire beam.

A D-shaped mirror was able to pick off the returning comb beam as the instrument was carefully built such that the beam was vertically offset compared to the input beams. The detection of the two comb interferogram output signals enabled balance detection to significantly lower the signal-to-noise ratio as the respective signals are anti-phase. The interferogram signals from the detectors were recorded on a 16-bit USB oscilloscope (Handyscope HS5, TiePie Engineering) at a rate of 6.25 million samples per second.

4.2 Data analysis procedure of the interferogram signals

The data analysis procedure for this experiment is well documented in Section 3 of Paper 1 - Compact Fourier-Transform Spectrometer for Comb-Mode Identification found in Appendix A.

4.3 Characterisation of Fourier-transform spectrometer

For the characterisation results of the instrument, please see Section 4.2 of Paper 1 - Compact Fourier-Transform Spectrometer for Comb-Mode Identification attached in Appendix A.

4.4 Modal subset identification

Once characterised, an experiment was set up to test the ability of the broadband Fourier-transform spectrometer (FTS) to identify modal subsets in a Fabry-Pérot-based astrocomb. As a proof of concept, the spectrometer was required to have sufficient spectral resolution and bandwidth to clearly distinguish all possible subsets across a broad range of frequencies. Therefore the 1-GHz Ti:sapphire supercontinuum beam picked off from the f-to-$2f$ interferometer with a dielectric mirror offered a bandwidth of 550–900 nm was used as the input to the Fabry-Pérot cavity (see Section 2.2).

The Fabry-Pérot cavity (as described in Section 2.3) was adjusted to a filter ratio of M=8, such that 7 out of 8 subsets were suppressed to produce a wide-mode spacing of $f_{\text{rep-astro}} = 8f_{\text{rep}} \approx 8$ GHz. The $\sim$8-GHz Fabry-Pérot-based astrocomb in this investigation had a stabilised repetition rate frequency and a monitored carrier-offset frequency. The dichroic mirror to pick off the 550–900 nm portion of the supercontinuum did not permit sufficient intensity of the f_{CEO} beat signal for active stabilisation, however the frequency was shown to be passively stable with a 5×10^{-9} relative precision over 1 second.

The data collection and results of this experiment are outlined in Paper 1 (Appendix A). The Fourier-transform spectrometer demonstrated sufficient resolution, despite its compact footprint, to be able to repeatably discriminate between each modal subset, as viewed in Figure 4.3.

The broadband capability of the FTS was also demonstrated by accurate identification of the same two neighbouring modal subsets across the supercontinuum beam, as is represented in Figure 4.4.
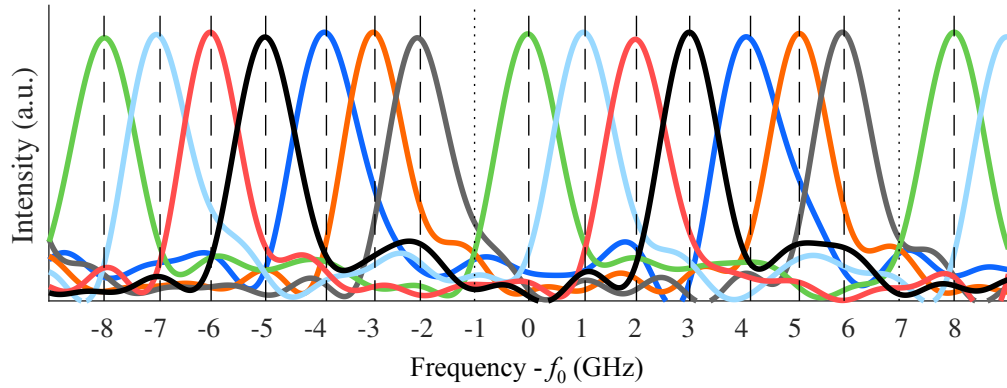
Figure 4.3: Fourier-transform spectrometer demonstration of sufficient resolution to accurately discriminate between modal subsets of a Fabry-Pérot-based astrocomb. Centred at $f_0 = c / 560\text{nm}$.
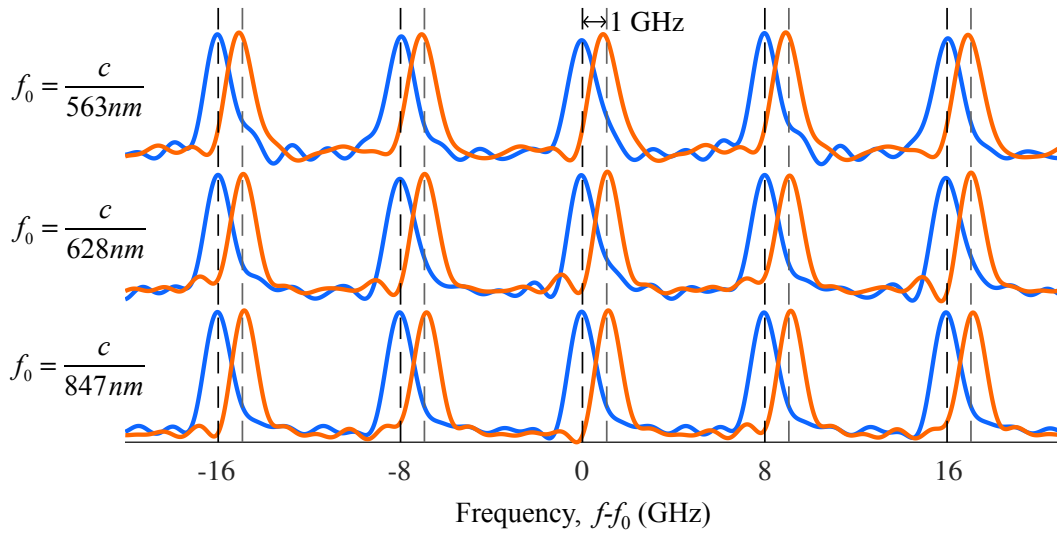
Figure 4.4: Fourier-transform spectrometer demonstration of subset identification over octave-spanning supercontinuum.

4.5 Conclusions

An exciting avenue presented from the data analysis involved in the FTS paper (Appendix A) is the possibility to characterise air dispersion for an accurate on-site compensation technique. This would be made possible from comparing the comb modes from the RF frequencies to the retrieved positions of the comb modes in the FTS analysis without any compensation. Initial proof-of-concept tests are planned to be performed using a long-travel FTS design.

Additional use of the long-travel stage is planned to characterise the effectiveness of the Fabry-Pérot cavity's sidemode suppression [81, 82].

Chapter 5

Conclusion

This report detailed the advances made towards the proposed turn-key astrocomb architecture for ELT HIRES described in Chapter 1.

Chapter 2 saw the demonstration of a fully-stabilised 1-GHz Ti:sapphire frequency comb with a design that permitted access to the Ti:sapphire supercontinuum beam, as well as the characterisation of a chirped-mirror-pair Fabry-Pérot filter for broadband modal selection.

Initial results were stated in Chapter 3 of an investigation to achieve a broadband synchronous degenerate OPO spanning 1–2 μm pumped by a 1-GHz Ti:sapphire laser. Before broadening in highly-nonlinear fibre, the 1-GHz degenerate OPO beam demonstrated $\sim$35% conversion efficiency, with a spectrum centred at $\sim$1.6 μm with a $\sim$100 nm bandwidth.

Chapter 4 detailed a compact broadband Fourier-transform spectrometer design as an ancillary technology for a Fabry-Pérot-based astrocomb system. As a proof-of-concept experiment, the spectrometer precisely identified the subset of filtered frequency-comb modes over a 1-GHz Ti:sapphire supercontinuum bandwidth.

Appendix A

Paper 1 - Compact Fourier-Transform Spectrometer for Comb-Mode Identification

Broadband Fourier-transform spectrometer enabling modal subset identification in Fabry-Pérot-based astrocombs

JAKE M. CHARSLEY,[*] RICHARD A. MCCRACKEN, LAUREN REID, AND DERRYCK T. REID

Scottish Universities Physics Alliance (SUPA), Institute of Photonics and Quantum Sciences, School of Engineering and Physical Sciences, Heriot-Watt University, Edinburgh EH14 4AS, UK
*jc50@hw.ac.uk

Abstract: A multi-GHz frequency comb (astrocomb) is typically realized by filtering modes of a sub-GHz frequency comb (source comb) in a Fabry-Pérot etalon, which can lead to ambiguities in determining which subset of source comb modes has been filtered. Here we demonstrate a broadband Fourier-transform spectrometer (FTS) with a resolving power of $R = 430,000$ at 550 nm, and apply it to the identification of comb subsets from a filtered 1-GHz supercontinuum. After apodization the FTS demonstrated an instrument line shape width of 1.26 GHz which enabled individual comb-line positions to be identified with an uncertainty of 17.6 MHz, a relative precision of 5×10^{-8}. Correcting for air dispersion allowed the instrument to determine the comb-mode spacing to an accuracy of 300 Hz and filtered subsets of source comb modes to be uniquely distinguished across the entire comb bandwidth from 550 to 900 nm. The inherently broadband design of the FTS makes it suitable in future applications for calibrating ultra-broadband astrocombs employed by instruments such as ELT HIRES.

References and links

1. T. Steinmetz, T. Wilken, C. Araujo-Hauck, R. Holzwarth, T. W. Hänsch, L. Pasquini, A. Manescau, S. D'Odorico, M. T. Murphy, T. Kentischer, W. Schmidt, and T. Udem, "Laser frequency combs for astronomical observations," Science **321**(5894), 1335–1337 (2008).
2. C.-H. Li, A. J. Benedick, P. Fendel, A. G. Glenday, F. X. Kärtner, D. F. Phillips, D. Sasselov, A. Szentgyorgyi, and R. L. Walsworth, "A laser frequency comb that enables radial velocity measurements with a precision of 1 cm s(-1)," Nature **452**(7187), 610–612 (2008).
3. A. G. Glenday, C.-H. Li, N. Langellier, G. Chang, L.-J. Chen, G. Furesz, A. A. Zibrov, F. Kärtner, D. F. Phillips, D. Sasselov, A. Szentgyorgyi, and R. L. Walsworth, "Operation of a broadband visible-wavelength astro-comb with a high-resolution astrophysical spectrograph," Optica **2**(3), 250–254 (2015).
4. R. A. McCracken, É. Depagne, R. B. Kuhn, N. Erasmus, L. A. Crause, and D. T. Reid, "Wavelength calibration of a high resolution spectrograph with a partially stabilized 15-GHz astrocomb from 550 to 890 nm," Opt. Express **25**(6), 6450–6460 (2017).
5. A. Bartels, D. Heinecke, and S. A. Diddams, "10-GHz self-referenced optical frequency comb," Science **326**(5953), 681 (2009).
6. M. Endo, I. Ito, and Y. Kobayashi, "Direct 15-GHz mode-spacing optical frequency comb with a Kerr-lens mode-locked Yb:Y(2)O(3) ceramic laser," Opt. Express **23**(2), 1276–1282 (2015).
7. J. M. Charsley, R. A. McCracken, D. T. Reid, G. Kowzan, P. Masłowski, A. Reiners, and P. Huke, "Comparison of astrophysical laser frequency combs with respect to the requirements of HIRES," in *Proc. SPIE, Optical Measurement Systems for Industrial Inspection X* (2017), pp. 10329–10333.
8. R. A. McCracken, J. M. Charsley, and D. T. Reid, "A decade of astrocombs: recent advances in frequency combs for astronomy," Opt. Express **25**(13), 15058–15078 (2017).
9. C.-H. Li, G. Chang, A. G. Glenday, N. Langellier, A. Zibrov, D. F. Phillips, F. X. Kärtner, A. Szentgyorgyi, and R. L. Walsworth, "Conjugate Fabry-Perot cavity pair for improved astro-comb accuracy," Opt. Lett. **37**(15), 3090–3092 (2012).
10. C.-H. Li, A. G. Glenday, A. J. Benedick, G. Chang, L.-J. Chen, C. Cramer, P. Fendel, G. Furesz, F. X. Kärtner, S. Korzennik, D. F. Phillips, D. Sasselov, A. Szentgyorgyi, and R. L. Walsworth, "In-situ determination of astro-

    comb calibrator lines to better than 10 cm s-1," Opt. Express **18**(12), 13239–13249 (2010).

11. G. G. Ycas, F. Quinlan, S. A. Diddams, S. Osterman, S. Mahadevan, S. Redman, R. Terrien, L. Ramsey, C. F. Bender, B. Botzer, and S. Sigurdsson, "Demonstration of on-sky calibration of astronomical spectra using a 25 GHz near-IR laser frequency comb," Opt. Express **20**(6), 6631–6643 (2012).

12. T. Steinmetz, T. Wilken, C. Araujo-Hauck, R. Holzwarth, T. W. Hänsch, and T. Udem, "Fabry–Pérot filter cavities for wide-spaced frequency combs with large spectral bandwidth," Appl. Phys. B **96**(2-3), 251–256 (2009).

13. A. Marconi, P. Di Marcantonio, V. D'Odorico, S. Cristiani, R. Maiolino, E. Oliva, L. Origlia, M. Riva, L. Valenziano, F. M. Zerbi, M. Abreu, V. Adibekyan, C. Allenda Prieto, P. J. Amado, W. Benz, I. Boisse, X. Bonfils, F. Bouchy, D. Buscher, A. Cabral, B. L. Canto Martins, A. Chiavassa, J. Coelho, E. Delgado, J. R. De Medeiros, I. Di Varano, P. Figueira, M. Fisher, J. P. U. Fynbo, A. C. H. Glasse, M. Haehnelt, C. Haniff, A. Hatzes, P. Huke, A. J. Korn, I. C. Leao, J. Liske, C. Lovis, I. Matute, R. A. McCracken, C. J. A. P. Martins, M. J. P. F. G. Monteiro, S. Morris, T. Morris, H. Nicklas, A. Niedzielski, N. Nunes, E. Palle, P. Parr-Burman, V. Parro, I. Parry, F. Pepe, N. Piskunov, D. Queloz, A. Quirrenbach, R. Rebolo Lopez, A. Reiners, D. T. Reid, N. Santos, W. Seifert, S. Sousa, H. C. Stempels, K. Strassmeier, X. Sun, S. Udry, M. Weber, and E. Zackrisson, "EELT-HIRES the high-resolution spectrograph for the E-ELT," Proc. SPIE **9908**, 990823 (2016).

14. A. Zybin, J. Koch, H. D. Wizemann, J. Franzke, and K. Niemax, "Diode laser atomic absorption spectrometry," Spectrochim. Acta B At. Spectrosc. **60**(1), 1–11 (2005).

15. G. Galbács, "A review of applications and experimental improvements related to diode laser atomic spectroscopy," Appl. Spectrosc. Rev. **41**(3), 259–303 (2006).

16. A. G. Glenday, D. F. Phillips, M. Webber, C.-H. Li, G. Furesz, G. Chang, L.-J. Chen, F. X. Kärtner, D. D. Sasselov, A. H. Szentgyorgyi, and R. L. Walsworth, "High-resolution Fourier transform spectrograph for characterization of echelle spectrograph wavelength calibrators," Proc. SPIE **8446**, 844696 (2012).

17. A. G. Glenday, C.-H. Li, N. Langellier, G. Chang, L.-J. Chen, G. Furesz, A. A. Zibrov, F. Kärtner, D. F. Phillips, D. Sasselov, A. Szentgyorgyi, and R. L. Walsworth, "Operation of a broadband visible-wavelength astro-comb with a high-resolution astrophysical spectrograph: supplementary material," Optica **2**(3), S1–S6 (2015).

18. V. Tsatourian, H. S. Margolis, G. Marra, D. T. Reid, and P. Gill, "Common-path self-referencing interferometer for carrier-envelope offset frequency stabilization with enhanced noise immunity," Opt. Lett. **35**(8), 1209–1211 (2010).

19. Z. Zhang, K. Balskus, R. A. McCracken, and D. T. Reid, "Mode-resolved 10-GHz frequency comb from a femtosecond optical parametric oscillator," Opt. Lett. **40**(12), 2692–2695 (2015).

20. J. Ye, S. Swartz, P. Jungner, and J. L. Hall, "Hyperfine structure and absolute frequency of the (87)Rb 5P(3/2) state," Opt. Lett. **21**(16), 1280–1282 (1996).

21. P. E. Ciddor, "Refractive index of air: new equations for the visible and near infrared," Appl. Opt. **35**(9), 1566–1573 (1996).

22. M. S. Bartlett, "Periodogram analysis and continuous spectra," Biometrika **37**(1-2), 1–16 (1950).

23. L. Rutkowski, P. Masłowski, A. C. Johansson, A. Khodabakhsh, and A. Foltynowicz, "Optical frequency comb Fourier transform spectroscopy with sub-nominal resolution," arXiv:1612.04808 (2016).

24. C. H. Knapp and G. C. Carter, "The generalized correlation method for estimation of time delay," IEEE Trans. Acoust. **24**(4), 320–327 (1976).

25. B. C. Smith, *Fundamentals of Fourier Transfom Spectroscopy* (CRC, 1996).

26. Spectratime, "iSource +TM Ultra LCR-900 Spec," www.spectratime.com/documents/lcr_spec.pdf.

27. "D2-100 DBR laser spec," http://www.vescent.com/products/lasers/d2-100-dbr-laser.

28. "PDA36A spec," https://www.thorlabs.com/thorproduct.cfm?partnumber=PDA36A-EC.

29. N. B. Hébert, S. K. Scholten, R. T. White, J. Genest, A. N. Luiten, and J. D. Anstie, "A quantitative mode-resolved frequency comb spectrometer," Opt. Express **23**(11), 13991–14001 (2015).

1. Introduction

The past decade has seen the development of various astrocomb architectures for astronomical spectrograph calibration [1–4] which exploit the stability and narrow linewidth of a frequency comb and deploy it as an optical ruler. The precisely-known frequency spacings of the comb lines are used to produce a wavelength solution of the cross-dispersed light that is incident on the CCD array of a high-resolution echelle spectrograph, enabling the identification of systematic errors and long-term instrument drifts.

    The optimal mode spacing for an astrocomb is determined by the resolving power of the spectrograph $R = \lambda/\Delta\lambda$ (normally > 40,000) and is typically 5–40 GHz, a repetition frequency range that is itself only achievable directly from a mode-locked laser in a few select cases [5,6], and at which the reduced peak powers become problematic for spectral broadening and other nonlinear conversion techniques. The prevailing approach to achieve a multi-GHz mode spacing is to filter the modes of a lower-repetition-rate laser in a Fabry-Pérot etalon (FP), and this technique has been used in every deployed astrocomb to date [7,8]. The filtering of a

frequency comb is non-trivial, and consideration of the etalon mirror coatings and curvature is necessary to ensure that unwanted modes are sufficiently suppressed [9,10].

An ambiguity exists in determining which subset of modes has been filtered from the dense source comb, as shown in Fig. 1(a). A common approach to address this problem for narrowband filtered combs has been to use a laser diode as an optical reference, locking it directly to (or beating it against) a comb tooth [11,12]. A wavemeter and an RF spectrum analyzer can provide sufficient diagnostic information to identify this comb tooth, from which the frequencies of the other comb modes can be calculated. The diode laser is then used to stabilize the Fabry-Pérot etalon, and therefore transmission of this reference laser also ensures transmission of a known subset of comb modes. This approach is only suitable for astrocomb systems comprising one Fabry-Pérot etalon (or set of etalons which filter a comb multiple times). Next-generation high resolution spectrographs demand extremely-broadband spectral coverage, such as the forthcoming HIRES instrument for the ELT [13] therefore multiple Fabry-Pérot etalons will need to be employed to provide the required modal spacing in each wavelength band [7]. Each etalon could therefore filter a different subset of comb modes which would lead to discontinuities at the edge of each wavelength band where the two subsets would overlap. Additionally, the approach of referencing all cavities to laser diodes is denied due to an absence of available narrow-linewidth sources and atomic references systematically spaced across the UV to the IR coverage [14,15].
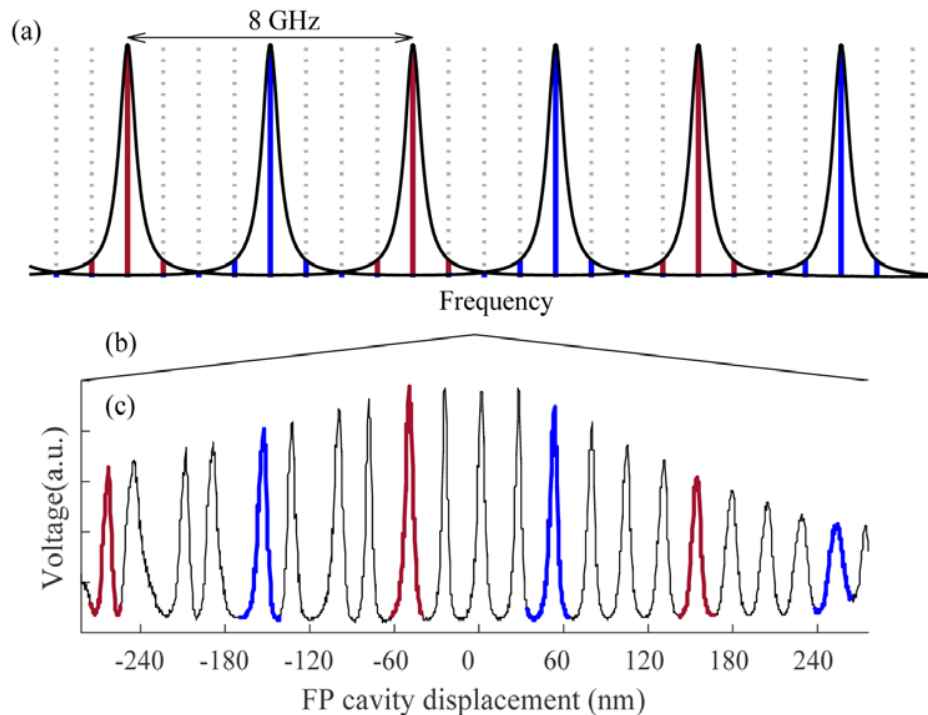
Fig. 1. (a) A Fabry-Pérot etalon can filter any subset of modes from a dense source comb. Here we illustrate two possible 8-GHz subsets selected from a 1-GHz comb. (c) The transmission profile of the Fabry-Pérot etalon as its length is swept by the triangular wave shown in (b). Red and blue lines indicate different 8-GHz subsets of the 1-GHz comb.

Here we demonstrate modal subset identification of an extremely-broadband astrocomb with a compact Fourier transform spectrometer (FTS). Previous examples of astrocombs deployed on an FTS have focused on employing high resolution (<100 MHz) instruments to characterize sideband suppression [16,17], requiring large optical paths and extreme

environmental stability. The compact FTS we report here is capable of resolving the modes of a supercontinuum pumped by a 1-GHz Ti:sapphire frequency comb, which are filtered by a Fabry-Pérot etalon locked to a comb transmission peak. The FTS path length is calibrated with an atomically-referenced diode laser and provides repeatable results from lock-to-lock, making it a promising on-site diagnostic tool for modal subset identification in broadband astrocombs for calibration of next-generation astronomical spectrographs for high-precision radial velocity measurements.

2. Experiment

The experimental layout is depicted in Fig. 2. Below we describe stabilization of the frequency comb and Fabry-Pérot etalon, and the design and operation of the FTS.

2.1 Frequency comb stabilization

A 1-GHz Ti:sapphire laser (Gigajet, Laser Quantum) produced 30-fs pulses with a central wavelength of 808 nm and 1.2-W average power. Approximately 500 mW was focused into a 12-cm-long photonic crystal fiber (PCF, FemtoWhite 800, NKT Photonics) with 70% coupling efficiency to generate an octave-spanning supercontinuum. Pre-compensation with dispersive mirrors ensured transform-limited pulses at the input facet of the PCF, maintaining supercontinuum phase coherence.

A dichroic mirror directed wavelengths from 550 to 900 nm towards the Fabry-Pérot etalon (see §2.2), with spectral components outside this range steered into a common-path f-to-2f interferometer with a design similar to that reported in [18] and illustrated in Fig. 2(c). A polarizer ensured a horizontal polarization at both visible and infrared wavelengths. Both spectral components were focused into a 2-mm-long LBO crystal cut for Type I SHG of 1060 nm, producing two orthogonally-polarized pulse sequences at 530 nm that propagated co-linearly. These pulses were focused into a Wollaston prism, splitting the polarizations with a 5° separation angle. The prism provided a differential group delay between the orthogonal polarizations, compensating for the group delay introduced within the PCF between the 1060-nm and 530-nm spectral components. The expanding beams were imaged back into the prism using a spherical silver mirror, and a slight vertical displacement allowed the recombined beams to be collected and directed towards an avalanche photodiode (APD430A2, Thorlabs). An interference filter with a 10-nm bandwidth removed unwanted spectral components, and a polarizer was used to balance the optical power between the fundamental and frequency-doubled 530-nm beams. The detected carrier-envelope offset frequency (f_{CEO}) had a 30-dB signal-to-noise ratio (SNR), sufficient for long-term monitoring. A stronger SNR is readily achievable with this interferometer, however the dichroic mirror used to direct light to the Fabry-Pérot etalon did not provide uniform reflectivity at the 530-nm and 1030-nm wavelengths required for beat detection. Previous measurements of f_{CEO} in this laser demonstrated a passive stability of 2.4 MHz hr^{-1} [4], thus active stabilization was not required for the purposes of the FTS demonstration. Detection of the repetition frequency (f_{REP}) was achieved by focusing a portion of the remaining Ti:sapphire power into a high-bandwidth GaAs photodiode (ET-3500, Electro-Optics Technology). The 8th harmonic of f_{REP} was compared against an RF synthesizer (FSL-0010, QuickSyn Lite), and the error signal used to provide feedback to a pair of piezoelectric transducers actuating mirror positions in the Ti:sapphire laser cavity.
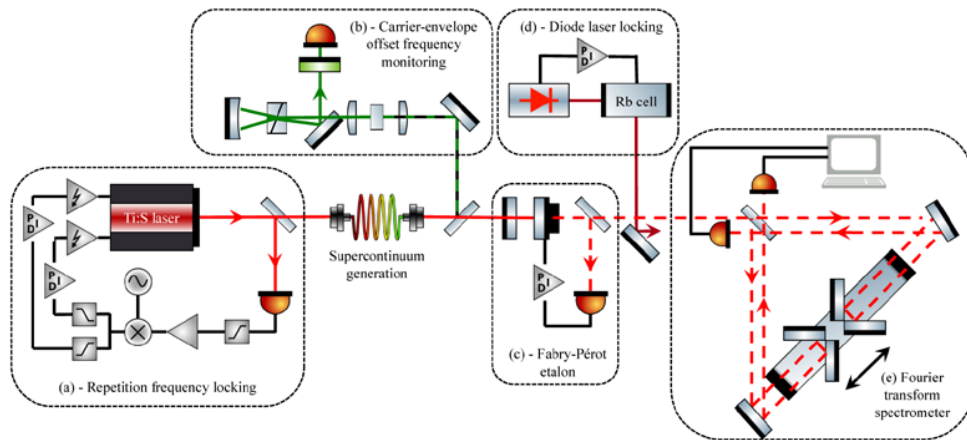
Fig. 2. Optical configuration of the experiment. (a), Ti:sapphire laser with f_{REP} locking loop. (b), common path f-to-$2f$ interferometer for f_{CEO} detection. (c), Fabry-Pérot etalon stabilized to a transmission peak. (d), narrow linewidth diode laser locked to a rubidium absorption line. (e), folded Fourier-transform spectrometer.

The design of the Fabry-Pérot etalon was identical to that reported in [4]. A pair of 98% reflectivity mirrors with complementary-dispersive coatings provided flat group delay across the 550–900nm region (Laseroptik). The cavity finesse of $F = 155$ provided a balance between sideband suppression and broadband operation. The etalon spacing was tuned to support an 8-GHz free spectral range, filtering the 1-GHz comb from the laser by a factor of eight. A triangular scan signal was applied to a 100-µm-travel piezoelectric actuator (NPM140, Newport) on which was mounted one of the etalon mirrors. Scanning the etalon spacing in this manner revealed the transmission profile shown in Fig. 1(c), with each transmission peak corresponding to an 8-GHz subset of the 1-GHz source-comb mode spacing. Dither locking was employed to stabilize the etalon spacing to a chosen transmission peak of the comb, providing a tight lock with sub-MHz uncertainty in the transmitted mode spacing.

2.2 Fourier transform spectrometer

The Fourier transform spectrometer is shown in Fig. 2(e). The design was based on that reported in [19] and comprised a pair of corner-cube retroreflectors mounted back-to-back on a long-travel motorized stage (DDSM100, Thorlabs), allowing the optical path difference (OPD) in each arm to be changed simultaneously and in opposite directions, effectively providing a 4-fold increase in the travel range of the stage for a spectral resolution as high as 750 MHz. Broadband operation was achieved by using all-metallic folding mirrors and a partially-silvered beam splitter, providing a linear instrument response with respect to chromatic dispersion. With appropriate dichroic beam splitters and detectors in the exit channel(s) of the FTS, this all-metallic design would enable astrocomb analysis from the UV to the mid-IR, however here we limit our measurements to the operational range of our Fabry-Pérot filter cavity.

Detection of the filtered comb was implemented using a pair of amplified silicon photodiodes (PDA36A-EC, Thorlabs), and the data acquired using a 16-bit USB oscilloscope at a sampling rate of 6.25 MS/s (Handyscope HS5, TiePie engineering). The OPD was calibrated using a narrow-linewidth single frequency diode laser (D2-100-DBR, Vescent Photonics) dither-locked to the ^{87}Rb F $= 2 \rightarrow$ F' $= 2,3$ crossover [20], providing absolute frequency traceability. Comb light detection and OPD calibration were carried out simultaneously to correct for stage jitter, with the filtered comb light and reference laser coupled into the FTS in a collinear, near-co-propagating geometry.

3. Data retrieval
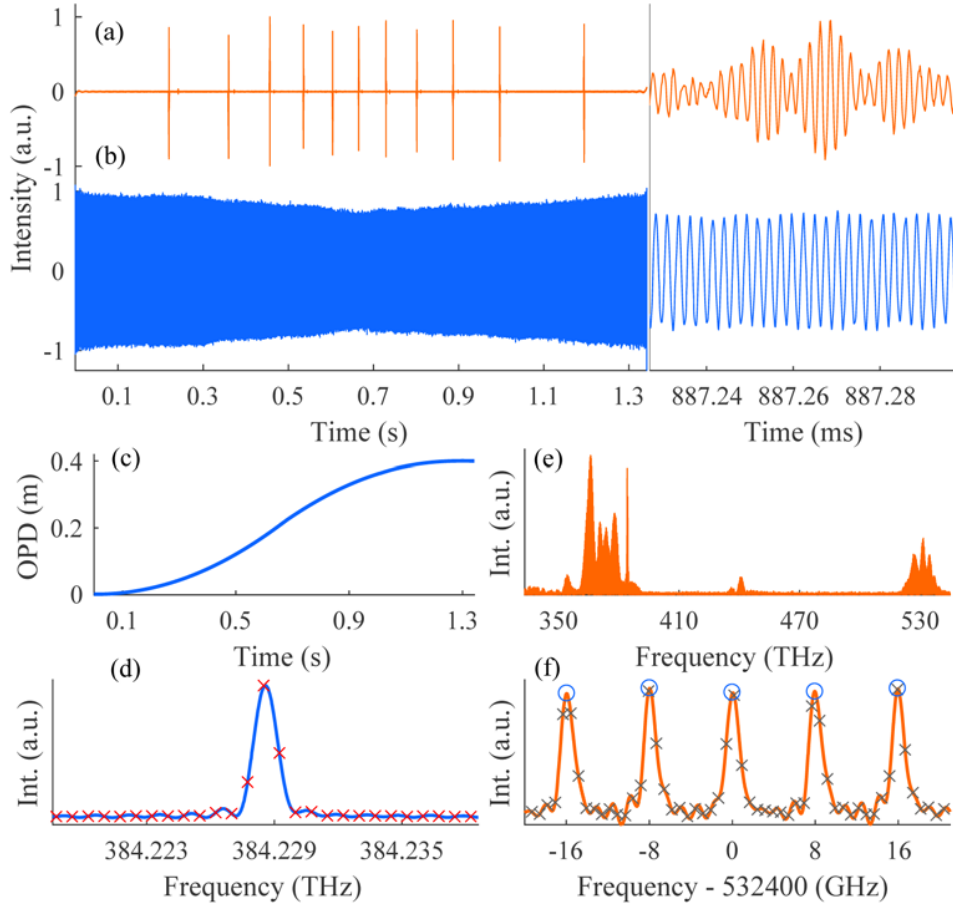
Fig. 3. FTS analysis protocol. Panels (a) and (b) show the balanced comb interferogram signal and the reference interferogram signal (centered about zero) respectively, over the course of the scan. The input is a 1-GHz supercontinuum FP-filtered to 8 GHz. Panel (c) illustrates the stage displacement over the scan calibrated by applying a zero-crossing algorithm to the reference signal. The instrument line shape of the spectrometer is revealed by upsampling the unresolved Rb spectral line (1.27-GHz apodized line width) shown in Panel (d). Panel (e) shows the retrieved supercontinuum spectrum. Finally, Panel (f) shows a selection of filtered comb modes, upsampled to illustrate the similarity of their line shapes with the instrument response. Cross-correlation was employed to find the peak positions (circled in blue).

The analysis protocol for the Fourier transform spectrometer is outlined in Fig. 3, which shows data for a Ti:sapphire supercontinuum comb, and the retrieval methodology is described below. Three signals were recorded for each scan of the FTS: the reference signal from the Rb-stabilized diode laser, and two anti-phase interferogram signals from the filtered frequency comb for balanced detection.

Firstly, the scan profile of the OPD was characterized using the reference signal, which was low-pass filtered to center the single-frequency oscillations about zero. An algorithm was applied to identify the half-fringe spacing across the scan, with upsampling by a factor of four utilized to increase the accuracy of the 'zero-crossing' positions in the central region of the scan (where the sampling is the most strained). These zero-crossing positions correspond to a half-wavelength separation of the interfering Rb-reference beams propagating in air, with the reference wavelength given by $\lambda_{REF} = \lambda_{Rb}/n_{air}(\lambda_{Rb})$ where $\lambda_{Rb} = 780.2465(8)$ nm is the Rb-

referenced wavelength of the narrow-line diode laser [20] and n_{air} is the refractive index of air given in the relations provided by Ciddor [21]. Using this method we characterized the optical path difference for the scan, with the maximum OPD of 40 cm corresponding to an unapodized instrument-limited resolution of 750 MHz.

As the linewidth of the diode laser is much narrower than the instrument-limited resolution, the line shape of the reference is unresolved by the FTS. The characteristic line shape of the instrument can therefore be determined from a Fourier transform of the reference interferogram. Characterization of the instrument line shape permits a thorough analysis of the modes of the FP-filtered frequency comb and is discussed in §4. In obtaining the instrument line shape the reference interferogram was linearly resampled in delay, apodized, and a fast Fourier transform (FFT) applied. The instrument line shape is affected by the chosen apodization function. We chose to implement a triangular apodization function on the reference signal which corresponds to an instrument line shape with a $sinc^2$ dependence [22].

The interferogram signals from the FP-filtered frequency comb were subjected to a similar low-pass filtering process and then balanced detection was implemented by subtracting one interferogram signal from the other. The resulting single comb interferogram was upsampled by the same factor used in the reference analysis and linearly resampled in delay with use of the obtained OPD profile. The comb interferogram was apodized and a FFT performed to retrieve the filtered comb modes. The same triangular apodization function used to condition the reference signal was imposed on the comb interferogram to ensure a consistent instrument line shape between the two retrieved spectra.

The frequency axis is determined by the maximum change in optical path. Compensation of the effects of dispersion of air throughout the spectrum was achieved through use of the relation [23]:

$$\lambda(air) = \lambda(vac)\frac{n_{air}(\lambda)}{n_{air}(\lambda = \lambda_{Rb})} \tag{1}$$

The frequency grid was converted to wavelength where the air dispersion compensation was performed, and then converted back to frequency. This step is vital for analysis of a broadband frequency comb where the wavelength dependence of the dispersion of air has the effect of displacing the retrieved mode positions from their true positions in a nonlinear way across the spectrum.

4. Results and discussion

4.1 Filtered subset identification

Analysis was performed of a Fabry-Pérot-filtered Ti:sapphire supercontinuum ranging in wavelength from 550 to 900 nm and with a mode spacing of 8 GHz. The 1.27-GHz apodized resolution is sufficient to distinguish neighboring subsets, and in Fig. 4 we present results demonstrating the identification of the possible modal subsets from the filtered comb structure near 560 nm. In the experiment, the Fabry-Pérot etalon was locked to all but one of the eight highest transmission peaks, shown in Fig. 1(b), with distinct subsets of the fundamental comb modes identified using the FTS for each lock. As Fig. 4 illustrates, the comb lines obtained for each different Fabry-Pérot lock lie on unique 8-GHz grids, with each grid displaced by a multiple of 1 GHz from the others, exactly as would be expected.
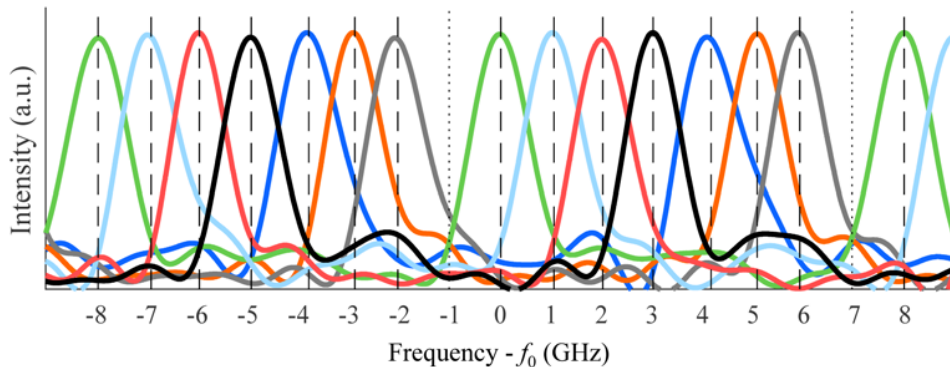
Fig. 4. Modal subset identification. A selection of the retrieved filtered comb modes near 560 nm are displayed. Each of the colored lines represents a distinct subset of the source-comb modes, where seven of the eight possible subsets were generated and identified in the experiment. The 8-GHz mode spacing is consistent with the FSR from the etalon mirror separation. The comb modes are displayed on a frequency scale centered at $f_0 = c$ / 560 nm.

The inherent broadband operation of the FTS is illustrated in Fig. 5. Interferograms were acquired for two neighboring transmission peaks of the Fabry-Pérot etalon. The corresponding upsampled comb spectra, displayed in red and blue in Fig. 5, show a 1-GHz difference in their comb-mode positions across the entire operating bandwidth of the Fabry-Pérot etalon (550–900nm). It is important to note that without correcting for the dispersion of air, the relative spacing between retrieved subsets would exhibit errors across this bandwidth.
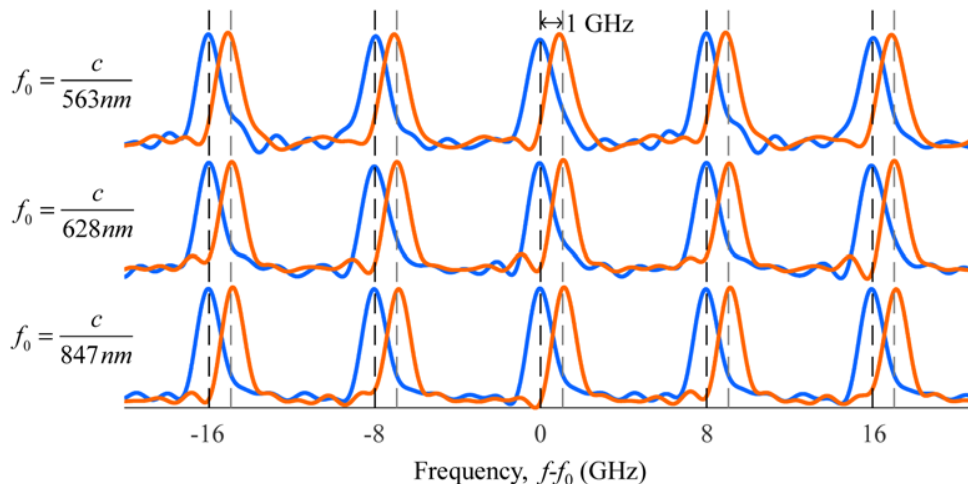
Fig. 5. A 1-GHz separation in the comb-mode positions of neighboring filtered subsets was identified across the full operational bandwidth of the Fabry-Pérot etalon. To allow inter-comparisons, each set of comb modes is displayed on a frequency scale centered at a different frequency, f_0.

4.2 Optical precision

In §4.1 we demonstrated that the instrument response of the FTS is sufficient for modal subset identification, however it is instructive to determine the precision to which the FTS can identify a single filtered comb line. Here we perform an analysis of the optical precision of the FTS, noting that this characterization need not be carried out for each use of the instrument.

The line shape of the instrument characterized by the unresolved Rb reference line enables a quantitative analysis of the retrieved comb-mode positions. The center frequency of each

comb mode in the supercontinuum (about 6000 in total) was obtained by a cross-correlation analysis with the instrument line shape, following the approach outlined in [24]. This is made possible because the comb modes and the Rb-referenced diode laser share a similar sub-MHz linewidth, neither of which is resolvable by the spectrometer. The cross-correlation technique effectively sweeps the instrument line shape through the comb spectrum, accurately registering the center positions of the comb modes, which correspond to local maxima of the cross-correlation function. The method guarantees a consistent way of obtaining the comb mode frequencies and also, as the instrument line shape is individually characterized for each scan, is insensitive to small differences in the instrument line shape observed from scan to scan. To obtain a clearer representation of the instrument line shape, the Rb-referenced diode laser line and the comb spectrum were upsampled by a factor of 128; the results shown in Fig. 3(d) and 3(f) illustrate the expected $sinc^2$ character of the instrument line function.

To evaluate the repeatability of the comb-line identification process we blocked the supercontinuum and steered a portion of the unbroadened Ti:sapphire comb into the Fabry-Pérot etalon, which was stabilized to a single transmission peak. We acquired 150 data sets over a 1-hour period, during which time both the Fabry-Pérot etalon and f_{REP} remained locked. A single filtered comb line near 371 THz was isolated and the peak of the comb line determined using the cross-correlation method described in §4.1. The distribution of the retrieved single mode position from each data set is shown in Fig. 6(a). The comb line was identified with a standard deviation of 17.6 MHz (bright red region), corresponding to a 5×10^{-8} relative precision. The extension of this approach to provide the standard deviation in the positions of 1000 comb modes over 150 acquisitions is shown in Fig. 6(b). The slight decrease in precision at lower frequencies may be attributable to imperfect compensation for air dispersion in the FTS, as higher frequencies lie closer to the reference wavelength of ~780.2 nm. With improved monitoring of local environmental conditions the compensation of air dispersion in the FTS can be more accurately applied, preventing a degradation of precision far from the reference wavelength.
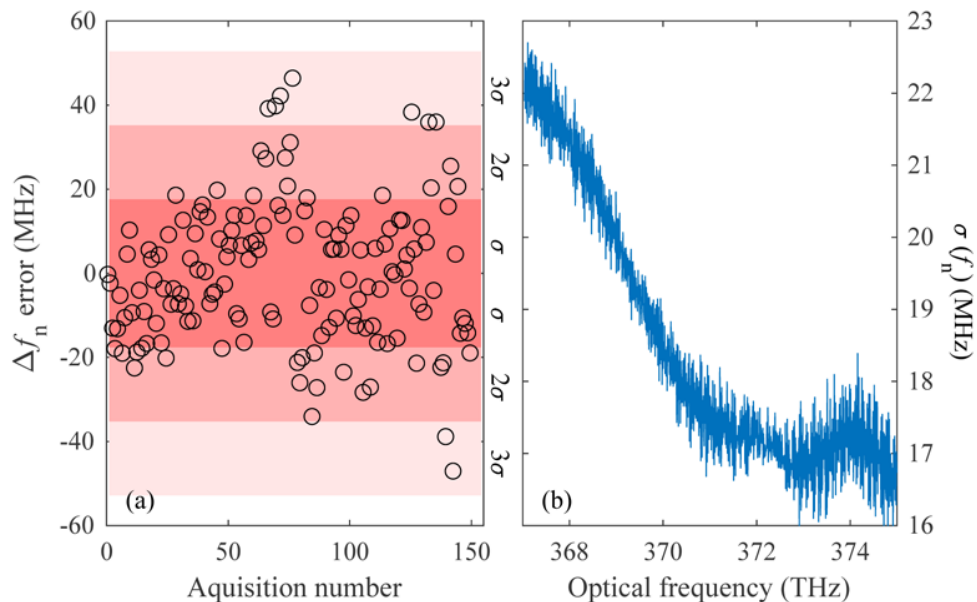
Fig. 6. (a) Uncertainty in the peak position of a single comb line near 371 THz, extracted from 150 data sets. Colored segments indicate standard deviations from the mean. (b) Standard deviations in the positions of each comb line from 367 to 375 THz, extracted from 150 data sets.

Additional data from multiple filtered subsets were acquired using the Ti:sapphire laser in order to determine the accuracy to which the FTS could identify the mode spacing of the astrocomb under test. This property is critical when analyzing combs in the UV-visible region, as they require extremely wide mode spacings (>40 GHz) and therefore very compact Fabry-Pérot etalons, where the change in mirror separation separating consecutive filter ratios is <100 µm. The peaks of 1000 comb modes were identified for 450 data sets recorded over three hours and the data combined to form a single data set containing the mean positions of 1000 comb modes. The frequency difference Δ between adjacent comb modes is a direct optical measurement of $8f_{REP}$, and this value was obtained for each data set by averaging the spacings between the 1000 comb modes. Conveniently, the laser repetition frequency was stabilized to the 8th harmonic of f_{REP} using a RF synthesizer (frequency, f_{SYNTH}), allowing us simply to subtract f_{SYNTH} from Δ in order to determine the accuracy to which $8f_{REP}$ could be measured using the FTS. Figure 7 shows the deviation between the synthesizer frequency and the optically calculated value of $8f_{REP}$. The mean mode spacing was found to be accurate to within 2.4 kHz of f_{SYNTH} (equivalent to optically determining f_{REP} to within 300 Hz) and the standard deviation was 26 kHz, indicating a 3×10^{-7} precision. It should be noted that the applied compensation for air dispersion is dependent on multiple variables, including air pressure, temperature, water vapor pressure and CO_2 concentration [16]. As such, the accuracy and precision stated here may decrease in any environment unless attention is paid to careful monitoring of local conditions.

The kHz-level and MHz-level uncertainties in the optically retrieved values for f_{REP} and f_n, respectively, are more than sufficient to consistently distinguish the filtered subset of an astrocomb, however limiting systematic uncertainties prevent direct optical retrieval of the carrier envelope offset (CEO) frequency, f_{CEO}. An additional measurement is therefore required to determine whether the CEO frequency measured with the f-to-$2f$ interferometer is f_{CEO} or f_{REP}-f_{CEO}, such as heterodyning the Ti:sapphire laser with the Rb-referenced diode laser.
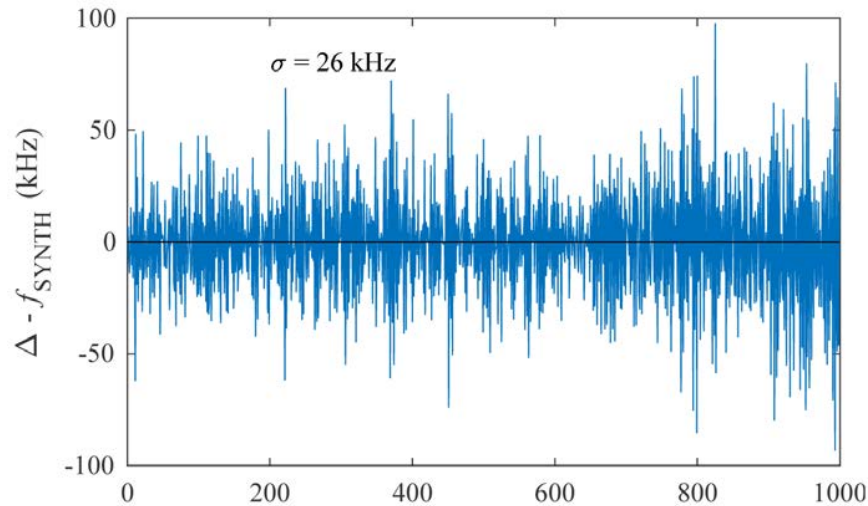
Fig. 7. Difference between the RF synthesizer frequency used for repetition rate stabilization (f_{SYNTH}) and the mean mode spacing between 1000 filtered comb modes ($8f_{REP}$) for 450 data sets. The standard deviation is 26 kHz and the mean offset of $8f_{REP}$ from f_{SYNTH} is 2.4 kHz, equivalent to optically determining f_{REP} with an accuracy of 300 Hz.

Sources of uncertainty in the instrument are listed in Table 1 along with an estimation of their contributions in the optical domain. The RF synthesizer was referenced to a Rb quartz oscillator with 5×10^{-11} accuracy and 3×10^{-11} precision over 1 second, which together with the locking loop used to stabilize f_{REP} results in a 300 Hz uncertainty at 384 THz (~780.2 nm). The diode laser had an approximate linewidth of 1 MHz, and was stabilized to an optical

transition with estimated line-position uncertainty of <1/200 of the 6-MHz linewidth. The reference laser module contributes an uncertainty of 1.06 MHz at optical frequencies. The carrier envelope offset frequency of the Ti:sapphire laser was not stabilized, resulting in a 1-MHz uncertainty over the 1-second acquisition time. Minute variations in air dispersion as a result of temperature and humidity fluctuations in the FTS resulted in changes to the OPD at each frequency, displacing the comb modes upon retrieval. While instantaneous changes will be very small, n_{air} changes by 10^{-6} per degree, resulting in a nonlinear shift in the frequency scale across the comb bandwidth. The bandwidth response of the detectors in the FTS will also affect the resolution of the instrument, introducing some systematic apodization prior to data retrieval [25].

Table 1. Contributions to optical uncertainties in the FTS

Source	Accuracy	Precision over 1-s acquisition time	Contribution in optical domain
RF synthesizer [26]	5×10^{-11}	3×10^{-11}	300 Hz
Diode laser [27]	-	2.6×10^{-9}	1.06 MHz
Rb-line [20]	1×10^{-10}	-	
CEO frequency [4]	-	5×10^{-9}	1 MHz
Air dispersion [21]	-	1×10^{-6}	1 kHz
Detector response [28]	-	-	Apodization

5. Conclusion

In summary, we have demonstrated a broadband, atomically traceable Fourier-transform spectrometer, capable of consistently identifying any subset of modes transmitted by a Fabry-Pérot etalon used to filter a frequency comb. This capability is needed by future high-resolution spectrographs such as ELT HIRES, whose ultra-broadband design implies the need for multiple Fabry-Pérot cavities operating at diverse wavelengths, rendering impractical the current referencing paradigm based on co-locking a narrow-line cw laser with the comb.

Cross-correlation analysis of the filtered comb with the 1.27-GHz instrument line shape enabled each comb-line position to be identified with a precision of 17.6 MHz, equivalent to 34 fm at 800 nm. The resolving power of ~2 pm in the optical domain is comparable with VIPA technology [29].

The precision to which individual comb modes can be identified could be used to recover the refractive index of air by observing the frequency-dependent shift in the spacing between filtered comb lines prior to correction, potentially providing an *in situ* compensation method without prior knowledge of local pressure, humidity and temperature.

Funding

Appendix B

Paper 2 - Astrocomb Review

A decade of astrocombs: recent advances in frequency combs for astronomy

RICHARD A. MCCRACKEN,[*] JAKE M. CHARSLEY, AND DERRYCK T. REID

Scottish Universities Physics Alliance (SUPA), Institute of Photonics and Quantum Sciences, School of Engineering and Physical Sciences, Heriot-Watt University, Edinburgh EH14 4AS, UK
*R.A.McCracken@hw.ac.uk

Abstract: A new regime of precision radial-velocity measurements in the search for Earth-like exoplanets is being facilitated by high-resolution spectrographs calibrated by laser frequency combs. Here we review recent advances in the development of astrocomb technology, and discuss the state of the field going forward.

References and Links

1. M. Mayor and D. Queloz, "A Jupiter-mass companion to a solar-type star," Nature **378**(6555), 355–359 (1995).
2. I. A. G. Snellen, R. J. de Kok, E. J. W. de Mooij, and S. Albrecht, "The orbital motion, absolute mass and high-altitude winds of exoplanet HD 209458b," Nature **465**(7301), 1049–1051 (2010).
3. A. Frebel, J. D. Simon, M. Geha, and B. Willman, "High-resolution spectroscopy of extremely metal-poor stars in the least evolved galaxies: Ursa Major II and Coma Berenices," Astrophys. J. **708**(1), 560–583 (2010).
4. K. Cunha and V. V. Smith, "Chemical evolution of the galactic bulge as derived from high-resolution infrared spectroscopy of K and M red giants," Astrophys. J. **651**(1), 491–501 (2006).
5. R. Maiolino, M. Haehnelt, M. T. Murphy, D. Queloz, L. Origlia, J. Alcala, Y. Alibert, P. J. Amado, C. Allende Prieto, M. Ammler-von Eiff, M. Asplund, M. Barstow, G. Becker, X. Bonfils, F. Bouchy, A. Bragaglia, M. R. Burleigh, A. Chiavassa, D. A. Cimatti, M. Cirasuolo, S. Cristiani, V. D'Odorico, D. Dravins, E. Emsellem, J. Farihi, P. Figueira, J. Fynbo, B. T. Gansicke, M. Gillon, B. Gustafsson, V. Hill, G. Israelyan, A. Korn, S. Larsen, P. De Laverny, J. Liske, C. Lovis, A. Marconi, C. Martins, P. Molaro, B. Nisini, E. Oliva, P. Petitjean, M. Pettini, A. Recio Blanco, R. Rebolo, A. Reiners, C. Rodriguez-Lopez, N. Ryde, N. C. Santos, S. Savaglio, I. Snellen, K. Strassmeier, N. Tanvir, L. Testi, E. Tolstoy, A. Triaud, L. Vanzi, M. Viel, and M. Volonteri, "A community science case for E-ELT HIRES," arXiv:1310.3163v2 (2013).
6. A. Sandage, "The change of redshift and apparent luminosity of galaxies due to the deceleration of selected expanding universes," Astrophys. J. **136**, 319–333 (1962).
7. C. Lovis, F. Pepe, F. Bouchy, G. Lo Curto, M. Mayor, L. Pasquini, D. Queloz, G. Rupprecht, S. Udry, and S. Zucker, "The exoplanet hunter HARPS: unequalled accuracy and perspectives toward 1 cm s −1 precision," Proc. SPIE **6269**, 62690P (2006).
8. R. P. Butler, G. W. Marcy, E. Williams, C. Mccarthy, P. Dosanjh, and S. S. Vogt, "Attaining Doppler precision of 3 m s-1," Publ. Astron. Soc. Pac. **108**, 500–509 (1996).
9. D. A. Fischer, G. Anglada-Escude, P. Arriagada, R. V. Baluev, J. L. Bean, F. Bouchy, L. A. Buchhave, T. Carroll, A. Chakraborty, J. R. Crepp, R. I. Dawson, S. A. Diddams, X. Dumusque, J. D. Eastman, M. Endl, P. Figueira, E. B. Ford, D. Foreman-Mackey, P. Fournier, G. Furesz, B. Scott Gaudi, P. C. Gregory, F. Grundahl, A. P. Hatzes, G. Hebrard, E. Herrero, D. W. Hogg, A. W. Howard, J. A. Johnson, P. Jorden, C. A. Jurgenson, D. W. Latham, G. Laughlin, T. J. Loredo, C. Lovis, S. Mahadevan, T. M. McCracken, F. Pepe, M. Perez, D. F. Phillips, P. P. Plavchan, L. Prato, A. Quirrenbach, A. Reiners, P. Robertson, N. C. Santos, D. Sawyer, D. Segransan, A. Sozzetti, T. Steinmetz, A. Szentgyorgyi, S. Udry, J. A. Valenti, S. X. Wang, R. A. Wittenmyer, and J. T. Wright, "State of the field: extreme precision radial velocities," Publ. Astron. Soc. Pac. **128**(964), 66001 (2016).
10. T. Wilken, C. Lovis, A. Manescau, T. Steinmetz, L. Pasquini, G. Lo Curto, T. W. Hänsch, R. Holzwarth, T. Udem, G. Lo Curto, T. W. Hansch, R. Holzwarth, and T. Udem, "High-precision calibration of spectrographs," Mon. Not. R. Astron. Soc. Lett. **405**(1), L16–L20 (2010).
11. M. T. Murphy, T. Udem, R. Holzwarth, A. Sizmann, L. Pasquini, C. Araujo-Hauck, H. Dekker, S. D'Odorico, M. Fischer, T. W. Hänsch, and A. Manescau, "High-precision wavelength calibration of astronomical spectrographs with laser frequency combs," Mon. Not. R. Astron. Soc. **380**(2), 839–847 (2007).
12. S. T. Cundiff and J. Ye, "Colloquium: femtosecond optical frequency combs," Rev. Mod. Phys. **75**(1), 325–342 (2003).
13. R. A. McCracken, É. Depagne, R. B. Kuhn, N. Erasmus, L. A. Crause, and D. T. Reid, "Wavelength calibration of a high resolution spectrograph with a partially stabilized 15-GHz astrocomb from 550 to 890 nm," Opt.

Express **25**(6), 6450–6460 (2017).

14. M. Lezius, T. Wilken, C. Deutsch, M. Giunta, O. Mandel, A. Thaller, V. Schkolnik, M. Schiemangk, A. Dinkelaker, A. Kohfeldt, A. Wicht, M. Krutzik, A. Peters, O. Hellmig, H. Duncker, K. Sengstock, P. Windpassinger, K. Lampmann, T. Hülsing, T. W. Hänsch, and R. Holzwarth, "Space-borne frequency comb metrology," Optica **3**(12), 1381–1387 (2016).

15. T. Wilken, T. W. Hänsch, R. Holzwarth, P. Adel, and M. Mei, "Low phase noise 250 MHz repetition rate fiber fs laser for frequency comb applications," in *Conference on Lasers and Electro-Optics (CLEO)* (2007), paper CMR3.

16. I. Hartl, H. A. Mckay, R. Thapa, B. K. Thomas, L. Dong, and M. E. Fermann, "GHz Yb-femtosecond-fiber laser frequency comb," in *Conference on Lasers and Electro-Optics (CLEO)* (2009), paper CMN1.

17. H.-W. Chen, G. Chang, S. Xu, Z. Yang, and F. X. Kärtner, "3 GHz, fundamentally mode-locked, femtosecond Yb-fiber laser," Opt. Lett. **37**(17), 3522–3524 (2012).

18. C. Li, Y. Ma, X. Gao, F. Niu, T. Jiang, A. Wang, and Z. Zhang, "1 GHz repetition rate femtosecond Yb:fiber laser for direct generation of carrier-envelope offset frequency," Appl. Opt. **54**(28), 8350–8353 (2015).

19. B. Xu, H. Yasui, Y. Nakajima, Y. Ma, Z. Zhang, and K. Minoshima, "Fully stabilized 750-MHz Yb:fiber frequency comb," Opt. Express **25**(10), 11910–11918 (2017).

20. D. Chao, M. Y. Sander, G. Chang, J. L. Morse, J. A. Cox, G. S. Petrich, L. A. Kolodziejski, F. X. Kärtner, and E. P. Ippen, "Self-referenced erbium fiber laser frequencycomb at a GHz repetition rate," in *Optical Fiber Communication (OFC)* (2012), paper OW1C.2.

21. F. Lücking, A. Assion, A. Apolonski, F. Krausz, and G. Steinmeyer, "Long-term carrier-envelope-phase-stable few-cycle pulses by use of the feed-forward method," Opt. Lett. **37**(11), 2076–2078 (2012).

22. A. Martinez and S. Yamashita, "Multi-gigahertz repetition rate passively modelocked fiber lasers using carbon nanotubes," Opt. Express **19**(7), 6155–6163 (2011).

23. A. Martinez and S. Yamashita, "10 GHz fundamental mode fiber laser using a graphene saturable absorber," Appl. Phys. Lett. **101**(4), 041118 (2012).

24. J. M. Dudley and S. Coen, "Coherence properties of supercontinuum spectra generated in photonic crystal and tapered optical fibers," Opt. Lett. **27**(13), 1180–1182 (2002).

25. R. A. McCracken, K. Balskus, Z. Zhang, and D. T. Reid, "Atomically referenced 1-GHz optical parametric oscillator frequency comb," Opt. Express **23**(12), 16466–16472 (2015).

26. T. M. Fortier, A. Bartels, and S. A. Diddams, "Octave-spanning Ti:sapphire laser with a repetition rate >1 GHz for optical frequency measurements and comparisons," Opt. Lett. **31**(7), 1011–1013 (2006).

27. A. Bartels, T. Dekorsy, and H. Kurz, "Femtosecond Ti:sapphire ring laser with a 2-GHz repetition rate and its application in time-resolved spectroscopy," Opt. Lett. **24**(14), 996–998 (1999).

28. A. Bartels, R. Gebs, M. S. Kirchner, and S. A. Diddams, "Spectrally resolved optical frequency comb from a self-referenced 5 GHz femtosecond laser," Opt. Lett. **32**(17), 2553–2555 (2007).

29. A. Bartels, D. Heinecke, and S. A. Diddams, "Passively mode-locked 10 GHz femtosecond Ti:sapphire laser," Opt. Lett. **33**(16), 1905–1907 (2008).

30. A. Bartels, D. Heinecke, and S. A. Diddams, "10-GHz self-referenced optical frequency comb," Science **326**(5953), 681 (2009).

31. D. Li, U. Demirbas, J. R. Birge, G. S. Petrich, L. A. Kolodziejski, A. Sennaroglu, F. X. Kärtner, and J. G. Fujimoto, "Diode-pumped passively mode-locked GHz femtosecond Cr:LiSAF laser with kW peak power," Opt. Lett. **35**(9), 1446–1448 (2010).

32. C. G. Leburn, A. A. Lagatsky, C. T. A. Brown, and W. Sibbett, "Femtosecond Cr4+:YAG laser with a 4GHz pulse repetition rate," in *Advanced Solid-State Photonics (ASSP)* (2004), paper WE4.

33. P. Wasylczyk, P. Wnuk, and C. Radzewicz, "Passively modelocked, diode-pumped Yb:KYW femtosecond oscillator with 1 GHz repetition rate," Opt. Express **17**(7), 5630–5635 (2009).

34. T. C. Schratwieser, C. G. Leburn, and D. T. Reid, "Highly efficient 1 GHz repetition-frequency femtosecond Yb3+:KY(WO4)2 laser," Opt. Lett. **37**(6), 1133–1135 (2012).

35. S. Yamazoe, M. Katou, T. Adachi, and T. Kasamatsu, "Palm-top-size, 1.5 kW peak-power, and femtosecond (160 fs) diode-pumped mode-locked Yb+3:KY(WO4)2 solid-state laser with a semiconductor saturable absorber mirror," Opt. Lett. **35**(5), 748–750 (2010).

36. M. Endo, A. Ozawa, and Y. Kobayashi, "Kerr-lens mode-locked Yb:KYW laser at 4.6-GHz repetition rate," Opt. Express **20**(11), 12191–12197 (2012).

37. M. Endo, A. Ozawa, and Y. Kobayashi, "6-GHz, Kerr-lens mode-locked Yb:Lu2O3 ceramic laser for comb-resolved broadband spectroscopy," Opt. Lett. **38**(21), 4502–4505 (2013).

38. M. Endo, I. Ito, and Y. Kobayashi, "Direct 15-GHz mode-spacing optical frequency comb with a Kerr-lens mode-locked Yb:Y2O3 ceramic laser," Opt. Express **23**(2), 1276–1282 (2015).

39. S. Pekarek, C. Fiebig, M. C. Stumpf, A. E. Oehler, K. Paschke, G. Erbert, T. Südmeyer, and U. Keller, "Diode-pumped gigahertz femtosecond Yb:KGW laser with a peak power of 3.9 kW," Opt. Express **18**(16), 16320–16326 (2010).

40. S. Pekarek, T. Südmeyer, S. Lecomte, S. Kundermann, J. M. Dudley, and U. Keller, "Self-referenceable frequency comb from a gigahertz diode-pumped solid-state laser," Opt. Express **19**(17), 16491–16497 (2011).

41. A. Klenner, M. Golling, and U. Keller, "A gigahertz multimode-diode-pumped Yb:KGW enables a strong frequency comb offset beat signal," Opt. Express **21**(8), 10351–10357 (2013).

42. N. Bucalovic, V. Dolgovskiy, M. C. Stumpf, C. Schori, G. Di Domenico, U. Keller, S. Schilt, and T. Südmeyer,

"Effect of the carrier-envelope-offset dynamics on the stabilization of a diode-pumped solid-state frequency comb," Opt. Lett. **37**(21), 4428–4430 (2012).

43. S. Pekarek, A. Klenner, T. Südmeyer, C. Fiebig, K. Paschke, G. Erbert, and U. Keller, "Femtosecond diode-pumped solid-state laser with a repetition rate of 4.8 GHz," Opt. Express **20**(4), 4248–4253 (2012).

44. A. Klenner, M. Golling, and U. Keller, "High peak power gigahertz Yb:CALGO laser," Opt. Express **22**(10), 11884–11891 (2014).

45. A. Klenner, S. Schilt, T. Südmeyer, and U. Keller, "Gigahertz frequency comb from a diode-pumped solid-state laser," Opt. Express **22**(25), 31008–31019 (2014).

46. A. Klenner and U. Keller, "All-optical Q-switching limiter for high-power gigahertz modelocked diode-pumped solid-state lasers," Opt. Express **23**(7), 8532–8544 (2015).

47. A. S. Mayer, C. R. Phillips, and U. Keller, "10-GHz straight-cavity SESAM-modelocked Yb:CALGO laser operating in the normal dispersion regime," in *Conference on Lasers and Electro-Optics (CLEO)* (2017), paper SM1I.2.

48. L. Krainer, R. Paschotta, S. Lecomte, M. Moser, K. J. Weingarten, and U. Keller, "Compact Nd:YVO4 lasers with pulse repetition rates up to 160 GHz," IEEE J. Quantum Electron. **38**(10), 1331–1338 (2002).

49. A. E. H. Oehler, M. C. Stumpf, S. Pekarek, T. Südmeyer, K. J. Weingarten, and U. Keller, "Picosecond diode-pumped 1.5 μm Er,Yb:glass lasers operating at 10–100 GHz repetition rate," Appl. Phys. B **99**(1-2), 53–62 (2010).

50. C. A. Zaugg, A. Klenner, M. Mangold, A. S. Mayer, S. M. Link, F. Emaury, M. Golling, E. Gini, C. J. Saraceno, B. W. Tilma, and U. Keller, "Gigahertz self-referenceable frequency comb from a semiconductor disk laser," Opt. Express **22**(13), 16445–16455 (2014).

51. A. Ishizawa, T. Nishikawa, A. Mizutori, H. Takara, A. Takada, T. Sogawa, and M. Koga, "Phase-noise characteristics of a 25-GHz-spaced optical frequency comb based on a phase- and intensity-modulated laser," Opt. Express **21**(24), 29186–29194 (2013).

52. K. Beha, D. C. Cole, P. Del'Haye, A. Coillet, S. A. Diddams, and S. B. Papp, "Self-referencing a continuous-wave laser with electro-optic modulation," arXiv:1507.06344v1 (2015).

53. T. J. Kippenberg, R. Holzwarth, and S. A. Diddams, "Microresonator-based optical frequency combs," Science **332**(6029), 555–559 (2011).

54. P. Del'Haye, A. Coillet, T. Fortier, K. Beha, D. C. Cole, K. Y. Yang, H. Lee, K. J. Vahala, S. B. Papp, and S. A. Diddams, "Phase-coherent microwave-to-optical link with a self-referenced microcomb," Nat. Photonics **10**(8), 516–520 (2016).

55. A. S. Mayer, A. Klenner, A. R. Johnson, K. Luke, M. R. E. Lamont, Y. Okawachi, M. Lipson, A. L. Gaeta, and U. Keller, "Frequency comb offset detection using supercontinuum generation in silicon nitride waveguides," Opt. Express **23**(12), 15440–15451 (2015).

56. T. Sizer, "Increase in laser repetition rate by spectral selection," IEEE J. Quantum Electron. **25**(1), 97–103 (1989).

57. D. A. Braje, M. S. Kirchner, S. Osterman, T. Fortier, and S. A. Diddams, "Astronomical spectrograph calibration with broad-spectrum frequency combs," Eur. Phys. J. D **48**(1), 57–66 (2008).

58. G. G. Ycas, F. Quinlan, S. A. Diddams, S. Osterman, S. Mahadevan, S. Redman, R. Terrien, L. Ramsey, C. F. Bender, B. Botzer, and S. Sigurdsson, "Demonstration of on-sky calibration of astronomical spectra using a 25 GHz near-IR laser frequency comb," Opt. Express **20**(6), 6631–6643 (2012).

59. T. Steinmetz, T. Wilken, C. Araujo-Hauck, R. Holzwarth, T. W. Hänsch, and T. Udem, "Fabry–Pérot filter cavities for wide-spaced frequency combs with large spectral bandwidth," Appl. Phys. B **96**(2-3), 251–256 (2009).

60. F. X. Kärtner, U. Morgner, R. Ell, T. Schibli, J. G. Fujimoto, E. P. Ippen, V. Scheuer, G. Angelow, and T. Tschudi, "Ultrabroadband double-chirped mirror pairs for generation of octave spectra," J. Opt. Soc. Am. B **18**(6), 882–885 (2001).

61. L.-J. Chen, G. Chang, C.-H. Li, A. J. Benedick, D. F. Philips, R. L. Walsworth, and F. X. Kärtner, "Broadband dispersion-free optical cavities based on zero group delay dispersion mirror sets," Opt. Express **18**(22), 23204–23211 (2010).

62. C.-H. Li, G. Chang, A. G. Glenday, N. Langellier, A. Zibrov, D. F. Phillips, F. X. Kärtner, A. Szentgyorgyi, and R. L. Walsworth, "Conjugate Fabry-Perot cavity pair for improved astro-comb accuracy," Opt. Lett. **37**(15), 3090–3092 (2012).

63. C.-H. Li, A. G. Glenday, A. J. Benedick, G. Chang, L.-J. Chen, C. Cramer, P. Fendel, G. Furesz, F. X. Kärtner, S. Korzennik, D. F. Phillips, D. Sasselov, A. Szentgyorgyi, and R. L. Walsworth, "In-situ determination of astro-comb calibrator lines to better than 10 cm s-1," Opt. Express **18**(12), 13239–13249 (2010).

64. A. G. Glenday, C.-H. Li, N. Langellier, G. Chang, L.-J. Chen, G. Furesz, A. A. Zibrov, F. Kärtner, D. F. Phillips, D. Sasselov, A. Szentgyorgyi, and R. L. Walsworth, "Operation of a broadband visible-wavelength astro-comb with a high-resolution astrophysical spectrograph," Optica **2**(3), S1–S6 (2015).

65. J. M. Dudley, G. Genty, and S. Coen, "Supercontinuum generation in photonic crystal fiber," Rev. Mod. Phys. **78**(4), 1135–1184 (2006).

66. T. A. Birks, W. J. Wadsworth, and P. S. J. Russell, "Supercontinuum generation in tapered fibers," Opt. Lett. **25**(19), 1415–1417 (2000).

67. D. T. Reid, "Engineered quasi-phase-matching for second-harmonic generation," J. Opt. A, Pure Appl. Opt. **5**(4), S97–S102 (2003).

68. A. Gambetta, R. Ramponi, and M. Marangoni, "Mid-infrared optical combs from a compact amplified Er-doped fiber oscillator," Opt. Lett. **33**(22), 2671–2673 (2008).
69. T. I. Ferreiro, J. Sun, and D. T. Reid, "Frequency stability of a femtosecond optical parametric oscillator frequency comb," Opt. Express **19**(24), 24159–24164 (2011).
70. Y. Kobayashi, K. Torizuka, A. Marandi, R. L. Byer, R. A. McCracken, Z. Zhang, and D. T. Reid, "Femtosecond optical parametric oscillator frequency combs," J. Opt. **17**(9), 94010 (2015).
71. S. T. Wong, T. Plettner, K. L. Vodopyanov, K. Urbanek, M. Digonnet, and R. L. Byer, "Self-phase-locked degenerate femtosecond optical parametric oscillator," Opt. Lett. **33**(16), 1896–1898 (2008).
72. J. M. Charsley, R. A. McCracken, D. T. Reid, G. Kowzan, P. Masłowski, A. Reiners, and P. Huke, "Comparison of astrophysical laser frequency combs with respect to the requirements of HIRES," in *Proc. SPIE, Optical Measurement Systems for Industrial Inspection X* (2017), pp. 10329–10333.
73. G. Chang, C.-H. Li, D. F. Phillips, A. Szentgyorgyi, R. L. Walsworth, and F. X. Kärtner, "Optimization of filtering schemes for broadband astro-combs," Opt. Express **20**(22), 24987–25013 (2012).
74. G. Chang, C.-H. Li, D. F. Phillips, R. L. Walsworth, and F. X. Kärtner, "Toward a broadband astro-comb: effects of nonlinear spectral broadening in optical fibers," Opt. Express **18**(12), 12736–12747 (2010).
75. R. A. Probst, T. Steinmetz, T. Wilken, H. Hundertmark, S. P. Stark, G. K. L. Wong, P. S. J. Russell, T. W. Hänsch, R. Holzwarth, and T. Udem, "Nonlinear amplification of side-modes in frequency combs," Opt. Express **21**(10), 11670–11687 (2013).
76. A. M. Weiner, "Ultrafast optical pulse shaping: A tutorial review," Opt. Commun. **284**(15), 3669–3692 (2011).
77. R. A. Probst, Y. Wu, T. Steinmetz, S. P. Stark, T. W. Hänsch, T. Udem, and R. Holzwarth, "Spectrally flattened, broadband astronomical frequency combs," in *Conference on Lasers and Electro-Optics (CLEO)* (2015), paper SW4G.7.
78. R. A. Probst, G. Lo Curto, G. Avila, B. L. Canto Martins, J. Renan De Medeiros, M. Esposito, J. I. González Hernández, T. W. Hänsch, R. Holzwarth, F. Kerber, I. C. Leão, A. Manescau, L. Pasquini, R. Rebolo-López, T. Steinmetz, T. Udem, and Y. Wu, "A laser frequency comb featuring sub-cm/s precision for routine operation on HARPS," Proc. SPIE **9147**, 91471C (2014).
79. R. A. Probst, G. Lo Curto, G. Avila, A. Brucalassi, B. L. Canto Martins, I. de Castro Leão, M. Esposito, J. I. González Hernández, F. Grupp, T. W. Hänsch, R. Holzwarth, H. Kellermann, F. Kerber, O. Mandel, A. Manescau, L. Pasquini, E. Pozna, R. Rebolo, J. Renan De Medeiros, S. P. Stark, T. Steinmetz, A. Suárez Mascareño, T. Udem, J. Urrutia, and Y. Wu, "Relative stability of two laser frequency combs for routine operation on HARPS and FOCES," Proc. SPIE **9908**, 990864 (2016).
80. J. Ye and S. T. Cundiff, *Femtosecond Optical Frequency Comb: Principle, Operation, and Applications* (Springer Science, 2005).
81. K. Saleh, J. Millo, A. Didier, Y. Kersalé, and C. Lacroûte, "Frequency stability of a wavelength meter and applications to laser frequency stabilization," Appl. Opt. **54**(32), 9446–9449 (2015).
82. S. A. Diddams, D. J. Jones, J. Ye, S. T. Cundiff, J. L. Hall, J. K. Ranka, R. S. Windeler, R. Holzwarth, T. Udem, and T. W. Hänsch, "Direct link between microwave and optical frequencies with a 300 THz femtosecond laser comb," Phys. Rev. Lett. **84**(22), 5102–5105 (2000).
83. A. Marconi, P. Di Marcantonio, V. D'Odorico, S. Cristiani, R. Maiolino, E. Oliva, L. Origlia, M. Riva, L. Valenziano, F. M. Zerbi, M. Abreu, V. Adibekyan, C. Allenda Prieto, P. J. Amado, W. Benz, I. Boisse, X. Bonfils, F. Bouchy, D. Buscher, A. Cabral, B. L. Canto Martins, A. Chiavassa, J. Coelho, E. Delgado, J. R. De Medeiros, I. Di Varano, P. Figueira, M. Fisher, J. P. U. Fynbo, A. C. H. Glasse, M. Haehnelt, C. Haniff, A. Hatzes, P. Huke, A. J. Korn, I. C. Leao, J. Liske, C. Lovis, I. Matute, R. A. McCracken, C. J. A. P. Martins, M. J. P. F. G. Monteiro, S. Morris, T. Morris, H. Nicklas, A. Niedzielski, N. Nunes, E. Palle, P. Parr-Burman, V. Parro, I. Parry, F. Pepe, N. Piskunov, D. Queloz, A. Quirrenbach, R. Rebolo Lopez, A. Reiners, D. T. Reid, N. Santos, W. Seifert, S. Sousa, H. C. Stempels, K. Strassmeier, X. Sun, S. Udry, M. Weber, and E. Zackrisson, "EELT-HIRES the high-resolution spectrograph for the E-ELT," Proc. SPIE **9908**, 990823 (2016).
84. H. Nasim and Y. Jamil, "Recent advancements in spectroscopy using tunable diode lasers," Laser Phys. Lett. **10**(4), 43001 (2013).
85. A. Zybin, J. Koch, H. D. Wizemann, J. Franzke, and K. Niemax, "Diode laser atomic absorption spectrometry," Spectrochim. Acta B At. Spectrosc. **60**(1), 1–11 (2005).
86. J. M. Charsley, R. A. McCracken, L. Reid, and D. T. Reid, "A broadband Fourier transform spectrometer enabling modal subset identification in Fabry-Pérot-based astrocombs," Opt. Express. submitted.
87. P. Masłowski, K. F. Lee, A. C. Johansson, A. Khodabakhsh, G. Kowzan, L. Rutkowski, A. A. Mills, C. Mohr, J. Jiang, M. E. Fermann, and A. Foltynowicz, "Surpassing the path-limited resolution of Fourier-transform spectrometry with frequency combs," Phys. Rev. A **93**, 021802 (2016).
88. L. Rutkowski, P. Masłowski, A. C. Johansson, A. Khodabakhsh, and A. Foltynowicz, "Optical frequency comb Fourier transform spectroscopy with sub-nominal resolution," arXiv:1612.04808 (2016).
89. J. Oaks, J. A. Buisson, and M. M. Largay, "A summary of the GPS constellation clock performance," in *Proceedings of the 39th Annual Precise Time and Time Interval (PTTI) Meeting* (2007).
90. J. A. King, J. K. Webb, M. T. Murphy, V. V. Flambaum, R. F. Carswell, M. B. Bainbridge, M. R. Wilczynska, and F. E. Koch, "Spatial variation in the fine-structure constant - new results from VLT/UVES," Mon. Not. R. Astron. Soc. **422**(4), 3370–3414 (2012).
91. J. Liske, A. Grazian, E. Vanzella, M. Dessauges, M. Viel, L. Pasquini, M. Haehnelt, S. Cristiani, F. Pepe, G. Avila, P. Bonifacio, F. Bouchy, H. Dekker, B. Delabre, S. D'Odorico, V. D'Odorico, S. Levshakov, C. Lovis, M.

Mayor, P. Molaro, L. Moscardini, M. T. Murphy, D. Queloz, P. Shaver, S. Udry, T. Wiklind, and S. Zucker, "Cosmic dynamics in the era of Extremely Large Telescopes," Mon. Not. R. Astron. Soc. **386**(3), 1192–1218 (2008).

92. T. Steinmetz, T. Wilken, C. Araujo-Hauck, R. Holzwarth, T. W. Hänsch, L. Pasquini, A. Manescau, S. D'Odorico, M. T. Murphy, T. Kentischer, W. Schmidt, and T. Udem, "Laser frequency combs for astronomical observations," Science **321**(5894), 1335–1337 (2008).

93. H. Doerr, T. J. Kentischer, T. Steinmetz, R. A. Probst, M. Franz, R. Holzwarth, T. Udem, T. W. Hänsch, and W. Schmidt, "Performance of a laser frequency comb calibration system with a high-resolution solar echelle spectrograph," Proc. SPIE **8450**, 84501G (2012).

94. D. F. Phillips, A. G. Glenday, C.-H. Li, C. Cramer, G. Furesz, G. Chang, A. J. Benedick, L.-J. Chen, F. X. Kärtner, S. Korzennik, D. Sasselov, A. Szentgyorgyi, and R. L. Walsworth, "Calibration of an astrophysical spectrograph below 1 m/s using a laser frequency comb," Opt. Express **20**(13), 13711–13726 (2012).

95. A. G. Glenday, C.-H. Li, N. Langellier, G. Chang, L.-J. Chen, G. Furesz, A. A. Zibrov, F. Kärtner, D. F. Phillips, D. Sasselov, A. Szentgyorgyi, and R. L. Walsworth, "Operation of a broadband visible-wavelength astro-comb with a high-resolution astrophysical spectrograph," Optica **2**(3), 250–254 (2015).

96. X. Yi, K. Vahala, J. Li, S. Diddams, G. Ycas, P. Plavchan, S. Leifer, J. Sandhu, G. Vasisht, P. Chen, P. Gao, J. Gagne, E. Furlan, M. Bottom, E. C. Martin, M. P. Fitzgerald, G. Doppmann, and C. Beichman, "Demonstration of a near-IR line-referenced electro-optical laser frequency comb for precision radial velocity measurements in astronomy," Nat. Commun. **7**, 10436 (2016).

97. S. D. Lord, "A new software tool for computing Earth's atmospheric transmission of near- and far-infrared radiation," NASA Tech. Memo. 103957 (1992).

98. A. Quirrenbach, P. J. Amado, J. A. Caballero, R. Mundt, A. Reiners, I. Ribas, W. Seifert, M. Abril, J. Aceituno, F. J. Alonso-Floriano, M. Ammler-von Eiff, R. Antona Jiménez, H. Anwand-Heerwart, M. Azzaro, F. Bauer, D. Barrado, S. Becerril, V. J. S. Béjar, D. Benítez, Z. M. Berdiñas, M. C. Cárdenas, E. Casal, A. Claret, J. Colomé, M. Cortés-Contreras, S. Czesla, M. Doellinger, S. Dreizler, C. Feiz, M. Fernández, D. Galadi, M. C. Gálvez-Ortiz, A. García-Piquer, M. L. García-Vargas, R. Garrido, L. Gesa, V. Gómez Galera, E. González-Álvarez, J. I. González Hernández, U. Grözinger, J. Guàrdia, E. W. Guenther, E. de Guindos, J. Gutiérrez-Soto, H.-J. Hagen, A. P. Hatzes, P. H. Hauschildt, J. Helming, T. Henning, D. Hermann, L. Hernández Castaño, E. Herrero, D. Hidalgo, O. Holgado, A. Huber, K. F. Huber, S. Jeffers, V. Joergens, E. de Juan, M. Kehr, R. Klein, M. Kürster, A. Lamert, S. Lalitha, W. Laun, U. Lemke, R. Lenzen, M. López del Fresno, B. López Martí, J. López-Santiago, U. Mall, H. Mandel, E. L. Martín, S. Martín-Ruiz, H. Martínez-Rodríguez, C. J. Marvin, R. J. Mathar, E. Mirabet, D. Montes, R. Morales Muñoz, A. Moya, V. Naranjo, A. Ofir, R. Oreiro, E. Pallé, J. Panduro, V.-M. Passegger, A. Pérez-Calpena, D. Pérez Medialdea, M. Perger, M. Pluto, A. Ramón, R. Rebolo, P. Redondo, S. Reffert, S. Reinhardt, P. Rhode, H.-W. Rix, F. Rodler, E. Rodríguez, C. Rodríguez-López, E. Rodríguez-Pérez, R.-R. Rohloff, A. Rosich, E. Sánchez-Blanco, M. A. Sánchez Carrasco, J. Sanz-Forcada, L. F. Sarmiento, S. Schäfer, J. Schiller, C. Schmidt, J. H. M. M. Schmitt, E. Solano, O. Stahl, C. Storz, J. Stürmer, J. C. Suárez, R.-G. Ulbrich, G. Veredas, K. Wagner, J. Winkler, M. R. Zapatero Osorio, M. Zechmeister, F. J. Abellán de Paco, G. Anglada-Escudé, C. del Burgo, A. Klutsch, J. L. Lizon, M. López-Morales, J. C. Morales, M. A. C. Perryman, S. M. Tulloch, and W. Xu, "CARMENES instrument overview," Proc. SPIE **9147**, 91471F (2014).

99. U. Conod, N. Blind, F. Wildi, and F. Pepe, "Adaptive optics for high resolution spectroscopy: A direct application with the future NIRPS spectrograph," Proc. SPIE **9909**, 990941 (2016).

100. S. P. Stark, T. Steinmetz, R. A. Probst, H. Hundertmark, T. Wilken, T. W. Hänsch, T. Udem, P. S. J. Russell, and R. Holzwarth, "14 GHz visible supercontinuum generation: calibration sources for astronomical spectrographs," Opt. Express **19**(17), 15690–15695 (2011).

101. T. Wilken, G. L. Curto, R. A. Probst, T. Steinmetz, A. Manescau, L. Pasquini, J. I. González Hernández, R. Rebolo, T. W. Hänsch, T. Udem, and R. Holzwarth, "A spectrograph for exoplanet observations calibrated at the centimetre-per-second level," Nature **485**(7400), 611–614 (2012).

102. P. Molaro, M. Esposito, S. Monai, G. Lo Curto, J. I. González Hernández, T. W. Hänsch, R. Holzwarth, A. Manescau, L. Pasquini, R. A. Probst, R. Rebolo, T. Steinmetz, T. Udem, and T. Wilken, "A frequency comb calibrated solar atlas," Astron. Astrophys. **560**, A61 (2013).

103. H.-P. Doerr, T. Steinmetz, R. Holzwarth, T. Kentischer, and W. Schmidt, "A laser frequency comb system for absolute calibration of the VTT echelle spectrograph," Adv. Eur. Sol. Phys. **280**(2), 663–670 (2012).

104. A. Brucalassi, F. Grupp, H. Kellerm, L. Wang, F. Lang-Bardl, N. Baisert, S. M. Hu, U. Hopp, and R. Bender, "Stability of the FOCES spectrograph using an astro-frequency comb as calibrator," Proc. SPIE **9908**, 99085W (2016).

105. H. Ye, J. Han, Y. Wu, and D. Xiao, "The fiber noise suppression of astro-comb fiber link system for Chinese 2.16m telescope," Proc. SPIE **9908**, 99087E (2016).

106. F. Quinlan, G. Ycas, S. Osterman, and S. A. Diddams, "A 12.5 GHz-spaced optical frequency comb spanning >400 nm for near-infrared astronomical spectrograph calibration," Rev. Sci. Instrum. **81**(6), 063105 (2010).

107. D. C. Hackett, G. Ycas, and S. Diddams, "A low-dispersion Fabry-Perot cavity for generation of a 30 GHz astrocomb spanning 140 nm," in *Conference on Lasers and Electro-Optics (CLEO)* (2015), paper SW4G.8.

108. L. Hou, H.-N. Han, W. Wang, L. Zhang, L.-H. Pang, D.-H. Li, and Z.-Y. Wei, "A 23.75-GHz frequency comb with two low-finesse filtering cavities in series for high resolution spectroscopy," Chin. Phys. B **24**(2), 024213 (2015).

109. G. Schettino, E. Oliva, M. Inguscio, C. Baffa, E. Giani, A. Tozzi, and P. Cancio Pastor, "Optical frequency comb

as a general-purpose and wide-band calibration source for astronomical high resolution infrared spectrographs," Exp. Astron. **31**(1), 69–81 (2011).

110. M. T. Murphy, C. R. Locke, P. S. Light, A. N. Luiten, and J. S. Lawrence, "Laser frequency comb techniques for precise astronomical spectroscopy," Mon. Not. R. Astron. Soc. **422**(1), 761–771 (2012).

111. Y. Ma, L. Zuo, F. Meng, C. Li, T. Jiang, A. Wang, F. Zhao, G. Zhao, and Z. Zhang, "A compact 30 GHz spaced astro-comb based on 1 GHz Yb:fiber laser," in *Conference on Lasers and Electro-Optics (CLEO)* (2016), paper JTh2A.137.

112. C.-H. Li, A. J. Benedick, P. Fendel, A. G. Glenday, F. X. Kärtner, D. F. Phillips, D. Sasselov, A. Szentgyorgyi, and R. L. Walsworth, "A laser frequency comb that enables radial velocity measurements with a precision of 1 cm s(-1)," Nature **452**(7187), 610–612 (2008).

113. A. Benedick, J. Birge, R. Ell, O. D. Mücke, M. Sander, and F. X. Kärtner, "Octave spanning 1GHz Ti:sapphire oscillator for HeNe CH4-based frequency combs and clocks," in *Conference on Lasers and Electro-Optics Europe (E-CLEO)* (2007), paper CF3.

114. A. J. Benedick, G. Chang, J. R. Birge, L.-J. Chen, A. G. Glenday, C.-H. Li, D. F. Phillips, A. Szentgyorgyi, S. Korzennik, G. Furesz, R. L. Walsworth, and F. X. Kärtner, "Visible wavelength astro-comb," Opt. Express **18**(18), 19175–19184 (2010).

115. D. F. Phillips, A. Glenday, C.-H. Li, G. Furesz, A. J. Benedick, G. N. Chang, L.-J. Chen, S. Korzennik, D. Sasselov, F. X. Kaertner, A. Szentgyorgyi, and R. L. Walsworth, "Calibration of an echelle spectrograph with an astro-comb: a laser frequency comb with very high repetition rate," Proc. SPIE **8446**, 84468O (2012).

116. N. Langellier, C.-H. Li, A. G. Glenday, G. Chang, H.-W. Chen, J. Lim, G. Furesz, F. Kärtner, D. F. Phillips, D. Sasselov, A. Szentgyorgyi, and R. Walsworth, "Green astro-comb for HARPS-N," Proc. SPIE **9147**, 91478N (2014).

117. G. Chang, L.-J. Chen, and F. X. Kärtner, "Fiber-optic Cherenkov radiation in the few-cycle regime," Opt. Express **19**(7), 6635–6647 (2011).

118. X. Dumusque, A. Glenday, D. F. Phillips, N. Buchschacher, A. C. Cameron, M. Cecconi, D. Charbonneau, R. Cosentino, A. Ghedina, D. W. Latham, C.-H. Li, M. Lodi, C. Lovis, E. Molinari, F. Pepe, S. Udry, D. Sasselov, A. Szentgyorgyi, and R. Walsworth, "Harps-N observes the Sun as a star," Astrophys. J. **814**(2), L21 (2015).

119. D. F. Phillips, A. G. Glenday, X. Dumusque, N. Buchschacher, A. C. Cameron, M. Cecconi, D. Charbonneau, R. Cosentino, A. Ghedina, R. Haywood, D. W. Latham, C.-H. Li, M. Lodi, C. Lovis, E. Molinari, F. Pepe, D. Sasselov, A. Szentgyorgyi, S. Udry, and R. L. Walsworth, "An astro-comb calibrated solar telescope to search for the radial velocity signature of Venus," Proc. SPIE **9912**, 99126Z (2016).

120. K. Kashiwagi, T. Kurokawa, Y. Okuyama, T. Mori, Y. Tanaka, Y. Yamamoto, and M. Hirano, "Direct generation of 12.5-GHz-spaced optical frequency comb with ultrabroad coverage in near-infrared region by cascaded fiber configuration," Opt. Express **24**(8), 8120–8131 (2016).

121. J. M. Chavez Boggio, A. A. Rieznik, M. Zajnulina, M. Böhm, D. Bodenmüller, M. Wysmolek, H. Sayinc, J. Neumann, D. Kracht, R. Haynes, and M. M. Roth, "Generation of an astronomical optical frequency comb in three fibre-based nonlinear stages," Proc. SPIE **8434**, 84340Y (2012).

122. J. M. Chavez Boggio, T. Fremberg, B. Moralejo, M. Rutowska, E. Hernandez, M. Zajnulina, A. Kelz, D. Bodenmüller, C. Sandin, M. Wysmolek, H. Sayinc, J. Neumann, R. Haynes, and M. M. Roth, "Astronomical optical frequency comb generation and test in a fiber-fed MUSE spectrograph," Proc. SPIE **9151**, 915120 (2014).

123. F. Wildi, B. Chazelas, and F. Pepe, "A passive, cost effective solution for the high accuracy wavelength calibration of radial velocity spectrographs," Proc. SPIE **8446**, 84468E (2012).

124. C. Schwab, J. Stürmer, Y. V. Gurevich, T. Führer, S. K. Lamoreaux, T. Walther, and A. Quirrenbach, "Stabilizing a Fabry-Perot etalon peak to 3 cm s-1 for spectrograph calibration," Publ. Astron. Soc. Pac. **127**(955), 880–889 (2015).

125. A. Reiners, R. K. Banyal, and R. G. Ulbrich, "A laser-lock concept to reach cm s−1-precision in Doppler experiments with Fabry-Pérot wavelength calibrators," Astron. Astrophys. **569**, A77 (2014).

126. F. F. Bauer, M. Zechmeister, and A. Reiners, "Calibrating echelle spectrographs with Fabry-Pérot etalons," Astron. Astrophys. **581**, A117 (2015).

127. F. Bouchy, F. Pepe, and D. Queloz, "Fundamental photon noise limit to radial velocity measurements," Astron. Astrophys. **374**(2), 733–739 (2001).

128. J. Baudrand and G. A. H. Walker, "Modal noise in high-resolution, fiber-fed spectra: a study and simple cure," Publ. Astron. Soc. Pac. **113**(785), 851–858 (2001).

129. X. Dumusque, S. Udry, C. Lovis, N. C. Santos, and M. J. P. F. G. Monteiro, "Planetary detection limits taking into account stellar noise I. Observational strategies to reduce stellar oscillation and granulation effects," Astron. Astrophys. **525**, A140 (2011).

130. G. Marra, H. S. Margolis, and D. J. Richardson, "Dissemination of an optical frequency comb over fiber with 3 × 10^-18 fractional accuracy," Opt. Express **20**(2), 1775–1782 (2012).

131. D. C. Heinecke, A. Bartels, T. M. Fortier, D. A. Braje, L. Hollberg, and S. A. Diddams, "Optical frequency stabilization of a 10 GHz Ti:sapphire frequency comb by saturated absorption spectroscopy in ^{87}rubidium," Phys. Rev. A **80**(5), 0538061 (2009).

132. J. Jennings, S. Halverson, R. Terrien, S. Mahadevan, G. Ycas, and S. A. Diddams, "Frequency stability characterization of a broadband fiber Fabry-Pérot interferometer," Opt. Express. submitted.

133. R. A. Probst, T. Steinmetz, T. Wilken, G. K. L. Wong, H. Hundertmark, S. P. Stark, P. S. J. Russell, T. W.

Hänsch, R. Holzwarth, and T. Udem, "Spectral flattening of supercontinua with a spatial light modulator," Proc. SPIE **8864**, 88641Z (2013).

134. M. Endo, T. Sukegawa, A. Silva, and Y. Kobayashi, "Development of compact and ultra-high-resolution spectrograph with multi-GHz optical frequency comb," Proc. SPIE **9147**, 91477Y (2014).

135. R. A. Probst, T. Steinmetz, Y. Wu, F. Grupp, T. Udem, and R. Holzwarth, "A compact echelle spectrograph for characterization of astro-combs," Appl. Phys. B **123**(3), 76 (2017).

1. Introduction

High resolution spectroscopy underpins most fields of astrophysics and has enabled major progress in multiple areas, such as the initial discovery of a planet orbiting a solar-type star [1] which led to the characterization of an exoplanet atmosphere [2], the study of metal-poor stars [3], as well as the chemical evolution of the Galactic bulge [4]. With suitably well-calibrated instruments, astronomical spectroscopy will explore some of the most fundamental concepts in physics and cosmology, including the search for dark energy and observing the expansion of the universe in real time [5].

A new generation of precision spectrographs (such as CARMENES, ESPRESSO and HIRES) is needed for experiments planned for the European Extremely Large Telescope (E-ELT), Very Large Telescope (VLT) and other projects. These experiments need to detect a radial velocity Doppler shift with a precision as high as 2 cm s^{-1} [6], implying the need for an extremely stable wavelength reference for spectrograph calibration. Current spectrographs are limited by the irregular line spacings, drifts and aging of the Th-Ar lamps [7] and I$_2$ cells [8] which are conventionally used, motivating the adoption of laser frequency combs as the preferred calibration sources for future instruments [9].

Frequency combs provide the precision needed by future high-resolution spectrographs in the form of a broadband, exactly-calibrated spectral 'ruler', whose accuracy is traceable to the SI second via a GPS radio-frequency reference. The uniformly-spaced, bright, and narrow features of the comb spectrum are ideal for optical frequency calibration, while the absolute traceability of the comb allows for comparisons of observations made on timescales from days to years, even at different observatories. A frequency comb can serve as both a perpetual calibrator, either solo or in tandem with a hollow cathode lamp, and as an identifier of systematic errors in the spectrograph, such as pixel mask stitching defects [10].

The potential for such 'astrocombs' to have a major impact on the astronomy community has been widely heralded [11], however multiple technical challenges stem from the conflicting requirements of providing comb-line spacings in the 5-50 GHz range across a wavelength bandwidth from 380 nm (Ca II H and K lines) to 2.4 μm (CO band at 2.3 μm), as high-peak-power pulses are typically only available at low pulse repetition frequencies.

The remainder of this article develops the core concepts underpinning astrocombs, starting from an understanding of the technical requirements of an astrocomb as a wavelength calibrator. We review the development of astrocomb systems, which can now be divided into fiber, solid-state and electro-optic comb approaches, which are each characterized by a distinct set of performance features and technological approaches. These comb configurations are explained in detail, allowing their relative performance to be critically compared. Finally, we discuss the state of the field going forward, examining the opportunities and challenges that lie ahead for the astrocomb community.

2. Astrocombs

A laser frequency comb provides a large number of narrow, equally spaced optical modes, the frequencies of which are given by $f_n = nf_{REP} + f_{CEO}$, where n is a large integer, f_{REP} is the mode spacing and f_{CEO} is an offset from a frequency grid that would pass through zero [12]. Stabilization of both f_{REP} and f_{CEO} is carried out to provide a set of comb lines whose frequencies are well known and are traceable to primary standards. In this section we detail the technical requirements of an astrocomb, such as mode spacing, spectral coverage and

frequency precision. We then describe common methods for creating astrocombs and review related technologies.

2.1 Concept

Astrocombs must fulfill a number of criteria for use as spectrograph calibrators. Aside from matching the wavelength coverage of the spectrograph itself, the comb spacing must be tailored to match the spectrograph resolving power $R = \lambda/\Delta\lambda$. Each comb tooth should be individually unresolved, yet adjacent comb modes must be resolved from one another. As a frequency comb is essentially a series of delta functions, the former requirement is easily fulfilled, and enables the comb to interrogate the instrument response. The latter requirement provides a series of frequency markers on the spectrograph CCD, with the frequency spacing selected to optimize the number of lines per resolution element [11]. With accurate centroiding of the comb lines on the CCD, a precise wavelength solution for the spectrograph can be constructed.

The two primary challenges facing practical astrocomb development are (i) achieving the required spectral coverage and (ii) matching the comb mode spacing to the spectrograph resolving power. Coverage can be addressed by combining the choice of laser gain medium with spectral broadening in suitable fiber or other well-established nonlinear techniques. The resolving power of a high-resolution spectrograph is typically >10,000, with corresponding optimal mode spacing >10 GHz, with the exact choice being wavelength dependent. This repetition frequency is not readily obtainable from typical femtosecond laser systems, and the most widely-adopted solution has been to optically filter the modes of a lower repetition frequency laser ($f_{REP} \leq 1$ GHz) in a Fabry-Pérot etalon, as discussed in §2.3.1 and shown in Fig. 1.

Figure 2 illustrates six system architectures (A-F) that have been employed in astrocombs. The simplest architecture (A) is to directly filter the output of the source comb to achieve the required mode spacing. This approach is intrinsically narrowband, restricting the range over which a spectrograph can be calibrated. Two simple extensions of this approach are to frequency double (B) or spectrally broaden (C) the laser output before filtering to extend the astrocomb coverage. Architectures (D) and (E) are commonly employed by fiber-based astrocombs, where low power, low-repetition-rate oscillators require significant filtering to remove unwanted modes, as well as amplification to achieve sufficient peak power for nonlinear frequency conversion processes. The approach illustrated in (F) is used in electro-optically modulated combs and is described in §2.2.3.

2.2 Astrocomb laser technologies

The photonics community has driven the majority of astrocomb development, and as a result a number of competing approaches have been advanced in parallel, separated by their different choices of laser technology. Below we discuss progress in the development of high repetition rate fiber and solid-state lasers, limiting the scope to systems that can be stabilized into frequency combs. We also describe alternative laser comb technologies such as electro-optically modulated CW lasers and microresonators.
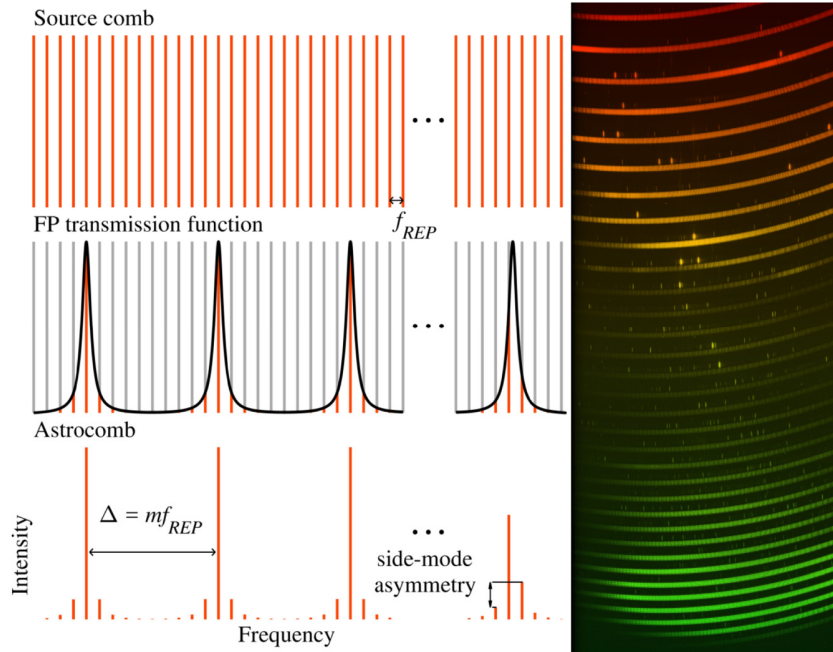
Fig. 1. Left: the dense modes of a low-repetition-rate frequency comb can be filtered in a Fabry-Pérot etalon to provide a wider mode spacing. If the group delay dispersion of the etalon is not zero then unwanted modes can be insufficiently or asymmetrically suppressed (exaggerated for effect). Right: a false-color CCD image of the 15-GHz astrocomb deployed at the Southern African Large Telesecope [13].
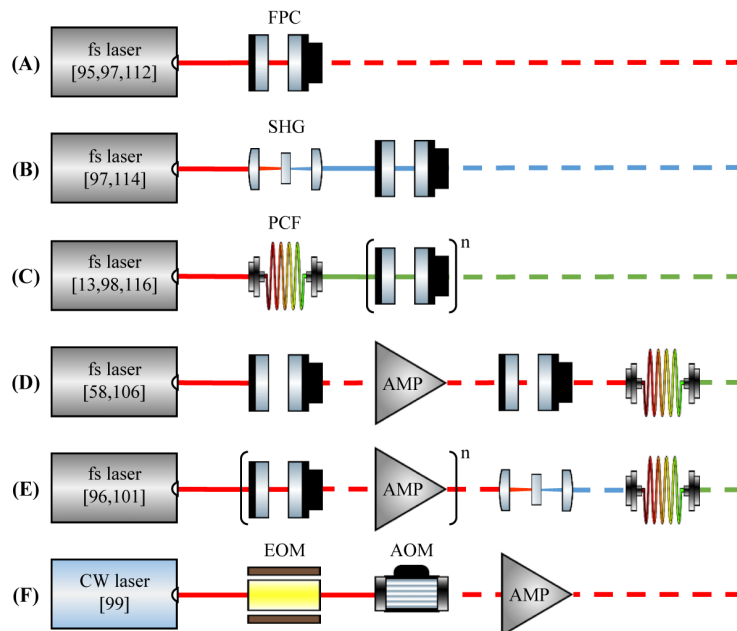
Fig. 2. Illustration of different astrocomb architectures. FPC, Fabry-Pérot cavity; SHG, second harmonic generation; PCF, photonic crystal fiber; AMP, amplifier; EOM; electro-optic modulator; AOM, acousto-optic modulator. See text in §2.1 for further details.

2.2.1 Fiber combs

Fiber laser frequency combs have proven to be compact and robust [14], with hands-free operation and little warm-up time. Erbium and ytterbium fiber lasers typically produce ~100 mW of average power which can be readily amplified to upwards of 10 W, with sub-ps compressed pulse durations. While the long-term stability and turnkey operation offered by fiber combs is highly desirable for telescope support staff or operators of non-robotic telescopes (who have little or no laser training), these systems still face significant technical challenges when used as the source laser for an astrocomb. The relatively narrow native spectral coverage of fiber systems requires broadening or wavelength shifting in order to match the operating region of many spectrographs. Commercially available fiber laser repetition rates are often limited to 250 MHz [15], particularly in all-fiber designs, and so the comb modes must be significantly filtered to achieve the >10 GHz mode spacing for spectrograph calibration. Both of these processes require amplification, however this can introduce unwanted side-effects such as third-order dispersion or sideband amplification due to four-wave mixing, and can also lead to component damage, particularly in the amplifier pump diodes and fibers.

Wider mode spacing fiber lasers have been developed using a variety of novel techniques. A 1.04-GHz Yb:fiber laser with a high doping level (up to 6 wt. %) produced 100 mW average power that was amplified in cladding-pumped fiber and compressed in order to produce an octave-spanning supercontinuum in suspended core fiber. This marked the first demonstration of a GHz fiber comb without mode filtering [16], however repetition rate scaling was limited by the use of bulky free-space dispersion compensation and the length of the gain fiber. A solution was found by employing a Yb-doped phosphate glass fiber with 15.2 wt. % for increased gain along with a dispersion compensating output coupler, producing 200 fs pulses at 3 GHz repetition rate [17]. Shorter pulses were achieved at 1 GHz using nonlinear-polarization-rotation mode-locking, which also provided higher output power for octave-spanning supercontinuum generation without prior amplification [18]. Recently a fully-stabilized 750-MHz Yb:fiber comb was reported which achieved f-to-$2f$ self-referencing without external amplification [19].

By using a saturable-absorber-mode-locked Er:fiber laser GHz repetition rates have also been also been demonstrated [20], with comb stabilization carried out using highly-nonlinear fiber (HNLF) for supercontinuum generation and an acousto-optic frequency shifter for f_{CEO} stabilization using the feed-forward technique [21]. An alternative approach uses the passive mode-locking of all-fiber Fabry-Pérot lasers by graphene or carbon-nanotube saturable absorbers to achieve multi-GHz repetition rates. These lasers use short lengths of Er:Yb phosphosilicate fiber, enabling compact footprints with low losses at the expense of increased pulse durations [22,23].

2.2.2 Solid-state combs

While fiber laser combs are compact and stable, solid-state systems offer shorter pulses and higher average powers directly from the oscillator, removing the need for external amplification stages. Moreover, GHz-repetition-rate Ti:sapphire lasers are now commercially available. Such higher repetition rates reduce the demands of the Fabry-Pérot filtering stages while still supplying sufficient pulse energies for coherent spectral broadening [24] or other nonlinear techniques [25]. Technical challenges facing these systems in an astrocomb include less-developed automation, noise factors associated with the free-space architecture, and long-term performance drift due to unwanted contaminants.

Ti:sapphire lasers exploit their large gain bandwidth and employ Kerr-lens mode-locking to routinely provide sub-40-fs pulses at GHz repetition rates. An octave-spanning 1-GHz Ti:sapphire laser enabled comb stabilization without additional spectral broadening [26], while 2-GHz and 5-GHz ring cavities have employed photonic crystal fiber (PCF) to achieve the same coverage [27,28]. The highest repetition rate reported so far has been 10 GHz [29],

and self-referencing was achieved with only 120 pJ pulse energy by coupling 560 mW of average power through a 2-m-long micro-structured fiber with a 1.5-μm core and zero-dispersion wavelength near 590 nm [30]. Diode-pumped Cr-doped lasers can operate at Ti:sapphire and Er:fiber wavelengths, providing femtosecond pulses at high repetition rates. A 1-GHz Cr:LiSAF laser producing 55-fs pulses at 863 nm was reported [31], which could potentially be broadened in standard PCF. A three-element Cr^{4+}:YAG laser with a 4-GHz repetition rate was developed for terabit communications, producing 82-fs pulses at 1525 nm [32].

Yb-doped gain media can be pumped by affordable and highly efficient laser diodes and can be subsequently amplified in Yb:fiber, making them excellent candidates for compact comb systems. The first passively mode-locked high repetition rate Yb:KYW laser was a 4-mirror ring cavity producing 1-GHz pulses [33]. A more compact and efficient design employed a semiconductor saturable absorber mirror (SESAM) for mode-locking [34], which also enabled the repetition rate to be extended to 2.8 GHz [35]. Recent efforts have exploited the high thermal conductivity and nonlinear refractive index of Yb:KYW to demonstrate a 4.6-GHz Kerr-lens mode-locked laser [36], which provides a broader spectrum and shorter pulses than SESAM mode-locking. Yb:ceramic lasers possess similar properties, and have been used to demonstrate repetition rates up to 15-GHz [37,38].

SESAM mode-locked Yb:KGW lasers have been developed extensively since 2010, when a 1-GHz laser producing 281-fs pulses with 1.1 W average power was reported [39]. This laser was subsequently broadened in PCF and f_{CEO} detected in an f-to-$2f$ interferometer [40], however despite a strong signal-to-noise level [41] locking was not achieved due to complexities in stabilizing the offset frequency using pump diode current modulation [42]. The highest repetition rate Yb:KGW laser reported thus far is 4.8 GHz [43], however the corresponding decrease in intracavity pulse energy resulted in insufficient self-phase modulation for coherent supercontinuum generation, with output pulse durations of 400 fs. Yb:CALGO (Yb:CaGdAlO$_4$) is a promising gain medium for the generation of sub-100fs pulses due to its low material dispersion (~100 fs^2/mm) and broad absorption and emission cross sections. A 1.8-GHz Yb:CALGO laser producing 60-fs pulses with 2.95 W average power was reported [44], and comb stabilization achieved without additional amplification or pulse compression [45]. This work has been extended to 5 GHz [46] and 10 GHz [47], however comb stabilization has not been attempted.

Higher repetition rates (10 – 160 GHz) are achievable in Nd:YVO$_4$ and Er:Yb:glass by combining compact cavity designs with suitable SESAMs [48,49], however pulse durations increase correspondingly to >1 ps, making coherent spectral broadening unfeasible. Semiconductor disk lasers such as VECSELs and MIXSELs offer wide mode spacings, but self-referencing has only been observed in limited circumstances [50].

2.2.3 Electro-optically modulated combs

In contrast to the laser systems described above, electro-optically modulated (EOM) frequency combs take an alternative approach to achieving the required optimal mode spacing, negating the use of Fabry-Pérot etalons at the expense of long-term stability [51] and increased modal position uncertainty. For self-referenced combs the positional uncertainty contains contributions from the microwave references used to stabilize f_{CEO} and f_{REP}, with the former frequency requiring an additional measurement to remove an aliasing ambiguity and the uncertainty in f_{REP} being the dominant factor when scaled up by n to the optical domain. In an EOM comb a narrow-line CW pump laser is phase modulated to produce sidebands with a spacing set by the modulation frequency. Absolute traceability is achieved by stabilizing the pump laser to an atomic reference (also preventing wavelength shifts) and through microwave referencing of the modulation frequency, and thus the dominant uncertainty becomes the precision to which the CW laser can be stabilized to $f_{atom} = f_{CEO}$. With commercial modulators primarily available at telecommunications wavelengths, EOM

combs have been limited to the 1-2 μm band, and octave-spanning coverage has only been demonstrated in a few instances [52].

2.2.4 Chip-scale frequency combs

Microresonators are chip-scale devices that exploit the nonlinear Kerr effect in a dielectric medium to produce multi-GHz line spacings without filtering [53]. While the promise of robust, compact and stable chip-scale frequency combs is appealing, this technology is still in an early developmental stage, with much work required to improve device repeatability, modal noise and spectral coverage. The development of microresonators has primary used silica or a crystalline material such as CaF_2 as a gain medium, with spectral output centered in the infrared. Recent work has enabled coherent f-to-$2f$ self-referencing of a 16.4 GHz microresonator comb via external broadening [54]. In the future this broadening could be achieved with chip-integrated highly nonlinear waveguides [55], with filtering and delay functions integrated onto the supercontinuum chip to create a compact visible frequency comb.

2.3 Ancillary astrocomb technologies

Aside from the master laser oscillator, an astrocomb typically contains one or more of the following ancillary components in order to produce the desired spectral coverage and mode spacing for spectrograph calibration.

2.3.1 Fabry-Perot etalons

The dense mode spacing of the typical frequency combs produced directly by mode-locked lasers (≤1 GHz) requires spectral filtering of >90% of the modes with one or more Fabry-Pérot etalons to produce a calibration grid matched to the resolving power of the spectrograph. A Fabry-Pérot etalon spectrally selects a set of modes from the input comb with frequency spacing f_{REP}, with the length of the cavity selected such that the free spectral range (FSR) of the etalon passes every mth comb mode, creating an output comb with frequency spacing mf_{REP} [56]. While simple in theory, in practice this approach is complicated by the broad bandwidths required for spectrograph calibration. Additional factors must be taken into account, including air dispersion inside the etalon, the phase contribution of the mirror coatings, and the Gouy phase shift [57]. The spectral transmission function of a Fabry-Pérot etalon consisting of two mirrors with reflectivity R separated by distance L is given by:

$$T\left(f, R, L(\lambda)\right) = \frac{(1-R)^2}{(1-R)^2 + 4R\sin^2\left(2\pi f L(\lambda)/c\right)} \qquad (1)$$

The dispersion of the etalon is included in the term $L(\lambda)$, and leads to a misalignment between the regular grid of comb modes and the FSR of the etalon. For demanding applications such as filtering the modes of a 250 MHz fiber laser to 25 GHz [58], the filter ratio of $m = 100$ would require a reflectivity of $R = 99.8\%$, extremely difficult to obtain over a broad bandwidth without introducing additional mirror dispersion. A solution is to use cascaded etalons, relaxing the reflectivity requirements on each individual cavity and increasing the operating bandwidth, with care taken to prevent the introduction of virtual cavities arising from spurious back reflections. Sideband suppression of 70 dB has been reported using this technique with a double etalon [59]. For extremely broadband applications the lower reflectivity of metallic coatings (<99%) can be combined with multiple filter stages to provide almost dispersion-free etalons. Advances in dielectric coating design and manufacturing have led to the production of mirror sets with highly tailored group delay dispersion (GDD), primarily for femtosecond laser applications [60]. Recently mirror pairs with complementary coatings designed to provide zero GDD have been reported [61]. When combined with the

dispersion of air, these mirror sets provide high fidelity filtering without FSR misalignment [62].

Inadequate filtering of the fundamental comb leads to poor suppression of unwanted modes, as well as intensity asymmetry between sidebands on either side of the transmitted mode. These sidebands cause a shift δf_m in the center of mass of an astrocomb line f_m as measured on the spectrograph, given by [63]:

$$\delta f_m \approx f_{REP} \left(\frac{\Delta_m / f_{REP}}{2F} \right)^2 \left[\frac{t_{m+1} I_{m+1} - t_{m-1} I_{m-1}}{t_m I_m} - 2 \frac{\delta \phi_m}{\pi} \frac{\Delta_m}{f_{REP}} \right] \tag{2}$$

where F is the etalon finesse, Φ_m is the round trip phase delay, I_m is the source comb line intensity and t_m is the resonant transmission of the Fabry-Pérot etalon at f_m. Analysis of this model has shown that centroid shifts of 7 cm s^{-1} can occur when neighboring comb lines differ by as little as 1%. Such systematic errors must be measured and corrected for when striving to achieve calibration accuracy at the 1 cm s^{-1} level. An in-depth analysis of the effects of sideband suppression and asymmetry indicated that long-term radial velocity accuracy is limited by drifts in the alignment of the Fabry-Pérot etalon [64].

2.3.2 Nonlinear frequency conversion

As shown by the dashed lines in Fig. 3, the spectral coverage of a high-resolution spectrograph is often extremely wide, making external frequency conversion of the source comb a necessity. The most common approach is to use PCF to generate a broadband supercontinuum [65], exploiting the high average powers or short pulses available to fiber and Ti:sapphire lasers respectively. Care must be taken to maintain phase coherence, otherwise there will be a shift in the position of the comb modes in the wings of the supercontinuum. In cases where pulse energies are low, tapered fibers can be employed to increase the nonlinear broadening effects [66].

Second harmonic generation enables access to green and blue wavelength regions that would otherwise be inaccessible using conventional PCF. Engineered grating periods in quasi-phase-matched crystals such as PPLN or PPKTP can produce top-hat spectra with increased phase-matching bandwidths compared to birefringent crystals such as BBO or LBO [67]. The tailoring of spectral profiles could be used to remove or relax the need for subsequent active spectral flattening, as described in §2.3.3.

Frequency down-conversion through parametric processes can be used to extend a comb to the near- and mid-infrared, however care must be taken to keep track of the comb offset frequency. Difference frequency generation (DFG) can produce offset-free combs [68], useful as they remove an ambiguity in the absolute frequency of each comb mode, however few spectrographs operate in the regions typically accessed through DFG. Optical parametric oscillator (OPO) frequency combs are as intrinsically stable as their pump [69], however the signal and idler offset frequencies are distinct from that of the pump laser [70]. Degenerate OPOs produce extremely broadband outputs at twice the pump wavelength, with a comb that is intrinsically locked to that of the pump laser [71]. Such systems are currently proposed in the calibration system for the planned HIRES spectrograph on the E-ELT [72].

Effective sideband suppression can be made more difficult by the use of nonlinear conversion techniques, particularly when using amplifiers in a fiber-based astrocomb. Chang *et al.* [73] studied a number of configurations of filtering schemes and amplifiers, and determined that the nonlinear phase introduced during chirped-pulse amplification reintroduces previously suppressed side modes, with two filter stages required prior to amplification to minimize this effect. The same team also studied the effects of nonlinear spectral broadening on filtered comb modes [74], noting that four-wave-mixing processes between astrocomb lines and side modes degraded the sideband suppression. Again, using multiple filter cavities prior to broadening was shown to alleviate this issue. In separate work,

Probst *et al.* [75] analyzed the effects of sideband amplification in PCF in SHG processes, drawing similar conclusions. While it may seem evident that broadening prior to filtering would remove this issue, it is worth noting that filtering is made relatively simpler when it is carried out at the pump wavelength due to the narrower spectral coverage and relaxed requirements of the mirror coatings.

2.3.3 Spectral flattening

As well as line spacing uniformity, an ideal calibrator provides a constant flux of photons per comb line to the CCD to maximize the signal-to-noise ratio in a given exposure time for the highest possible precision, and therefore the uniformity of the spectral intensity of the astrocomb must be considered. Most nonlinear broadening processes result in a highly-modulated envelope due to Raman soliton and four-wave mixing processes. Spectral shaping [76] of a lab-based astrocomb has been demonstrated using a spatial light modulator placed at the image plane of a grating spectrometer and between a pair of crossed polarizers, with a CCD spectrometer used in an adaptive feedback loop [77,78], and a spectral flattening module was added to the HARPS astrocomb in a recent upgrade [79] (see §3.1). Further work is required to extend this flattening process to the infrared.

2.3.4 Absolute comb mode identification and traceability

For precision calibration it is necessary to identify the absolute frequency of each comb tooth, requiring knowledge of the mode number as well as f_{REP} and f_{CEO}. Two ambiguities in this identification process exist and must be addressed. The first is in the determination of the offset frequency, as standard f-to-$2f$ interferometry techniques are unable to distinguish between f_{CEO} and f_{REP}-f_{CEO} without an additional measurement, typically beating a stabilized CW laser with a comb line then fractionally shifting f_{REP} to observe how this beat frequency shifts. The second ambiguity arises in determining which subset of modes has been filtered by the Fabry-Pérot etalon, as the filtering process can transmit any subset that falls within the free spectral range of the mirrors.

A common approach to address this issue has been to use a narrow linewidth CW laser as a reference frequency. If the CW laser is locked to the comb then a wavemeter must be used to determine the absolute frequency of one comb tooth, from which the remaining comb teeth can be calculated [80]. The frequency stability of a wavemeter is not suitable for long-term precision measurements of a single comb line [81], however it does allow the modal number ambiguity to be resolved. Alternatively, the CW laser can be stabilized to an atomic transition to provide absolute traceability, and the comb offset frequency stabilized relative to this reference [82]. The offset frequency ambiguity can be resolved by shifting f_{REP} by a known value and observing the shift in f_{CW}-f_n. In either case the CW reference can also be used to stabilize the Fabry-Pérot etalon spacing using the Pound-Drever-Hall method, ensuring that transmitting the CW laser also transmits a known subset of modes.

The above method is well suited for narrow bandwidth astrocombs that employ filter cavities operating over a single spectral region, however future spectrographs such as E-ELT-HIRES require astrocombs which can provide a calibration scale extending over nearly three octaves of optical frequency [72,83]. The design approach taken in such spectrographs is to divide the light into discrete wavelength channels (up to eight in E-ELT-HIRES) from the UV to the mid-IR, implying a requirement not only for a broadband astrocomb but also for multiple Fabry-Pérot etalons, each filtering the astrocomb within a unique wavelength region. Narrow-line and atomically referenceable CW lasers are not generally available across such a wide spectral range, with most diode lasers used for atomic spectroscopy operating in the UV-visible region [84,85]. We recently proposed an alternative technique in which the Fabry-Pérot cavity is locked directly to the comb and a Fourier-transform spectrometer (FTS) with resolution sufficient to resolve the filtered comb is employed as a mode identifier [86]. Calibrating the scanned optical path length of the FTS with a single atomically-stabilized

diode laser ensures traceability, and an all-metallic design enables broadband operation. Combined with retrieval techniques that can surpass the path-limiting resolution of conventional FTS [87,88], the absolute comb frequencies could be identified without the need for additional CW lasers or a wavemeter.

For absolute traceability to SI standards the RF synthesizers used to stabilize f_{REP} and f_{CEO} can be referenced to GPS disciplined microwave clocks. These clocks are the primary source of uncertainty in the comb mode positions, as small fluctuations in f_{REP} in the RF domain are multiplied by the mode number n, creating larger errors in the optical domain. Long-term averaging can reduce the uncertainty to below the 10^{-12} level, with the one-day frequency stability of almost all the satellite clocks forming the GPS constellation being reported as $< 2 \times 10^{-13}$ [89]. Referencing and archiving of GPS timing signals against a terrestrial master clock operated by the US Department of Defense ensures long-term traceability of these data can limit their daily drift to $< 2 \times 10^{-14}$ [89]. This long-term precision, which is ultimately determined by the terrestrial primary Cs standard, is important for several ambitious science cases which require consistent comb performance over many observations, such as measuring the radial velocity variations over the long orbital period of an Earth-like exoplanet, testing the postulated variation with redshift and direction on the sky of the fundamental fine structure constant α [90], and directly measuring the dynamical evolution of the Universe over time (the Sandage test) [91]. Observational campaigns conducted on a single instrument are likely to be precision limited, but in cases where observations from more than one telescope might be combined then the question of absolute calibration accuracy also becomes important and would be subject to the same limitations imposed by GPS referencing.

3. Review of demonstrated astrocombs

In this section we review the systems that have been deployed or identified as potential astrocombs. Where possible, we present work chronologically by research group, reflecting advances in the field, and separating the discussion by laser system. Figure 3 illustrates the wavelength coverage of several spectrographs and the astrocombs that have been deployed to calibrate them, with further detail provided in Table 1 and the text below. Note that the spectral gap from 900 to 1400 nm in Fig. 3 does not reflect a lack of suitable comb sources, but is due to a combination of other factors including increased atmospheric water vapor absorption [97], a decrease in detector performance for instruments typically designed for operation in the visible or IR, and a lack of science justification for high detail observations in this region, although this will change with the advent of instruments such as CARMENES [98] and NIRPS [99].

3.1 Fiber lasers

Researchers working in collaboration with Menlo Systems have utilized fiber combs to calibrate multiple spectrographs. The initial field demonstration of an astrocomb was carried out in 2008 on the solar spectrograph at the Vacuum Tower Telescope (VTT) at Tenerife, Canary Islands [92]. A Fabry-Pérot etalon with <40-nm bandwidth at 1570 nm filtered the modes of a 250 MHz Er:fiber comb to 15 GHz, with >30-dB sideband suppression. The etalon was dither-locked to a transmission maximum, with mode number identification carried out by locking a CW laser to a comb line and measuring this frequency with a wavemeter. As the VTT spectrograph is not stabilized, drifts of 8 m s^{-1} min^{-1} were clearly evident using the comb, which were not observable with thorium lamp calibration.

After this initial promising demonstration, the Menlo Systems comb was installed as the calibrator for the High Accuracy Radial velocity Planet Searcher (HARPS) spectrograph at European Southern Observatory's 3.6-m telescope at La Silla, Chile [10]. HARPS has a resolving power of $R = 115000$ and covers the 380-690 nm range, with a long term precision of 1 m s^{-1}. The HARPS comb consisted of a 250-MHz Yb:fiber laser filtered to 18 GHz in two Fabry-Pérot etalons with different FSRs, providing >50-dB sideband suppression. The

cavities were tilt-locked to a CW laser, itself locked to the comb and frequency monitored with a wavemeter, enabling the same subset of modes to be transmitted by both etalons. Amplifiers were employed before, between, and after the etalons to provide adequate power for frequency doubling to 515 nm, with sufficient bandwidth to cover a single spectral order. The uncertainty in the comb line positions was 2.1 cm s^{-1} after subtracting instrument drift. Analysis of the residuals in the calibration curve revealed detector inhomogeneities every 512 pixels, deriving from the mask used in the manufacturing process.

Table 1. Summary of astrocombs implemented at an on-site spectrograph

Spectrograph	VTT [92]	VTT [93]	HARPS/ FOCES [79]	Pathfinder [58]	TRES [94]	HARPS-N [95]	HRS [13]	NIRSPEC [96]
Comb source	Er:fiber	Yb:fiber	Yb:fiber	Er:fiber	Ti:sapphire	Ti:sapphire	Ti:sapphire	EOM
Source f_{REP} (GHz)	0.25	0.25	0.25	0.25	1	1	1	CW
Astrocomb f_{REP} (GHz)	15	5.5	18 / 25	25	30/50	16	15/25	12
Bandwidth (nm)	1530-1600	480-640	440-600	1450-1700	400-420 / 780-880	500-620	555-890	1430-1640
No. Fabry-Perot etalons	1	2	3	2	1	2	1	N/A
Fabry-Perot finesse	2400	3000	2600	2000	250	105	155	N/A
Sidemode suppression (dB)	46	94	55	50	22	45	20	N/A
No. amplification stages	0	3	3	2	0	0	0	2

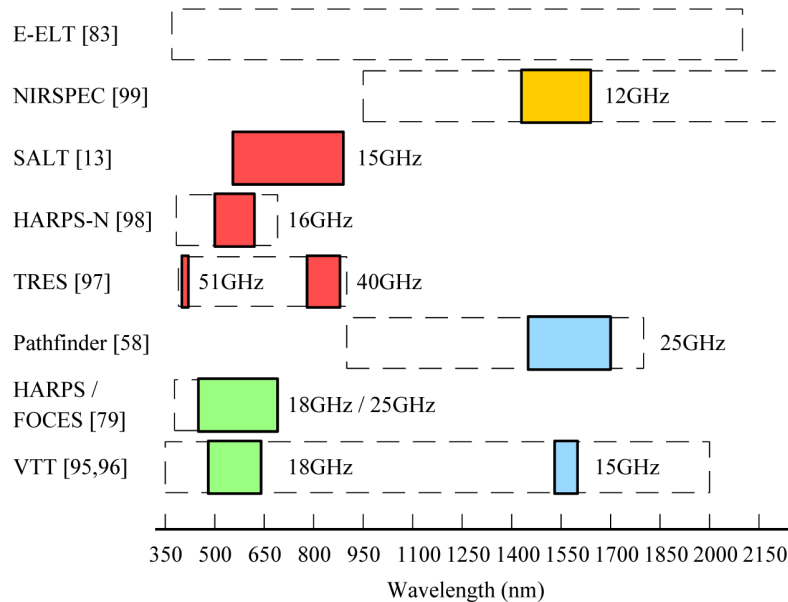Fig. 3. Comparison of the astrocomb calibration campaigns on astronomical spectrographs. Colored boxes show the achieved spectral coverage of the astrocomb, with colours indicating the employed laser technology, where blue is Er:fibre, green is Yb:fibre, red is Ti:sapphire and orange is an EOM comb. Dashed lines indicate the entire spectral coverage of the spectrograph. The coverage of NIRSPEC extends to 5500 nm.

To calibrate further spectral orders the frequency-doubled filtered comb was broadened in tapered PCF with a core diameter <1 μm [100]. With 90-mW input pulses at 18 GHz (5 pJ pulse energy), the output spectrum was 140 nm wide at 20 dB below the peak [101]. This astrocomb was used to calibrate the radial velocity shifts of the star HD 75289, orbited by a Jupiter-mass exoplanet with a period of 3.5 days. The orbit of the planet was reconstructed with the same uncertainty as previous measurements using a Thorium lamp, suggesting that additional factors were limiting the calibration. The HARPS comb was also used to calibrate a solar atlas using sunlight reflected from the surface of the moon, in which CCD stitching errors revealed previously were measured for multiple spectral orders [102].

A similar Yb:fiber comb was installed on the VTT telescope in 2011. Filtering of the pump laser was carried out using a pair of identical Fabry-Pérot etalons locked with the Pound-Drever-Hall method to the transmission of an orthogonally-polarized CW laser stabilized to a comb mode [103]. The etalon finesse was increased to ~3000, with sideband suppression >94dB. Simultaneous coupling of sunlight and calibration light into the same single mode fiber removed systematic effects related to grating illumination. Results identified a number of systematic errors in the calibration, including camera vibrations from a cooling fan, imperfections in the microlens array, and variations in the point-spread function arising from changes in the fiber coupling [93].

A Menlo Systems astrocomb was used to determine the calibration precision and stability of the upgraded Fiber Optic Cassegrain Échelle Spectrograph (FOCES), previously installed at the Calar Alto 2.2m telescope and current housed at the Wendelstein Observatory, Germany. The astrocomb architecture is similar to those described above but with 25-GHz mode spacing, and spectral broadening achieved directly in tapered fiber rather than after an intermediate frequency-doubling stage [104]. An identical astrocomb has been installed at the Xinglong station of the National Astronomical Observatory of China [105], however further results have not yet been reported. The HARPS astrocomb was upgraded to a similar architecture in 2015 while maintaining a 18-GHz mode spacing, and the FOCES astrocomb transported to La Silla in order to compare the relative stability of these two calibration sources [79]. An additional temporally incoherent spectral background was observed in the new HARPS comb that was not previously present, and was attributed to amplified spontaneous emission (ASE) produced in the power amplification stage. The calibration repeatability of 1 cm s^{-1} was attainable on a time scale of a few hours, with other systematics in the spectrograph such as multimode fiber noise and spectrograph channel cross-talk currently preventing longer-term calibration.

Researchers at NIST generated a 12.5-GHz comb by filtering a 250-MHz Er:fiber laser in a pair of high finesse (F = 2000) etalons that were dither locked to a peak of transmitted power [106]. The etalons were constructed from curved rather than planar mirrors, with the curvature selected to offset higher order spatial modes by + 1.75 GHz from the main 12.5-GHz spaced modes. Intermediate amplification after the first etalon with a pair of semiconductor optical amplifiers preserved the spectral bandwidth before launching into a high power EDFA and subsequently into the second etalon. The filtered pulse train was broadened in 50 m of HNLF. The sideband suppression was measured by optically heterodyning the 12.5-GHz comb with a tunable CW laser. While asymmetry was noted after amplification, it was not detected after broadening. The frequency accuracy of this comb was evaluated throughout the optical chain by referencing a single mode to a 10-MHz hydrogen-maser reference. At each stage the optical mode fluctuations tracked the GPS disciplined oscillator used for f_{REP} locking, suggesting that this was the limiting factor. In separate work [58], this laser was further filtered to 25 GHz with 50dB sideband suppression and used to calibrate the Pathfinder spectrograph on the Hobby-Eberly telescope in Texas with a radial velocity precision of 10 m s^{-1}. This is currently being extended to 30 GHz in the near infrared through the use of three low dispersion etalons [107]. Complementary work in Yb:fiber has

been carried out by Hou *et al.* [108], generating a 23.75-GHz comb with 43dB sideband suppression.

An astrocomb is being developed for the infrared (0.9-2.5 μm) GIANO spectrograph located on the Telescopio Nazionale Galileo (TNG) in La Palma, Spain [109]. A 100-MHz Er:fiber laser will be filtered to 16 GHz in two moderate finesse etalons ($F = 600$) before amplification and broadening in HNLF. Alternatively, should sideband suppression be insufficient, the etalons will be composed of metallic mirrors to minimize dispersion, allowing broadening to be undertaken at 100 MHz with no amplification but requiring additional etalon stages.

Murphy *et al.* [110] demonstrated the measurement of both the instrument line shape and inter-pixel sensitivity variation on the Ultra-High-Resolution Facility (UHRF) spectrograph at the Anglo-Australian Telescope (ATT), Australia. With $R \approx 10^6$, a mode spacing of 1 GHz was sufficient to resolve the comb lines. A 94-MHz Er:fiber laser was stabilized to the 100th harmonic of f_{REP} and the offset frequency was monitored using the $2f$-to-$3f$ technique.

Ma *et al.* [111] have developed an astrocomb based on a 1-GHz Yb:fiber laser with sufficient bandwidth and output power for comb stabilization [18]. The laser output was amplified to 2.8 W in 4.5 m of double-cladding Yb:fiber and compressed to < 100 fs using a grating pair in order to generate a supercontinuum in a tapered PCF. A Zerodur-spaced Fabry-Pérot etalon composed of a complementary pair of zero-GDD mirrors [61] for transmission over 430–700 nm with 26 dB sideband suppression. Initial tests at the Xinglong station of the National Astronomical Observatory of China show an estimated RV resolution of 29 cm s^{-1}, but with asymmetric filtered comb lines due to etalon phase errors.

3.2 Ti:sapphire lasers

The first laboratory demonstration of an astrocomb was carried out in 2008 by Li *et al.* [112] by employing an octave-spanning Ti:sapphire laser with 1-GHz mode spacing [113], enabling direct stabilization of f_{CEO} without further spectral broadening. A Fabry-Pérot etalon locked to a Rb-stabilized diode laser provided up to 40-GHz mode spacing in the range of 770-920 nm. This work was extended to the visible by frequency doubling the Ti:sapphire output in a 1-mm-thick BBO crystal, proving more robust and reliable than broadening in PCF. The comb was installed on the TRES spectrograph at the Fred Laurence Whipple Observatory (FLWO) on Mt. Hopkins, Arizona. A Fabry-Pérot etalon operating over 400–420 nm provided a mode spacing of 51 GHz with 20-dB sideband suppression [114]. Both the near-infrared and blue astrocombs were used to calibrate TRES, indicating that 1-m s^{-1} resolution should be achievable once temperature, pressure and vibration controls are installed [94,115].

The same research group designed and installed an astrocomb at HARPS-N, located on the TNG in the Canary Islands [116]. In contrast to the heavily filtered and amplified Yb:fiber comb used to calibrate HARPS, the 1-GHz Ti:sapphire employed in this system requires less demanding mode filtering in order to achieve the optimal spacing, however tapered PCF was still required to satisfy the spectral coverage demands of the spectrograph. An 11-mm length of solid core PCF (NKT PM850) was adiabatically tapered from an initial core size of 3 μm to 1.7 μm, generating an output from 500 to 620 nm through fiber optic Cherenkov radiation [117]. The green comb modes were filtered to 16 GHz in an etalon stabilized with a low noise frequency doubled Nd:YAG laser, using the Pound-Drever-Hall method and a high-bandwidth piezo for cavity length feedback. The entire Fabry-Pérot system was isolated from DC to 2 kHz, and the temperature held at 5 K above ambient to better than 100 mK. Tests showed that the system was capable of sub-10-cm s^{-1} stability over long time scales [95]. This comb was also used in a series of experiments to observe the Sun as a star, measuring sub-m s^{-1} Earth-Sun RV shifts [118]. Ongoing work will attempt to extract the signature of Venus from the measured RV profile, demonstrating the capability of HARPS-N in detecting Earth-like exoplanets [119].

A partially-stabilized 1-GHz Ti:sapphire laser was used by McCracken *et al.* [13] as the source comb for calibrating the High Resolution Spectrograph (HRS) on the Southern African Large Telescope (SALT). The Ti:sapphire comb was repetition-rate stabilized, with f_{CEO} monitored by heterodyning the comb against a narrow linewidth diode laser stabilized to a hyperfine Rb transition. The offset frequency shifted by less than 2% (20 MHz) over an 8-hour observation window, and could be accounted for in the calibration process. The Ti:sapphire laser was spectrally broadened in a short length of PCF and the modes filtered in a tunable Fabry-Pérot etalon, offering 15-25 GHz spacing over 550–890 nm, fully covering the red arm of the spectrograph. Comb calibration improved the wavelength solution by a factor of two and established a higher resolving power for the high stability mode of HRS than was previously assumed.

3.3 Electro-optically modulated lasers

An EOM comb constructed entirely from commercial off-the-shelf components was deployed by Yi *et al.* [96] at the NASA Infrared Telescope Facility (IRTF) and the W. M. Keck observatory (Keck) 10-m telescope, with campaigns in 2014 and 2015 respectively. A narrow-line CW laser was stabilized to a pressure-broadened transition in hydrogen cyanide at 1559.9 nm. Out-of-loop measurements showed a stability of <60 cm s^{-1} for averaging times greater than 20 s, and a frequency drift of <1.2 cm s^{-1} per day, suitable for short-term measurements but implying that further investigations would be required for multi-year campaigns. The CW laser was modulated in both phase and amplitude using a series of LiNbO$_3$ modulators before being amplified, resulting in a 1-W, 12-GHz, 2-ps pulse train. Broadening from 4 nm to over 100 nm was carried out in 20 m of HNLF. While observation time at IRTF was plagued by bad weather, the campaign at Keck revealed a sub-pixel drift in the comb line positions on the CCD over a period of one hour, directly correlated to temperature drifts within the spectrograph itself.

An EOM comb is being designed for the Subaru Telescope by Kashiwagi *et al.* [120] using a similar pump scheme. By modeling a series of cascaded HNLFs with carefully selected zero-dispersion wavelengths a 12.5-GHz comb spanning over 100 THz was achieved. A Fabry-Pérot etalon was employed prior to amplification and broadening to remove unwanted ASE, resulting in high contrast comb lines.

In a complementary approach, Chavez Boggio *et al.* [121,122] demonstrated a novel astrocomb generated from two amplified narrow linewidth CW lasers near 1550nm that were co-launched into 1.5 m of low dispersion HNLF. Four-wave mixing products resulted in a 60-THz comb centered at 1600 nm which was subsequently frequency doubled in BBO to produce a comb at 800 nm with a modal separation of 708.5 GHz. While in its early stages, this work is promising for the generation of extremely-widely-spaced astrocombs.

4. Outlook

In this article we have highlighted the advances made in the development of frequency combs for astronomical spectrograph calibration. With metallic cathode Th-Ar lamps no longer available on the market [9], astrocombs may soon be considered the primary source for spectrograph calibration rather than a luxury, and their performance must improve to meet this challenge accordingly.

4.1 Challenges

While nonlinear optics enables the broadening of a relatively narrow source comb, many practical astrocombs provide far narrower wavelength coverage than the spectrograph upon which they are deployed. The limiting factors lie in the inherent trade off between sideband suppression and operational bandwidth of the Fabry-Pérot etalons required for mode filtering, requiring multiple etalons to cover different spectral regions. The proposed spectrograph for the E-ELT will require a calibration source that covers 0.37–2.1 μm and an operational

lifetime of 10 years – no astrocomb to date has demonstrated this requirement [72]. An alternative technology may be Fabry-Pérot etalons illuminated by a broadband white-light source, producing a comb-like structure. Fixed etalons have been employed as calibration sources demonstrating ~1-m s^{-1} stability demonstrated over several months [123], with primary challenges including vacuum and temperature stabilization and dispersion drifts. Tunable etalons must be stabilized to an optical reference such as an atomically stabilized diode laser or a laser frequency comb. Such stabilization can enable few-cm s^{-1} accuracy [124–126], however the use of a reference places additional demands on the engineering of the etalon coatings.

Full automation remains a technical challenge. The astrocomb at HARPS-N has been upgraded to include auto-alignment of the flat-mirror Fabry-Pérot etalons and coupling into the tapered PCF. Care must still be taken to ensure that contaminants do not damage sensitive components, particularly in fiber systems with high average powers. Ti:sapphire systems require periodic adjustment of the crystal position to prevent damage from the optical tweezing of dust, which alters f_{CEO}. This can be compensated for using motorized intracavity wedges, however this is currently a manual process. The recent upgrade to the astrocomb at HARPS includes a significant redesign to aid automation, with studies of long-term fail-safe operation underway [79].

Within the astronomy community, questions remain over whether astrocombs are truly required to achieve the greatest radial velocity precision from a spectrograph. Lovis *et al.* performed an in-depth study of Th-Ar lamp spectra at the HARPS spectrograph, estimating a global uncertainty in the wavelength calibration of 0.2–0.4 m s^{-1} in observations taken over a 1-month window [7]. A comparison of the spectra from different Th-Ar lamps taken during the same night revealed 1 m s^{-1} line shifts, which may have been attributable to instrument drifts or CCD limitations rather than calibration standard variation. In short, astronomers have had many decades of experience working with Th-Ar lamps, reducing the calibration uncertainty to near-cm-s^{-1} level, and thus far the performance issues and technological difficulties associated with astrocombs have not yielded the promised benefits or results.

While sub-cm-s^{-1} wavelength calibration may be soon be achievable with an astrocomb, the choice of calibration source is not the limiting factor in the radial velocity precision achievable with a high-resolution spectrograph. Technological issues include photon noise [127], guiding and modal noise associated with optical fibers [128], and CCD stitching errors [10], although these can all be addressed with a sufficiently stable instrument. Stellar phenomena such as sunspots, meridional flows, p-mode oscillations and jitter must be accounted for and, where possible, averaged out in order to keep the RV precision below 1 m s^{-1} [129]. Going forward, the astrophotonics community must continue to develop calibration tools that ensure that the wavelength solution is an order of magnitude more precise than other sources of uncertainty, removing this factor from the overall error budget.

4.2 Opportunities

The continual progression of laser technology is opening up new avenues of exploitation within astronomy. The relative expense of a frequency comb makes it affordable by only the largest facilities, however small and medium scale spectrographs would also benefit from comb calibration. Where multiple telescopes are located in one geographical location a single frequency comb could be distributed from a central hub via low-loss single mode fiber, and the structure of the comb can be preserved over multiple km [130].

New and emerging laser sources will find applications as astrocombs in the future, particularly the microresonators and compact solid-state lasers previously mentioned. The wide mode spacing offered by these systems would also enable direct optical frequency stabilization to an atomic reference through saturated absorption spectroscopy [131], providing intrinsic atomic traceability for each comb line without an additional CW laser.

Astrocombs may have a role in the pre-calibration and validation of lower cost calibration technologies such as white-light etalons [132].

As spectral flattening improves there is an opportunity to use the astrocomb not only as a precision wavelength calibrator, but also as an ideal white light source for flat-fielding of the CCD. Tungsten filaments are currently employed for this purpose and flat-fielding is carried out daily, however the filaments age over time and therefore suffer from intensity variations. They are also subject to the same manufacturing limitations as hollow cathode lamps, making it difficult to compare data sets. The intensity profile of a filament is not constant with wavelength, introducing signal-to-noise errors in the flat-field calibration. With photon-flux-per-few-comb-lines shaping possible [133], the comb could be used for this purpose, providing identical, traceable flat-fielding.

Compact laboratory spectrographs constructed from commercial off-the-shelf components for the analysis of astrocombs have recently been reported [134,135]. While they lack the environmental stability of large-scale systems, their comparative resolving power of $R > 150,000$ enables the analysis of sideband suppression and other systematics.

Appendix C

Paper 3 - Astrocomb Proposal for ELT HIRES

Comparison of astrophysical laser frequency combs with respect to the requirements of HIRES

Jake M. Charsley[a], Richard A. McCracken[a], Derryck T. Reid[a], Grzegorz Kowzan[b], Piotr Maslowski[b], Ansgar Reiners[c] and Philipp Huke[c]

[a]Scottish Universities Physics Alliance (SUPA), Institute of Photonics and Quantum Sciences, School of Engineering and Physical Sciences, Heriot-Watt University, Edinburgh EH14 4AS, UK
[b]Institute of Physics, Faculty of Physics, Astronomy and Informatics, Nicolaus Copernicus University, ul. Grudziądzka 5, 87-100 Toruń, Poland
[c]Georg-August Universität Göttingen, Institut für Astrophysik, Friedrich-Hund-Platz 1, Göttingen, Germany

ABSTRACT

Precise astronomical spectroscopy with the forthcoming E-ELT and its high resolution spectrograph HIRES will address a number of important science cases,[1] e.g. detection of atmospheres of exoplanets. Challenging technical requirements have been identified to achieve these cases, principal among which is the goal to achieve a radial velocity precision on the order of 10 cms^{-1}. HIRES will experience systematic errors like intrapixel variations and random variations like fiber noise, caused by the non-uniform illumination of the coupling fibers, with these and other systematic errors affecting the performance of the spectrograph. Here, we describe the requirements for the calibration sources which may be used for mitigating such systematic errors in HIRES. Precise wavelength calibration with wide-mode-spacing laser frequency combs (LFCs), so called astrocombs, has been demonstrated with different astronomical spectrographs. Here we present a comparison of currently used astrocombs and outline a possible solution to meet the requirements of HIRES with a single broadband astrocomb.

Keywords: Astrocombs, Astronomical instrumentation, Calibration, HIRES, Laser frequency combs, Spectroscopy

1. INTRODUCTION

The instrumentation programme[2] of the E-ELT foresees a high-resolution spectrograph (HIRES) as one of the instruments located on the Nasmyth B platform. The instrument's concept evolved from the combined studies for CODEX (an ultra-stable high resolution spectrograph in the visible[3]) and SIMPLE (a high-resolution near-infrared spectrometer[4]). Flagship science drivers were identified based on the scientific needs of the astrophysics community.[5] These science drivers were categorized and prioritized into five science cases.[1] The science cases impose requirements on the calibration in a way that only laser frequency combs (LFCs) and Fabry-Pérot etalons (FPs) can be used as wavelength calibration sources:

1. **Wavelength coverage**
   The wavelength coverage is driven by all science cases differently. Most of the science cases, including the characterisation of exoplanet atmospheres, require an almost continuous coverage from 0.4 to 1.8μm. The blue end (0.37–0.4μm) is essential for the Sandage test[5] as well as the measurement of important characteristics of exoplanets, protoplanetary disks and for the velocity (RV) survey on M dwarfs. The wavelength coverage is driven by all science cases differently. An almost continuous coverage until 2.1μm is desirable for a radial velocity (RV) survey of M dwarfs, the detection of exoplanet atmospheres, and studying the evolution of galaxies and the intergalactic medium.

Further author information: (Send correspondence to Jake M. Charsley or Philipp Huke)
Jake M. Charsley: E-mail: jc50@hw.ac.uk
Philipp Huke: E-mail: huke@astro.physik.uni-goettingen.de

2. **Resolving Power**

Most of the science cases require a resolving power $R = \lambda/\Delta\lambda \approx 100,000$. A higher resolving power (R≈150,000) is desirable for some stellar atmosphere studies and RV measurements. Lower resolving power (R<50,000) as well as a multiplexing capability is desirable by some extragalactic science.

3. **Precision and Accuracy**

The most stringent requirement on precision comes from RV exoplanet measurements down to 10 cms^{-1}, while the most stringent requirement in terms of accuracy comes from the Sandage test with a goal value down to 1 ms^{-1} or similar for long-term stability.

Precision is mostly driven by the stability of the instrument, while the accuracy is driven by the precision of the calibration. Therefore, the calibration unit (CU) aims at a precision of 1 mms^{-1} and an accuracy on the same order. To ensure this, the calibration sources are measured against internal calibration standards. The most stable light source that enables a transfer of its stability to the whole spectral range required by all scientific cases is the LFC.

Comparing these requirements to those of calibration units in other spectrographs (SPIRou,[6] ESPRESSO,[7] HARPS,[8,9] CARMENES[10]) shows that new solutions have to be found. The concept of how these solutions work together is explained in Ref. 11. Here we describe the primary module of the calibration unit, a LFC covering the full wavelength range and locked to traceable calibration standards.

The main requirements for this LFC can be extracted from the calibration requirements for HIRES as follows:

- Full wavelength coverage 0.4–1.8 μm (goal 0.37–2.4 μm)

- Repetition rate adjusted so that one comb line is available for every ∼2.4 resolution elements for calibration (details explained in Section 2.1)

- Flat spectral intensity distribution

- Full automatization

- Precision better than 0.1 cms^{-1}

- Stability better than 0.1 cms^{-1} over 10 years

In the following section we will describe the principles of astrocombs and give a comparison between existing combs. The principal setup of our comb is explained in Section 3.

2. ASTROCOMBS

2.1 Principles of Astrocombs

A laser frequency comb[12] produces a series of extremely-narrow, equally-spaced lines in the frequency domain, the positions of which can be stabilized to a precision approaching 10^{-12} with a standard RF reference.[13] The frequency of any comb line (mode) is given by

$$f_n = n f_{\mathrm{rep}} + f_{\mathrm{CEO}}, \tag{1}$$

where f_{rep} is the spacing between the comb modes and corresponds to the repetition rate of the laser that is set by the cavity length, f_{CEO} is the carrier-envelope offset frequency, a value set by the laser cavity dispersion, and n is a large integer ($\approx 10^5$). Without active feedback the absolute position of the comb modes will vary with time. The mode spacing will fluctuate due to changes in the length of the laser cavity, and this can be stabilized using intracavity piezo actuators. The offset frequency will fluctuate with minute changes in the intracavity dispersion, and multiple techniques have been developed to detect and stabilize this frequency.[14]

The appeal of using a frequency comb for spectrograph calibration lies in its stability, traceability and precision. A stabilized frequency comb will produce the same spectral output over its operating lifetime, providing

thousands of equally-spaced comb lines, the positions of which can be traced back to optical standards. The width of each comb tooth is much narrower than the instrument response given by the resolving power of the spectrograph, allowing the true instrument function to be characterized. The spectral brightness of all comb lines can be adjusted such that they are roughly equal, precluding pixel saturation.

The primary barrier to the wide-spread adoption of frequency comb technology, aside from cost, is a fundamental mismatch between the native comb spacing and the spectrograph resolving power. As outlined in the seminal paper of Murphy *et al.*,[15] the ideal repetition rate for a frequency comb for the calibration of an astronomical spectrograph would have each comb line be individually resolvable on the CCD, with frequency spacing corresponding to around three resolution elements. Typically for a high resolution spectrograph, this sees an optimal repetition-rate requirement of 10–40 GHz, while commercially available frequency combs have repetition rates of 80 MHz,[16] 250 MHz,[17] or 1 GHz.[18] Higher repetition rate frequency combs have been demonstrated but only in a laboratory setting,[19,20] while emerging alternative technologies have not yet shown the requisite stability and spectral coverage for astrocomb use.[21–23]
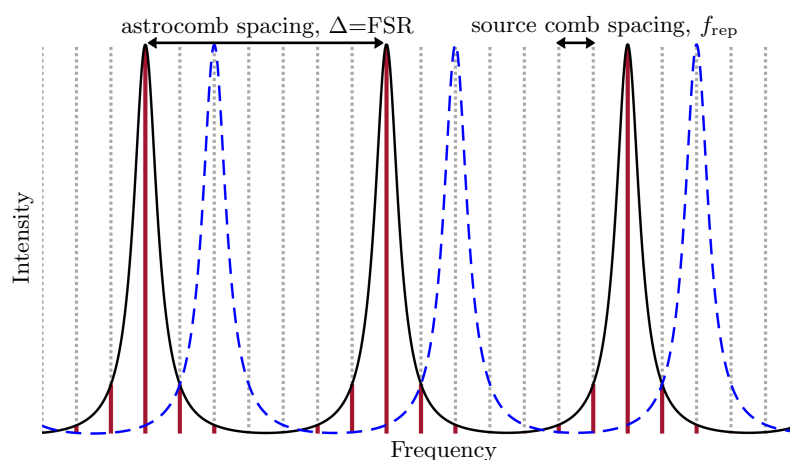

Figure 1. Astrocomb via the Fabry-Pérot filtering technique. The locked Fabry-Pérot transmission function (black outline) transmits every M^{th} mode of the source comb (in red). Identification of which modal subset has been filtered is critical for repeatability of measurements from lock-to-lock as the cavity does not discriminate between filtering alternative subsets (e.g. blue outline).

A common approach to obtain a widely-mode-spaced frequency comb is to optically filter a lower repetition rate comb through a Fabry-Pérot cavity. Imposing the condition that the free spectral range of the Fabry-Pérot cavity be an integer multiple M of the source comb repetition rate, the cavity can be effectively tuned to transmit only a subset of source comb modes, as illustrated in Figure 1. The resultant astrocomb structure sees one comb line every $\Delta = M f_{\rm rep}$, equal to the FSR of the Fabry-Pérot, where M can be arbitrarily chosen such that the filtered line spacing is well resolved by the astronomical spectrograph.

The dispersion provided by the mirrors and air in the filter cavity limits the useable spectral bandwidth transmitted, as after a certain operational bandwidth the filter transmission function 'walks off' from the source comb modes. Significant walk-off sees the selected subset no longer centered around the source comb line incident on the etalon. This walk-off between the Fabry-Pérot transmission regions and the astrocomb modes can be partially abated by decreasing the finesse of the filter cavity, essentially extending the point at which the intended source comb line is no longer centered by widening the transmission region. However, there is a compromise to be had as widening the filter transmission window leads to non-negligible transmission of the comb-mode neighbours (side-modes) of the intended transmitted comb modes. Due to the walk-off effect, these non-negligible side-modes can be asymmetric around the center of the transmission function of the filter cavity and, therefore, be transmitted with unequal weighting. In this case, the position of the astrocomb line will appear shifted as resolved by the astronomical spectrograph (which is typically much wider than both the source comb spacing and the filter cavity transmission function FWHM) as the center-of-mass resolvable by the spectrograph is no longer

centered around the intended astrocomb line. Braje *et al.*[24] first noted this shift from insufficient suppression of side-modes in their in-depth study on the importance of the Fabry-Pérot cavity mirror design. Side-mode suppression is commonly used to gauge the extent of this effect, which is the main obstacle of implementing the filtering calibration technique.

A number of techniques to improve side-mode suppression over a broad range of optical frequencies have been investigated. Filtering the source comb through a succession of Fabry-Pérots, first proposed by Steinmetz *et al.*,[25] can be used to improve side-mode suppression and has been predominantly used to filter a fiber source comb as the amplification stages required in such a system also amplify side-modes and generate amplified spontaneous emission (ASE) noise. The various ways of combining filter cavities were modelled comprehensively by Chang *et al.*[26] and identified the most efficient configuration for side-mode suppression to be a conjugate Fabry-Pérot pair whereby the free spectral range of the first cavity is $\Delta_1 = M f_{\rm rep}$ and the second is $\Delta_2 = M f_{\rm rep}/(M - 1)$.[27]

Limiting the net dispersion in the Fabry-Pérot cavity increases the bandwidth of the filtered astrocomb. Two ways of limiting the filter cavity dispersion have been demonstrated. The first, rather intuitive, method uses state-of-the-art mirror coatings with an extremely-low group delay dispersion.[25,28] A second method uses a chirped-mirror pair Fabry-Pérot cavity. The mirror coatings are dispersive, but oppositely so, such that the pair provide a low net dispersion over a very wide range of frequencies.[29]

Post-measurement, the useable filtered bandwidth can be extended by a technique proposed by Li *et al.*[30] which analytically recovers the astrocomb line center in each of the resolved calibration lines imaged on the spectrograph by on-site diagnosis of the finesse of the Fabry-Pérot cavity and the phase deviation of the astrocomb lines.

Another subtlety that arises from filtering is a possible ambiguity in which modal subset of the source comb is filtered by the stabilized Fabry-Pérot cavity, as shown in Figure 1. The transmission of the same subset through the cavity from lock-to-lock is critical for the repeatability of radial velocity measurements. For a narrowband astrocomb this ambiguity can be removed by locking a narrow linewidth diode laser to one comb tooth (see supplementary material in Ref. 31). This laser acts as a fiducial marker, and is used to stabilize the Fabry-Pérot cavity, ensuring that the transmission of the marker also transmits a known subset of modes. The diode laser output is then measured using a wavemeter, allowing the frequencies of all filtered comb modes to be calculated. Alternatively, the diode laser can be stabilized to an atomic transition, providing absolute traceability for each comb tooth.

Spectral flatness of the filtered comb is highly desirable, as it enables controllable CCD exposure times without saturation, minimizing photon noise and improving calibration accuracy. A spatial light modulator (SLM) placed at the image plane of a grating spectrometer can provide broadband intensity shaping, as demonstrated by Probst *et al.*[32] This technique is particularly useful when the astrocomb utilizes a fiber for spectral broadening, as this process results in a heavily structured spectral envelope (for an illustration please see Figure 11 in Ref. 33). While no deployed astrocombs have employed spectral flattening, a proposed future update to the HARPS calibrator will use a SLM.[33]

2.2 Comparison of Astrocombs

Since its conception in 2007,[15] two dominant approaches for building an astrocomb have emerged which are separated by the choice of laser oscillator; fiber or solid-state. Each has their subtleties, and in this section we review the implications of the different laser oscillators and the progression made in the respective approaches toward an ideal calibration source for astronomical spectrographs.

Fiber laser technology has long set the benchmark for compact design with user-friendly operation. Turn-key operation is routine, and long-term performance is repeatable without the need for regular cleaning or realignment. Fiber laser oscillators typically produce a low power output that is externally amplified in low-loss fiber, for a highly stable and scalable architecture.[34] For astrocomb applications, fiber sources require additional effort to achieve the requisite mode spacing and spectral coverage. The repetition rate is typically limited to 250MHz, increasing the demands of FP filtering. Multiple amplification stages are required for broadband operation of fiber oscillator-based astrocombs (i) to compensate for power lost in filter cavities, (ii) to obtain sufficient power for nonlinear broadening, and (iii) for any frequency conversion process. Any amplification

process also produces unwanted effects, such as amplification of side-modes due to four-wave mixing processes. These amplification stages are prone to component damage, requiring replacement on a monthly timescale.

Solid-state laser technology routinely provides sub-50fs pulses with Watt-level average powers and GHz-level repetition rates. The high peak power available directly from the oscillator enables nonlinear frequency conversion without amplification. With an initial repetition rate of 1 GHz the FP cavity filtering demands are relaxed, allowing mode filtering over large instantaneous bandwidths. For astrocomb applications, solid-state lasers have additional engineering challenges that must be overcome for long-term operation. The free-space architecture of the laser cavity introduces additional noise not present in fiber systems, and the high-power pump laser focused into the gain crystal introduces an optical tweezing effect onto the crystal surface which traps particulate matter, decreasing the laser performance over time if not addressed. Turn-key operation is available, but is not typically as robust as in fiber systems.

The following sections review the current state of deployed astrocombs and the progress made towards an ideal calibration source for astronomical spectrographs. For the purposes of discussion the implemented astrocombs are grouped by laser oscillator, with key information summarised in Table 1.

2.2.1 Fiber laser sources

Steinmetz et al.[31] conducted the first experiment to use frequency-comb light for wavelength calibration of an astronomical spectrograph. This proof-of-concept experiment employed a 250-MHz Erbium-doped fiber (Er:fiber) laser frequency comb filtered by a single Fabry-Pérot cavity to produce an astrocomb with a 15-GHz repetition rate. The results from coupling the astrocomb calibration light with sunlight from the German Vacuum Tower Telescope (VTT) onto an astronomical spectrograph empirically confirmed the value of using laser frequency combs for astronomy.

The High Accuracy Radial velocity Planet Searcher (HARPS) optical spectrograph has been used for a number of collaborative campaigns between the European Southern Observatory, Menlo Systems, and the Max-Planck-Institute of Quantum Optics.[35] The collaboration were the first to use an astrocomb to study the orbit of an exoplanet. Wilken et al.[36] studied an already-known, Jupiter-sized exoplanet orbiting the star HD75289 and reported the same level of uncertainty as previous measurements which used a Thorium lamp calibration source. The deployed astrocomb consisted of a 250-MHz Ytterbium-doped fiber (Yb:fiber) source comb, frequency-doubled to partially match the visible coverage of HARPS. The source comb was filtered by up to four Fabry-Pérot cavities to increase the suppression of side-modes for broadband operation and produced an astrocomb with a spectrograph-specific 18-GHz mode spacing. Probst et al.[33] outline the future plans for astrocomb calibration at HARPS, which notably includes introducing heavy automation of the calibration system towards the realisation of a turn-key system, as well as the implementation of an SLM for improved spectral flatness.[32]

The VTT is the setting for a ~5.5 GHz line spacing astrocomb planned for absolute wavelength calibration for measurement of the limb-effect as well as Sun-as-a-star tests.[37] The astrocomb is a 250-MHz Yb:fiber laser (Menlo Systems FC 1000) filtered such that one in every 22 comb lines is transmitted by two identical plano-convex Fabry-Pérot cavities. The laser power is amplified before each of the filter cavities, as well as after the filtering process. The pulses are then compressed to a level permitting efficient nonlinear frequency conversion using second harmonic generation (SHG) and broadening in photonic crystal fiber (PCF). The resultant astrocomb spans 480nm to 640nm and is almost completely fiber coupled, except for free-space sections for SHG and broadening in PCF.

Ycas et al.[38] installed an astrocomb calibration source for the Pathfinder spectrograph at the Hobby-Eberly telescope in Davis Mountains, Texas. The deployed astrocomb followed on from previous lab-based work by Quinlan et al.[39] and uses a 250-MHz Er:fiber source comb, twice filtered by identical Fabry-Pérot cavities. The filter cavities are dither-locked at 50kHz to the peak of transmitted power and had a high finesse of 2000 to produce a 12.5-GHz astrocomb with side-mode suppression of 20–45-dB after amplification and broadening, varying across the broadened 1380nm to 1630nm bandwidth. Comb calibration at the Hobby-Eberly telescope provided a radial velocity precision of <6 cms^{-1} from 1450nm to 1630nm which enabled radial velocity precision at the ~10 ms^{-1} level for the measurement of stellar targets on three echelle orders of the Pathfinder spectrograph.

2.2.2 Solid-state laser sources

The very first lab-based demonstration of an astrocomb was reported by Li *et al.*,[40] and was driven by an octave-spanning Titanium-sapphire (Ti:sapphire) frequency comb with a 1-GHz repetition rate.[41] The laser modes were filtered in a Fabry-Pérot cavity composed of plane-parallel mirrors with $\sim$99% reflectivity over the range 770nm to 920nm and a finesse of $\sim$250. The filter cavity provided up to 40-GHz line spacing, and was stabilized by locking a resonance peak to an atomically-referenced diode laser. The filtered frequency comb was observed on an optical spectrum analyser with 8-GHz resolution ($R \approx 47,000$).

A campaign headed by Harvard University and Massachusetts Institute of Technology (MIT) conducted a series of astrocomb calibration experiments on the Tillinghast Reflector Echelle Spectrograph (TRES) at the Fred Lawrence Whipple Observatory on Mt. Hopkins, Arizona.[30,42,43] First, Li *et al.*[30] modelled and implemented an on-site characterisation technique of the center-of-mass shift due to the unwanted side-mode effects as described in Section 2.1. The astrocomb was built from a fully-locked 1-GHz octave-spanning Ti:sapphire source comb (Octavius, Menlo Systems Inc.) filtered through a single Fabry-Pérot cavity (finesse $\approx$ 180) consisting of two $\sim$98.5% reflective flat mirrors each with a low group delay dispersion of $<$10 fs^2 over the intended spectral range. Benedick *et al.*[42] demonstrated an astrocomb operating over $\sim$10nm FWHM around 410nm, a challenging spectral region not easily accessible by any of the well-established laser gain media either for solid-state or fiber. The astrocomb used the same source comb, now frequency doubled using a BBO crystal. This was filtered by a single Fabry-Pérot cavity with dielectric Bragg-stack mirrors, tuneable from 20–51 GHz line spacing. The previous TRES campaigns were combined to calibrate the red and blue channels of the spectrograph by Phillips *et al.*[43] which provided calibration sensitivity below the 1 ms^{-1} level. The red and blue channels were calibrated using a 1-GHz home-built Ti:sapphire laser with coverage from 700nm to 1000nm,[41] with the blue calibrator being frequency doubled using a BBO crystal. The Fabry-Pérot mirrors were again dielectric Bragg-stack mirrors, correspondingly coated to suit the red and blue astrocombs, producing a 30-GHz red astrocomb ($\sim$100nm FWHM centered at 820nm) and a 50-GHz blue astrocomb ($\sim$10nm FWHM centered at 410nm), both with $\sim$22-dB sidemode-suppression.

The Harvard and MIT partnership followed up the TRES campaigns with the astrocomb calibration of HARPS North (HARPS-N), the high resolution spectrograph at the Roque de los Muchachos Observatory in the Canary Islands. A green astrocomb (500nm to 620nm) with 16-GHz line spacing was deployed by Glenday *et al.*[44] and calibrated to an accuracy of $\sim$6 cms^{-1} in a single exposure of reflected sunlight from an asteroid. The source comb was a 1-GHz Ti:sapphire octave-spanning comb spectrally broadened and shifted to the green in 11-mm-long tapered PCF through the fiber-optic Cherenkov radiation process. The authors state the power per line of the PCF output remained constant over months of operation, with no signs of component degradation. The 16-GHz line spacing was achieved using two Fabry-Pérot cavities in series, consisting of 97.5% reflective, plane-parallel, chirped-mirror pairs, with a slight wedge given to the substrate to diminish back-reflection effects. The side-mode suppression was comprehensively examined in three separate approaches: heterodyne detection, the characterisation technique for the center-of-mass shift, and direct measurement with a Fourier transform spectrometer. All approaches agreed on a value of side-mode suppression at $>$40-dB, which enables RV measurement precision of $<$10 cms^{-1}. The green astrocomb was notably used in a Sun-as-a-star experiment to further understand RV variation associated with stellar noise,[45] and is being used in an ongoing HARPS-N experiment which aims to indirectly detect Venus using its RV signature from spectral measurements of the Sun.[46]

The high resolution echelle spectrograph HRS on the Southern African Large Telescope (SALT) was recently calibrated using an astrocomb by McCracken *et al.*[47] The astrocomb was a 1-GHz Ti:sapphire source comb spectrally broadened in PCF and then spectrally filtered by a single Fabry-Pérot cavity, whose mirrors were complementarily coated for minimal dispersion over the intended bandwidth, to obtain a 15-GHz line spacing across the spectrograph's full wavelength coverage from 550nm to 900nm. The Ti:sapphire-based astrocomb calibration improved the radial velocity accuracy to 10 ms^{-1}, a two-fold improvement in comparison to the resident Thorium-Argon calibration source.

Table 1. Specifications of implemented astrocombs

Project	VTT	HARPS	Hobby-Eberly	TRES red/blue	VTT	HARPS (planned)	HARPS North	SALT
Project Reference	Steinmetz, 2008[31]	Wilken, 2012[36]	Ycas, 2012[38]	Phillips, 2012[43]	Doerr, 2012[37]	Probst, 2014[33]	Glenday, 2015[44]	McCracken, 2017[47]
Source comb	Er:fiber	Yb:fiber	Er:fiber	Ti:sapphire	Yb:fiber	Yb:fiber	Ti:sapphire	Ti:sapphire
Supplier	Menlo Systems	Menlo Systems	home built	home built	Menlo Systems	Menlo Systems	Harvard University	Laser Quantum
Spectrograph coverage (nm)	Solar	378-691	1000-1800	390-900	Solar	378-691	383-690	555-890
Astrocomb coverage (nm)	1530-1600	450-590	1450-1700	780-880/ 400-420	440-600	440-600	500-620	555-890
On-sky measurement	yes	yes	yes	no	no	expected	yes	yes
Source repetition rate (GHz)	0.250	0.250	0.250	1	0.250	0.250	1	1
Spectral flatness (max int./min int.)	100	100	no info	50/60	no info	1.1 expected	5	100
Astrocomb repetition rate (GHz)	15	18	25	30/50	5.5	18	16	15
Filter ratio, M	60	72	100	30/50	22	72	16	15
Precision of f_0	$<10^{-11}$	$<10^{-10}$	no info	no info	$<10^{-12}$	no info	no info	$<10^{-10}$
Precision of f_r	$<10^{-11}$	$<10^{-10}$	$<10^{-9}$	no info	$<10^{-12}$	no info	no info	$<10^{-10}$
Radio frequency standard	Rb clock	Rb clock	GPS	Rb clock	GPS	GPS	GPS	Rb clock
Optical frequency standard	CW laser	CW laser	CW laser	CW laser	no info	CW laser	none	CW laser
Optical reference measurement	wavemeter	wavemeter	wavemeter	none	no info	wavemeter	none	none
Broadening in PCF	no	yes	yes	no	yes	yes	yes	yes
Amplification stages	none	4	2	none	3	3	none	none
Filtering stages	1	4	2	1	2	3	2	1
Sidemode suppression (dB)	46	55	<50	22	94	50	45	20
Fabry-Pérot finesse	2400	390	2000	250	3000	2000	105	155

3. PROPOSED DESIGN OF AN ASTROCOMB FOR HIRES

The wavelength calibration proposal for HIRES spans the specified spectral region of 0.37μm to 2.1μm with a single, traceable source comb. Fiber laser technology is at present seen as unsuitable as it is unable to fulfil the coverage requirements of HIRES set out in Section 1, nor has it yet been proven to be sufficiently reliable to serve as a long-term calibrator due to component lifetime issues, particularly the PCFs. The length of tapered PCF required for spectral broadening in fiber astrocombs are typically tens of centimeters with core diameters of $\sim0.5\mu$m,[33] as compared with more robust tapered PCFs available for shorter-pulse, solid-state astrocombs (with typical lengths of $\sim$1cm).[48] The astrocomb architecture will consist of a Ti:sapphire mode-locked laser with three modules to span the required bandwidth: a second-harmonic generation module, a spectrally-broadened Ti:sapphire module, and a degenerate doubly-resonant OPO (DRO) module, outlined in Figure 2.

Below we describe each of these modules, along with subsequent Fabry-Pérot filter cavity stages, spectral flattening architecture, and our approach for broadband modal subset identification.
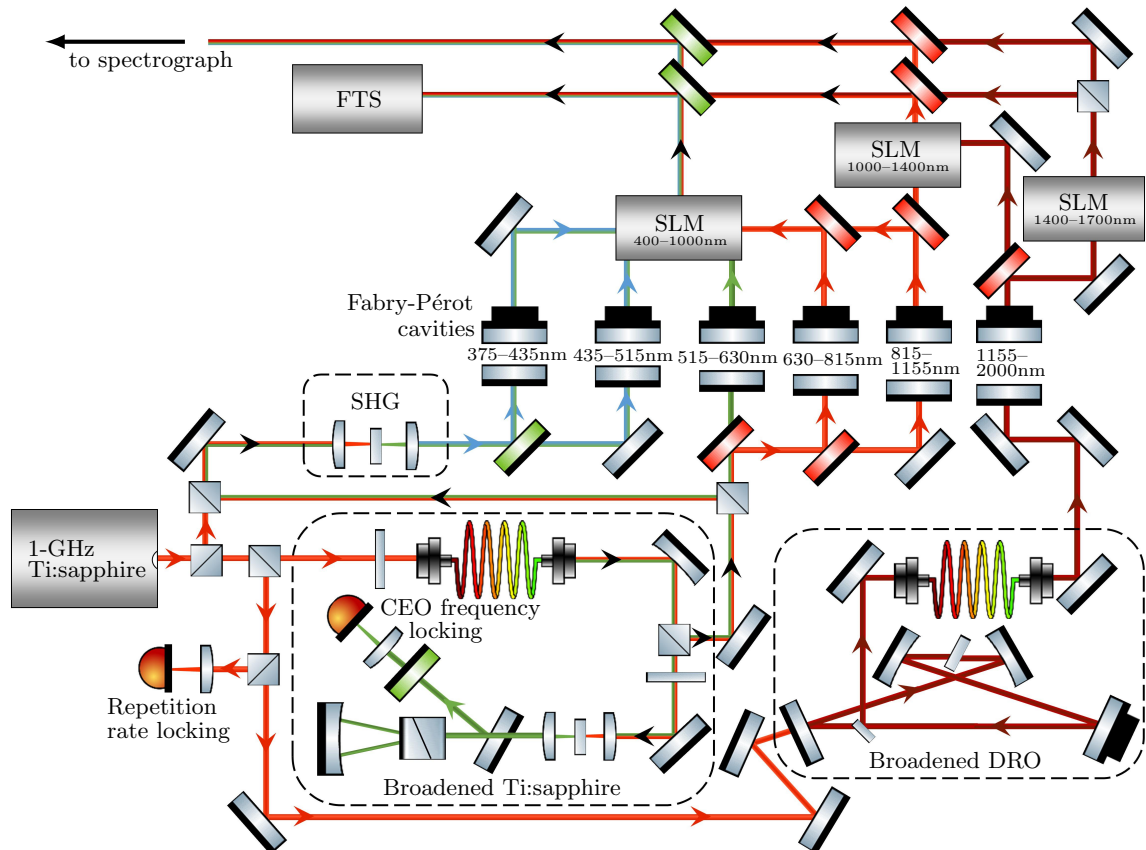

Figure 2. Proposed architecture of the LFC calibrator for HIRES.

3.1 Source Comb

The proposed source comb is a robust, turn-key 1-GHz Ti:sapphire laser, selected for its high average power and short pulses, negating the requirement for complicated amplification schemes. The native spectral coverage of the Ti:sapphire laser is $\sim$785–815 nm with typical pulse widths of $\sim$30 fs. The repetition rate of the laser is stabilized by comparing a high harmonic of $f_{\rm rep}$ with an RF synthesizer, with cavity length control achieved using a pair of intracavity piezoelectric transducers. Carrier-envelope offset frequency detection is carried out using a common-path f-to-$2f$ interferometer,[49] providing common-mode noise rejection in a compact footprint. The offset frequency is controlled through diode-current modulation, which enables long-term high-bandwidth locking.

3.2 Wavelength Coverage

The shorter wavelength range of the E-ELT spectrograph will be matched by frequency doubling a portion of the Ti:sapphire laser power in a suitable nonlinear crystal, achieving 390–410nm of spectral coverage. The PCF in the f-to-$2f$ interferometer provides a supercontinuum which spans ∼500–1100nm, however only components at 530nm and 1060nm are required for f_{CEO} detection. The remainder of the supercontinuum can therefore be exploited in the astrocomb. The calibration range from 410–500nm is demanding as it is unsuited for any established mode-locked laser gain media, including Ti:sapphire. To cover this awkward spectral region, we look to take a similar approach to Phillips *et al.* when calibrating the blue channel of TRES[43] by which we frequency double part of the supercontinuum from the PCF. Spectral coverage in the mid-IR from around 1100nm to 2100nm will be achieved by pumping a degenerate doubly-resonant optical parametric oscillator (DRO) with the Ti:sapphire source comb, and broadening the resulting spectrum centered at 1.6μm in a highly nonlinear fiber. At degeneracy the DRO acts as a broadband wavelength converter that maintains the comb structure of the pump comb, with the IR comb remaining intrinsically locked to the source comb laser.[50]

3.3 Mode Filtering

A number of Fabry-Pérot cavities will be used to match the different wavelength-dependences of the many echelle orders. A practical solution is to divide the 0.37–2.1μm bandwidth of the spectrograph into spectral regions that cover equal frequency bandwidths, exploiting the fact that the dielectric mirror coatings intrinsically operate in frequency rather than wavelength space, and striking a balance between bandwidth, coating engineering requirements, and overall complexity.

3.4 Flat Spectral Intensity Distribution

As discussed in Section 2.1, spectral flatness is desirable for high-precision radial velocity measurements, but has not yet been demonstrated for an astrocomb. We propose to implement three SLMs designed for spectral shaping in the visible-NIR-IR, however there will be limited capability to flatten below 400nm and above 1700nm, due to the lack of suitable SLMs operating at these wavelengths. This can be addressed through the use of dielectric mirror coatings with tailored reflection/transmission profiles, designed to provide coarse spectral flattening over limited bandwidths.

3.5 Comb Diagnostics and Absolute Traceability

In Section 2.1 we described a common approach to remove the modal subset ambiguity issue, namely the pinning of a comb tooth to a narrow-line diode laser. This technique is not viable for broadband astrocombs that employ multiple Fabry-Pérot cavities, as suitable narrow-line diode lasers (and traceable atomic transitions) are not universally throughout the UV to the IR. Our approach is to use a broadband Fourier transform spectrometer (FTS) with resolution sufficient for mode-subset identification.

The FTS design is similar to that employed in Zhang *et al.*,[51] which used a folded push-pull configuration to achieve an unapodized 750-MHz resolution in a compact footprint. The FTS employs all metallic optics for broadband operation, and balanced detection for improved signal-to-noise. The path length of the FTS is calibrated using a narrow-line diode laser stabilized to an atomic transition in rubidium, providing absolute measurement traceability. Increasing the resolution below 500 MHz with a longer-travel linear motor stage would enable unambiguous comb mode identification of the 1-GHz source comb, beyond the aliasing uncertainty of the f-to-$2f$ system. Alternatively, precision windowing of the interferogram trace can provide sub-nominal resolution of the comb lines for measurements providing increased accuracy in the identification of the filtered subset, with a shorter required scan length.[52,53]

For complete system traceability, all RF synthesizers will be referenced to GPS disciplined microwave clocks.

4. SUMMARY

We have proposed a broadband astrocomb architecture as a calibration source for HIRES fulfilling the requirements for all science cases outlined in Section 1, with consideration given to previous astrocomb calibration campaigns on astronomical spectrographs in Section 2.2. The proposed astrocomb will be driven by a single source comb, branching out to three frequency conversion modules for full wavelength coverage of the spectrograph, as illustrated in Figure 2. Multiple low-dispersion Fabry-Pérot cavities will achieve the required mode spacings, and spatial light modulators will provide spectral flattening. By employing a low-noise GPS disciplined microwave clock and an atomically referenced diode laser for absolute traceability, the astrocomb will enable cms^{-1} precision RV measurements for next-generation exoplanet hunting campaigns.

ACKNOWLEDGMENTS

REFERENCES

[1] Marconi, A., Di Marcantonio, P., D'Odorico, V., Cristiani, S., Maiolino, R., Oliva, E., Origlia, L., Riva, M., Valenziano, L., Zerbi, F. M., et al., "EELT-HIRES the high-resolution spectrograph for the E-ELT," *Proc. SPIE* **9908**, 990823 (2016).

[2] Ramsay, S., D'Odorico, S., Casali, M., González, J. C., Hubin, N., Kasper, M., Käufl, H. U., Kissler-Patig, M., Marchetti, E., Paufique, J., Pasquini, L., Siebenmorgen, R., Richichi, A., Vernet, J., and Zerbi, F. M., "An overview of the E-ELT instrumentation programme," *Proc. SPIE* **7735**, 773524 (2010).

[3] Pasquini, L., Cristiani, S., Garcia-Lopez, R., Haehnelt, M., and Mayor, M., "CODEX: An Ultra-stable High Resolution Spectrograph for the E-ELT," *ESO: The Messenger 140* (2010).

[4] Origlia, L., Oliva, E., Maiolino, R., Gustafsson, B., Piskunov, N., Kochucov, O., Vanzi, L., Minniti, D., Zoccali, M., Hatzes, A., and Guenther, E., "SIMPLE: a high-resolution near-infrared spectrometer for the E-ELT," *Proc. SPIE* **7735**, 77352B (2010).

[5] Maiolino, R. and Haehnelt, M. and Murphy, M. T. and Queloz, D. and Origlia, L. et al., "A community science case for E-ELT HIRES." arXiv:1310.3163 [astro-ph.IM] (2013).

[6] Wildi, F., Chazelas, B., and Pepe, F., "A passive cost-effective solution for the high accuracy wavelength calibration of radial velocity spectrographs," *Proc. SPIE* **8446**, 84468E (2012).

[7] Pepe, F., Molaro, P., Cristiani, S., Rebolo, R., Santos, N., Dekker, H., Mégevand, D., Zerbi, F., Cabral, A., Di Marcantonio, P., et al., "ESPRESSO: The next European exoplanet hunter," *Astronomische Nachrichten* **335**(1), 8–20 (2014).

[8] Rupprecht, G., Pepe, F., Mayor, M., Queloz, D., Bouchy, F., et al., "The exoplanet hunter HARPS: performance and first results," *Proc. SPIE* **5492**, 148–159 (2004).

[9] Lovis, C., Pepe, F., Bouchy, F., Lo Curto, G., Mayor, M., Pasquini, L., Queloz, D., Rupprecht, G., Udry, S., and Zucker, S., "The exoplanet hunter HARPS: unequalled accuracy and perspectives toward 1 cm s^{-1} precision," *Proc. SPIE* **6269**, 62690P (2006).

[10] Quirrenbach, A., Amado, P. J., Caballero, J. A., Mundt, R., Reiners, A., Ribas, I., Seifert, W., et al., "CARMENES instrument overview," *Proc. SPIE* **9147**, 91471F (2014).

[11] Huke, P., Origlia, L., Riva, M., Pepe, F., Reiners, A., Charsley, J. M., McCracken, R. A., Reid, D. T., Kowzan, G., Maslowski, P., Korhonen, H., Broeg, C., Dolon, F., Boisse, I., Disseau, K., Perruchot, S., Ottogalli, S., and Bandy, T., "Phase A: Calibration concepts for HIRES," in [*Optical Measurement Systems for Industrial Inspection X*], *Proc. SPIE* , 10329–91 (2017).

[12] Cundiff, S. T. and Ye, J., "Colloquium: Femtosecond optical frequency combs," *Rev. Mod. Phys.* **75**, 325–342 (2003).

[13] Diddams, S. A., Jones, D. J., Ye, J., Cundiff, S. T., Hall, J. L., Ranka, J. K., Windeler, R. S., Holzwarth, R., Udem, T., and Hänsch, T. W., "Direct link between microwave and optical frequencies with a 300 THz femtosecond laser comb," *Phys. Rev. Lett.* **84**, 5102–5105 (2000).

[14] Jones, D. J., Diddams, S. A., Ranka, J. K., Stentz, A., Windeler, R. S., Hall, J. L., and Cundiff, S. T., "Carrier-envelope phase control of femtosecond mode-locked lasers and direct optical frequency synthesis," *Science* **288**(5466), 635–639 (2000).

[15] Murphy, M. T., Udem, T., Holzwarth, R., Sizmann, A., Pasquini, L., Araujo-Hauck, C., Dekker, H., D'Odorico, S., Fischer, M., Hänsch, T., and Manescaur, A., "High-precision wavelength calibration of astronomical spectrograps with laser frequency combs," *Mon. Not. R. Aston. Soc.* **380**, 839–847 (2007).

[16] http://www.toptica.com/products/frequency-combs/dfc-core-dfc-core/. Accessed: 1 April 2017.

[17] http://www.menlosystems.com/products/optical-frequency-combs/. Accessed: 1 April 2017.

[18] http://www.laserquantum.com/products/detail.cfm?id=100. Accessed: 1 April 2017.

[19] Bartels, A., Heinecke, D., and Diddams, S. A., "10-GHz self-referenced optical frequency comb," *Science* **326**, 681–681 (2009).

[20] Endo, M., Ito, I., and Kobayashi, Y., "Direct 15-GHz mode-spacing optical frequency comb with a Kerr-lens mode-locked Yb:Y2O3 ceramic laser," *Opt. Express* **23**, 1276–1282 (2015).

[21] Yi, X., Vahala, K., Li, J., Diddams, S., Ycas, G., Plavchan, P., Leifer, S., Sandhu, J., Vasisht, G., Chen, P., Gao, P., Gagne, J., Furlan, E., Bottom, M., Martin, E. C., Fitzgerald, M. P., Doppmann, G., and Beichmann, C., "High-precision calibration of spectrographs," *Nature Communications* **7**, 10436 (2016).

[22] Del'Haye, P., Arcizet, O., Schliesser, A., Holzwarth, R., and Kippenberg, T. J., "Full stabilization of a microresonator-based optical frequency comb," *Phys. Rev. Lett.* **101**, 053903 (2008).

[23] Reiners, A., Banyal, R. K., and Ulbrich, R. G., "A laser-lock concept to reach cms^{-1}-precision in Doppler experiments with Fabry-Pérot wavelength calibrators," *A&A* **569**, A77 (2014).

[24] Braje, D. A., Kirchner, M. S., Osterman, S., Fortier, T., and Diddams, S. A., "Astronomical spectrograph calibration with broad-spectrum frequency combs," *The European Physical Journal D* **48**, 57–66 (2008).

[25] Steinmetz, T., Wilken, T., Araujo-Hauck, C., Holzwarth, R., Hänsch, T. W., and Udem, T., "Fabry–Pérot filter cavities for wide-spaced frequency combs with large spectral bandwidth," *Applied Physics B* **96**, 251–256 (2009).

[26] Chang, G., Li, C.-H., Phillips, D. F., Szentgyorgyi, A., Walsworth, R. L., and Kärtner, F. X., "Optimization of filtering schemes for broadband astro-combs," *Opt. Express* **20**, 24987–25013 (2012).

[27] Li, C.-H., Chang, G., Glenday, A. G., Langellier, N., Zibrov, A., Phillips, D. F., Kärtner, F. X., Szentgyorgyi, A., and Walsworth, R. L., "Conjugate Fabry-Perot cavity pair for improved astro-comb accuracy," *Opt. Lett.* **37**, 3090–3092 (2012).

[28] Hackett, D., Ycas, G., and Diddams, S., "A low-dispersion Fabry-Perot cavity for generation of a 30 GHz astrocomb spanning 140 nm," *CLEO 2015 Conference Digest*, SW4G.8 (2015).

[29] Chen, L.-J., Chang, G., Li, C.-H., Benedick, A. J., Philips, D. F., Walsworth, R. L., and Kärtner, F. X., "Broadband dispersion-free optical cavities based on zero group delay dispersion mirror sets," *Opt. Express* **18**, 23204–23211 (2010).

[30] Li, C.-H., Glenday, A. G., Benedick, A. J., Chang, G., Chen, L.-J., Cramer, C., Fendel, P., Furesz, G., Kärtner, F. X., Korzennik, S., Phillips, D. F., Sasselov, D., Szentgyorgyi, A., and Walsworth, R. L., "In-situ determination of astro-comb calibrator lines to better than 10 cm s^{-1}," *Opt. Express* **18**, 13239–13249 (2010).

[31] Steinmetz, T., Wilken, T., Araujo-Hauck, C., Holzwarth, R., Hänsch, T. W., Pasquini, L., Manescau, A., D'Odorico, S., Murphy, M. T., Kentischer, T., Schmidt, W., and Udem, T., "Laser frequency combs for astronomical observations," *Science* **321**, 1335–1337 (2008).

[32] Probst, R. A., Steinmetz, T., Wilken, T., Wong, G. K. L., Hundertmark, H., Stark, S. P., Russell, P. S. J., Hänsch, T. W., Holzwarth, R., and Udem, T., "Spectral flattening of supercontinua with a spatial light modulator," *Proc. SPIE* **8864**, 88641Z (2013).

[33] Probst, R. A. et al., "A laser frequency comb featuring sub-cm/s precision for routine operation on HARPS," *Proc. SPIE* **9147**, 91471C (2014).

[34] Lezius, M. et al., "Space-borne frequency comb metrology," *Optica* **3**(12), 1381–1387 (2016).

[35] Wilken, T., Lovis, C., Manescau, A., Steinmetz, T., Pasquini, L., Lo Curto, G., Hänsch, T. W., Holzwarth, R., and Udem, T., "High-precision calibration of spectrographs," *Mon. Not. R. Aston. Soc.* **405**, L16–L20 (2010).

[36] Wilken, T., Lo Curto, G., Probst, R. A., Steinmetz, T., Manescau, A., Pasquini, L., González Hernández, J., Rebolo, R., Hänsch, T., Udem, T., and Holzwarth, R., "A spectrograph for exoplanet observations calibrated at the centimetre-per-second level," *Nature* **485**, 611–614 (2012).

[37] Doerr, H.-P., Kentischer, T. J., Steinmetz, T., Probst, R. A., Franz, M., Holzwarth, R., Udem, T., Hänsch, T. W., and Schmidt, W., "Performance of a laser frequency comb calibration system with a high-resolution solar echelle spectrograph," *Proc. SPIE* **8450**, 84501G (2012).

[38] Ycas, G. G., Quinlan, F., Diddams, S. A., Osterman, S., Mahadevan, S., Redman, S., Terrien, R., Ramsey, L., Bender, C. F., Botzer, B., and Sigurdsson, S., "Demonstration of on-sky calibration of astronomical spectra using a 25 GHz near-IR laser frequency comb," *Opt. Express* **20**, 6631–6643 (2012).

[39] Quinlan, F., Ycas, G., Osterman, S., and Diddams, S. A., "A 12.5 GHz-spaced optical frequency comb spanning >400nm for near-infrared astronomical spectrograph calibration," *Review of Scientific Instruments* **81**, 063105 (2010).

[40] Li, C.-H., Benedick, A. J., Fendel, P., Glenday, A., Kärtner, F., Phillips, D. F., Sasselov, D., Szentgyorgyi, A., and Walsworth, R., "A laser frequency comb that enables radial velocity measurements with a precision of 1 cm s^{-1}," *Nature* **452**, 610–612 (2008).

[41] Benedick, A., Birge, J., Ell, R., Mücke, O. D., Sander, M., and Kärtner, F. X., "Octave spanning 1GHz Ti:sapphire oscillator for HeNe CH4-based frequency combs and clocks," *CLEO/Europe and IQEC 2007 Conference Digest* , CF3_1 (2007).

[42] Benedick, A. J., Chang, G., Birge, J. R., Chen, L.-J., Glenday, A. G., Li, C.-H., Phillips, D. F., Szentgyorgyi, A., Korzennik, S., Furesz, G., Walsworth, R. L., and Kärtner, F. X., "Visible wavelength astro-comb," *Opt. Express* **18**, 19175–19184 (2010).

[43] Phillips, D. F., Glenday, A. G., Li, C.-H., Cramer, C., Furesz, G., Chang, G., Benedick, A. J., Chen, L.-J., Kärtner, F. X., Korzennik, S., Sasselov, D., Szentgyorgyi, A., and Walsworth, R. L., "Calibration of an astrophysical spectrograph below 1 m/s using a laser frequency comb," *Opt. Express* **20**, 13711–13726 (2012).

[44] Glenday, A., Li, C.-H., Langellier, N., Chang, G., Chen, L.-J., Furesz, G., Zibrov, A., Kärtner, F., Phillips, D., Sasselov, D., Szentgyorgyi, A., and Walsworth, R., "Operation of a broadband visible-wavelength astro-comb with a high-resolution astrophysical spectrograph," *Optica* **2**, 250–254 (2015).

[45] Dumusque, X., Glenday, A., Phillips, D. F., et al., "HARPS-N observes the Sun as a star," *The Astrophysical Journal Letters* **814**(2), L21 (2015).

[46] Phillips, D. F., Glenday, A. G., Dumusque, X., et al., "An astro-comb calibrated solar telescope to search for the radial velocity signature of Venus," *Proc. SPIE* **9912**, 99126Z (2016).

[47] McCracken, R. A., Depagne, É., Kuhn, R. B., Erasmus, N., Crause, L. A., and Reid, D. T., "Wavelength calibration of a high resolution spectrograph with a partially stabilized 15-GHz astrocomb from 550 to 890 nm," *Opt. Express* **25**(6), 6450–6460 (2017).

[48] Langellier, N., Li, C.-H., Glenday, A. G., Chang, G., Chen, H.-W., Lim, J., Furesz, G., Kärtner, F., Phillips, D. F., Sasselov, D., Szentgyorgyi, A., and Walsworth, R., "Green astro-comb for HARPS-N," *Proc. SPIE* **9147**, 91478N (2014).

[49] Tsatourian, V., Margolis, H. S., Marra, G., Reid, D. T., and Gill, P., "Common-path self-referencing interferometer for carrier-envelope offset frequency stabilization with enhanced noise immunity," *Opt. Lett.* **35**(8), 1209–1211 (2010).

[50] Wong, S. T., Vodopyanov, K. L., and Byer, R. L., "Self-phase-locked divide-by-2 optical parametric oscillator as a broadband frequency comb source," *J. Opt. Soc. Am. B* **27**(5), 876–882 (2010).

[51] Zhang, Z., Balskus, K., McCracken, R. A., and Reid, D. T., "Mode-resolved 10-GHz frequency comb from a femtosecond optical parametric oscillator," *Opt. Lett.* **40**(12), 2692–2695 (2015).

[52] Rutkowski, L., Maslowski, P., Johansson, A. C., Khodabakhsh, A., and Foltynowicz, A., "Optical frequency comb Fourier transform spectroscopy with sub-nominal resolution." arXiv:1612.04808 [physics.ins-det] (2016).

[53] Maslowski, P., Lee, K. F., Johansson, A. C., Khodabakhsh, A., Kowzan, G., Rutkowski, L., Mills, A. A., Mohr, C., Jiang, J., Fermann, M. E., and Foltynowicz, A., "Surpassing the path-limited resolution of Fourier-transform spectrometry with frequency combs," *Phys. Rev. A* **93**, 021802 (2016).

Appendix D

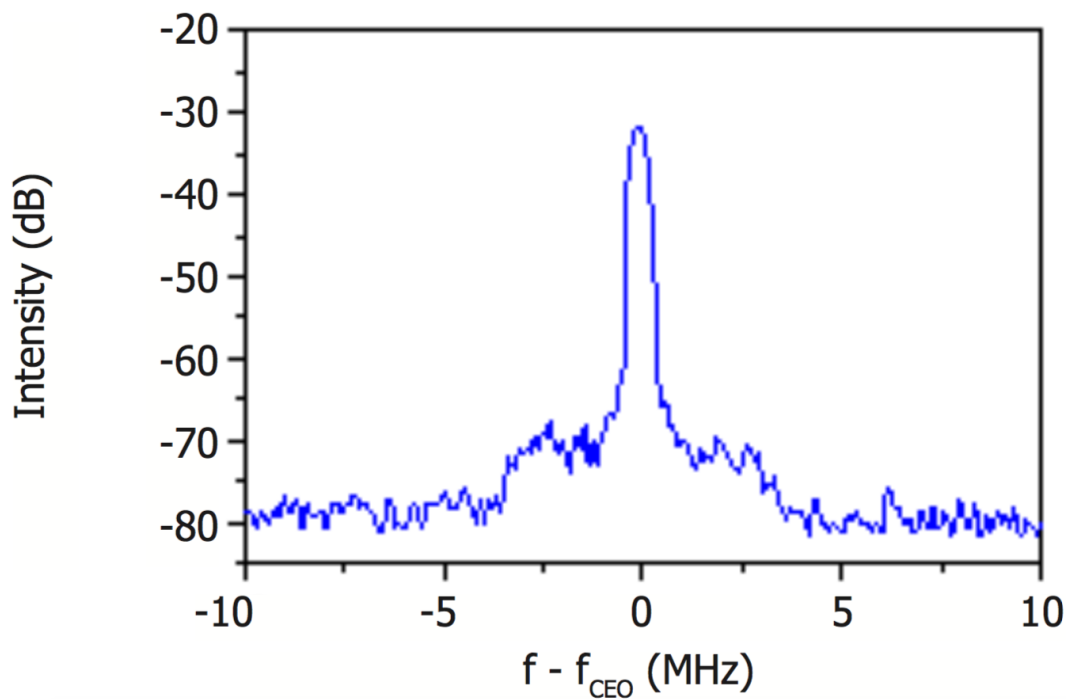# Profile of Carrier-envelope-offset beat achieved by Laser Quantum

Figure D.1: The 1-GHz taccor Ti:sapphire laser carrier-envelope-offset beat frequency measured at Laser Quantum.

Appendix E

GUI Instruction Manual for Fourier-Transform Spectrometer Data Retrieval Software

Upload data into work space

To start click 'New file'. A pop-up window enables the user to select the raw data file you wish to investigate. The contents of the file require an array named 'Data0'
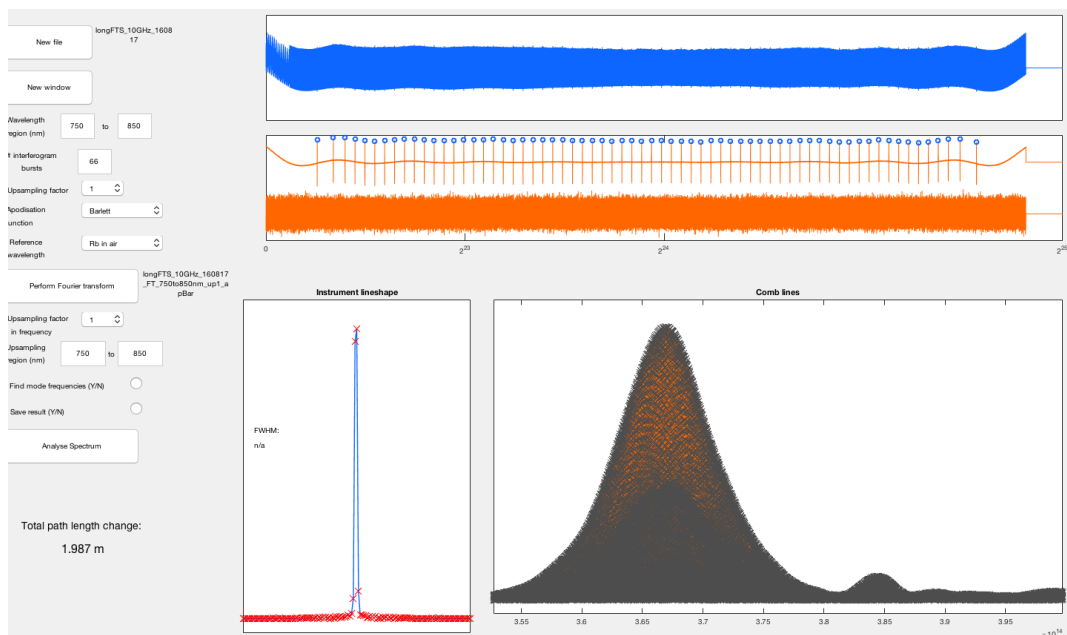

Figure E.1: GUI for FTS data retrieval.

Figure E.2: GUI for FTS data retrieval: Fourier transform options.

of size N×L, where N is the number of channels (N=2 if reference and single in-terferogram signal, N=3 for balanced detection) and L is the length of the sampled points. The file name of the file chosen will be displayed underneath the 'New file' button. The code will then perform a low-pass filter on the input signals and then detect which of the signals is the reference by a simple maximum algorithm which works due to the reference signal being a single frequency and, as such, many points are close to the maximum point in comparison with the interferogram signal. The reference signal will appear in the top figure, and the interferogram signal(s) will appear in the figure below. If a window has previously been chosen for the data file, the window will be displayed by red lines at the extremes of the window. Similarly, if the number of interferogram bursts has previously been set and a Fourier trans-form performed, the interferogram signal(s) in the second figure will show green rings indicating the algorithms ability to detect the interferogram bursts.

Remove data recorded before and after scan from analysis

Click 'New window' on initial investigation. If window selection has already been successfully chosen there is no need to select a new window. However, if the user is investigating a new raw data file, or they wish to overwrite a previous window,
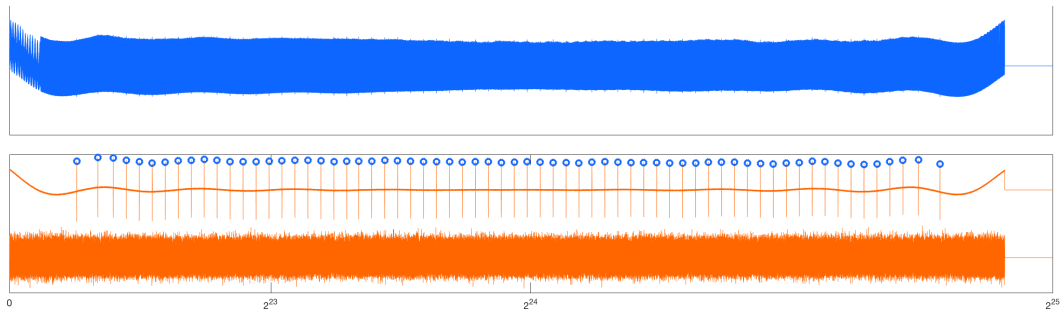
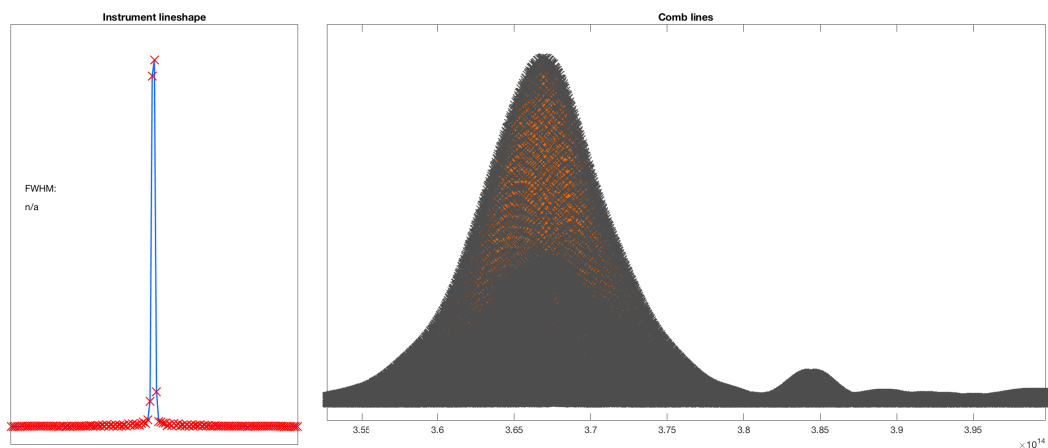**Figure E.3:** GUI for FTS data retrieval: Fourier transform options.

Figure E.4: GUI for FTS data retrieval: Retrieved spectrum.

perform this procedure. On clicking 'New window' a ginput cursor will appear on the figure and prompts will direct the user to choose the window extremes. The prompts will direct you to first pick the left window frame by twice zooming into a region for accurate placement. Then the same procedure is used to choose the right window frame. The selected window will be displayed by red lines at the extremes of the window.

Fast Fourier transform analysis

Select Fourier-transform settings

The software allows the user to specify the (i) wavelength region to keep from the Fourier analysis, (ii) upsampling factor by which the raw data signals can be better formatted for the zero-crossing algorithm, (iii) apodisation function to effect the instrument line shape, (iv) reference wavelength in air.

Figure E.5: GUI for FTS data retrieval: Spectrum analysis options.

Input number of interferogram bursts

The number of interferogram bursts must be specified for the software to run successfully. This is necessary to remove any back-reflections present in the interferograms. If the number of interferogram bursts has previously been specified for the data file, the previously-specified number will appear in the box when the file loads.

Perform Fourier transform

On clicking 'Perform Fourier transform' the majority of the analysis occurs; namely: (i) a zero-crossing algorithm is applied to the reference signal to obtain the path length difference, (ii) the interferogram signal(s) is redistributed linearly with the acceleration profile from the zero-crossing algorithm, (iii) a fast-fourier transform is computed on both the reference and interferogram signals After the Fourier analysis, the spectral data along with the acceleration profile of the scan is saved in the host folder with a file name which contains the raw data file name with the selected settings appended. The instrument lineshape, the path length profile, and the signal spectrum are then plotted in the bottom three figures, respectively.
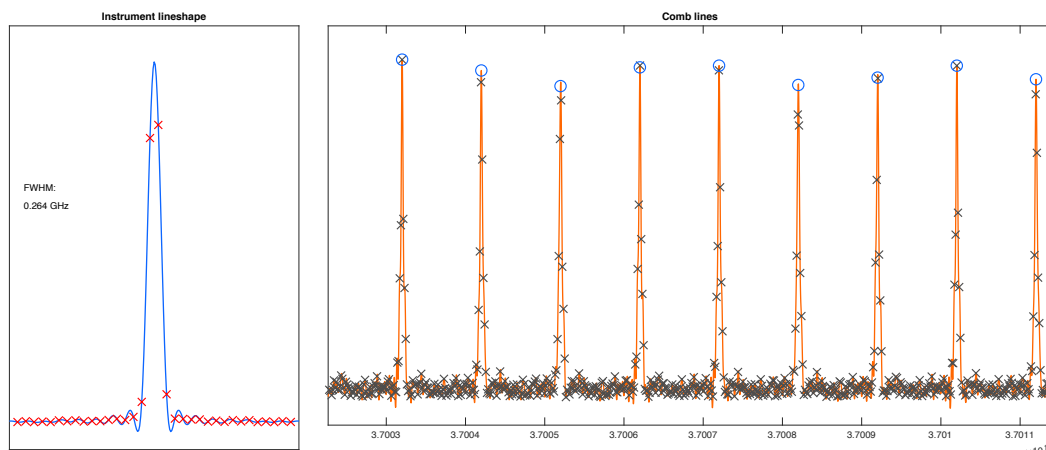
Figure E.6: GUI for FTS data retrieval: Spectrum analysis.

Analyse spectrum

Select analysis settings

Analysis software enables the user to specify the (i) wavelength region to analyse further, (ii) upsampling factor in frequency by which the reference and signal spectra can better reveal the instrument line shape, (iii) whether to save the resultant spectra.

Assess results of FFT

Click 'Analyse spectra'. A pop-up window enables the user to select the spectra data file you wish to investigate from the 'Fast Fourier transform analysis' process. If the spectra data file already exists the user can start at the 'Analyse spectrum' section. The spectral analysis software process performs the following: (i) the interferogram spectrum is windowed to match the chosen upsampling region (ii) the reference and interferogram spectra are upsampled by the frequency upsample factor (iii) a simple zero-crossing algorithm is used to ascertain the full-width at half-maximum of the unresolved reference line which is taken to be the resolution of the instrument. (iv) if the 'Save result' button is activated, the resultant spectra will be saved to a file in the host folder with the file name similar to the original spectra file with the selected settings appended. The save file contains the following arrays: 'r_orig' - the original reference spectrum, 'r_up' - the upsampled reference spectrum, 'c_orig'

- the original interferogram spectrum, 'c_up' - the upsampled interferogram spectrum, and 'fwhm' - the linewidth of the unresolved reference line. Note each of the spectrum arrays contains the frequency content in the first column and the intensity information in the second column. The upsampled instrument lineshape, the path length profile, and the upsampled signal spectrum are then plotted in the bottom three figures, respectively.

Bibliography

[1] J. M. Charsley, R. A. McCracken, L. Reid, and D. T. Reid, "Broadband Fourier-transform spectrometer enabling modal subset identification in Fabry-Pérot-based astrocombs," Opt. Express **25**, 19251–19262 (2017).

[2] R. A. McCracken, J. M. Charsley, and D. T. Reid, "A decade of astrocombs: recent advances in frequency combs for astronomy," Opt. Express **25**, 15058–15078 (2017).

[3] J. M. Charsley, R. A. McCracken, D. T. Reid, G. Kowzan, P. Maslowski, A. Reiners, and P. Huke, "Comparison of astrophysical laser frequency combs with respect to the requirements of HIRES," in "Optical Measurement Systems for Industrial Inspection X," (2017), Proc. SPIE 10329, pp. 10329–12.

[4] P. Huke, L. Origlia, M. Riva, F. Pepe, A. Reiners, J. M. Charsley, R. A. McCracken, D. T. Reid, G. Kowzan, P. Maslowski, H. Korhonen, C. Broeg, F. Dolon, I. Boisse, K. Disseau, S. Perruchot, S. Ottogalli, and T. Bandy, "Phase A: Calibration concepts for HIRES," in "Optical Measurement Systems for Industrial Inspection X," (2017), Proc. SPIE 10329, pp. 10329–91.

[5] M. T. Murphy, T. Udem, R. Holzwarth, A. Sizmann, L. Pasquini, C. Araujo-Hauck, H. Dekker, S. D'Odorico, M. Fischer, T. Hänsch, and A. Manescaur, "High-precision wavelength calibration of astronomical spectrographs with laser frequency combs," Mon. Not. R. Aston. Soc. **380**, 839–847 (2007).

[6] T. Steinmetz, T. Wilken, C. Araujo-Hauck, R. Holzwarth, T. W. Hänsch, L. Pasquini, A. Manescau, S. D'Odorico, M. T. Murphy, T. Kentischer,

W. Schmidt, and T. Udem, "Laser frequency combs for astronomical observations," Science **321**, 1335–1337 (2008).

[7] F. Roques and J. Schneider, "The exoplanet encyclopaedia," `http://www.exoplanet.eu/catalog`. Accessed: 7 May 2017.

[8] D. A. Fischer, G. Anglada-Escude, P. Arriagada, R. V. Baluev, J. L. Bean, F. Bouchy, L. A. Buchhave, T. Carroll, A. Chakraborty, J. R. Crepp, R. I. Dawson, S. A. Diddams, X. Dumusque, J. D. Eastman, M. Endl, P. Figueira, E. B. Ford, D. Foreman-Mackey, P. Fournier, G. Frsz, B. S. Gaudi, P. C. Gregory, F. Grundahl, A. P. Hatzes, G. Hbrard, E. Herrero, D. W. Hogg, A. W. Howard, J. A. Johnson, P. Jorden, C. A. Jurgenson, D. W. Latham, G. Laughlin, T. J. Loredo, C. Lovis, S. Mahadevan, T. M. McCracken, F. Pepe, M. Perez, D. F. Phillips, P. P. Plavchan, L. Prato, A. Quirrenbach, A. Reiners, P. Robertson, N. C. Santos, D. Sawyer, D. Segransan, A. Sozzetti, T. Steinmetz, A. Szentgyorgyi, S. Udry, J. A. Valenti, S. X. Wang, R. A. Wittenmyer, and J. T. Wright, "State of the field: Extreme precision radial velocities," Publications of the Astronomical Society of the Pacific **128**, 066001 (2016).

[9] G. W. Marcy and R. P. Butler, "Precision radial velocities with an iodine absorption cell," Publications of the Astronomical Society of the Pacific **104**, 270 (1992).

[10] R. P. Butler, G. W. Marcy, E. Williams, C. McCarthy, P. Dosanjh, and S. S. Vogt, "Attaining Doppler Precision of 3 m s^{-1}," PASP **108**, 500 (1996).

[11] H. Leopardi, J. Davila-Rodriguez, F. Quinlan, S. Diddams, and T. Fortier, "Er:fiber frequency comb for synthesis of optical frequencies at the 10^{-18} level," in "2016 IEEE Photonics Conference (IPC)," (2016), pp. 186–187.

[12] D. J. Jones and S. T. Cundiff, "Optical frequency electronics," IEEE Circuits and Devices Magazine **19**, 28–35 (2003).

[13] D. E. Spence, P. N. Kean, and W. Sibbett, "60-fsec pulse generation from a self-mode-locked Ti:sapphire laser," Opt. Lett. **16**, 42–44 (1991).

[14] L. Spinelli, B. Couillaud, N. Goldblatt, and D. K. Negus, "Starting and Generation of Sub-100fs Pulses in Ti:Al2O3 by Self-Focusing," in "Conference on Lasers and Electro-Optics," (Optical Society of America, 1991), p. CPD7.

[15] F. Salin, M. Piché, and J. Squier, "Mode locking of Ti:Al2O3 lasers and self-focusing: a Gaussian approximation," Opt. Lett. **16**, 1674–1676 (1991).

[16] T. Brabec, C. Spielmann, P. F. Curley, and F. Krausz, "Kerr lens mode locking," Opt. Lett. **17**, 1292–1294 (1992).

[17] J. Herrmann, "Theory of Kerr-lens mode locking: role of self-focusing and radially varying gain," J. Opt. Soc. Am. B **11**, 498–512 (1994).

[18] I. P. Christov, M. M. Murnane, H. C. Kapteyn, and V. D. Stoev, "Mode locking with a compensated space–time astigmatism," Opt. Lett. **20**, 2111–2113 (1995).

[19] J. Reichert, R. Holzwarth, T. Udem, and T. Hänsch, "Measuring the frequency of light with mode-locked lasers," Optics Communications **172**, 59–68 (1999).

[20] T. Udem, R. Holzwarth, and T. W. Hänsch, "Optical frequency metrology," Nature **416**, 233–237 (2002).

[21] L.-S. Ma, Z. Bi, A. Bartels, L. Robertsson, M. Zucco, R. S. Windeler, G. Wilpers, C. Oates, L. Hollberg, and S. A. Diddams, "Optical Frequency Synthesis and Comparison with Uncertainty at the 10^{-19} Level," Science **303**, 1843–1845 (2004).

[22] H. Telle, G. Steinmeyer, A. Dunlop, J. Stenger, D. Sutter, and U. Keller, "Carrier-envelope offset phase control: A novel concept for absolute optical frequency measurement and ultrashort pulse generation," Applied Physics B **69**, 327–332 (1999).

[23] D. J. Jones, S. A. Diddams, J. K. Ranka, A. Stentz, R. S. Windeler, J. L. Hall, and S. T. Cundiff, "Carrier-envelope phase control of femtosecond mode-

locked lasers and direct optical frequency synthesis," Science **288**, 635–639 (2000).

[24] T. A. Birks, J. C. Knight, and P. S. J. Russell, "Endlessly single-mode photonic crystal fiber," Opt. Lett. **22**, 961–963 (1997).

[25] J. K. Ranka, R. S. Windeler, and A. J. Stentz, "Visible continuum generation in air–silica microstructure optical fibers with anomalous dispersion at 800 nm," Opt. Lett. **25**, 25–27 (2000).

[26] J. L. Hall and J. Ye, "A new era of frequency standards and optical frequency measurement," Opt. Photon. News **12**, 44–50 (2001).

[27] R. Ell, U. Morgner, F. X. Kärtner, J. G. Fujimoto, E. P. Ippen, V. Scheuer, G. Angelow, T. Tschudi, M. J. Lederer, A. Boiko, and B. Luther-Davies, "Generation of 5-fs pulses and octave-spanning spectra directly from a Ti:sapphire laser," Opt. Lett. **26**, 373–375 (2001).

[28] W. J. Wadsworth, A. Ortigosa-Blanch, J. C. Knight, T. A. Birks, T.-P. M. Man, and P. S. J. Russell, "Supercontinuum generation in photonic crystal fibers and optical fiber tapers: a novel light source," J. Opt. Soc. Am. B **19**, 2148–2155 (2002).

[29] F. W. Helbing, G. Steinmeyer, U. Keller, R. S. Windeler, J. Stenger, and H. R. Telle, "Carrier-envelope offset dynamics of mode-locked lasers," Opt. Lett. **27**, 194–196 (2002).

[30] T. C. Schratwieser, K. Balskus, R. A. McCracken, C. Farrell, C. G. Leburn, Z. Zhang, T. P. Lamour, T. I. Ferreiro, A. Marandi, A. S. Arnold, and D. T. Reid, "[87]Rb-stabilized 375-MHz Yb:fiber femtosecond frequency comb," Opt. Express **22**, 10494–10499 (2014).

[31] M. Hoffmann, S. Schilt, and T. Südmeyer, "CEO stabilization of a femtosecond laser using a SESAM as fast opto-optical modulator," Opt. Express **21**, 30054–30064 (2013).

[32] B. R. Washburn, S. A. Diddams, N. R. Newbury, J. W. Nicholson, M. F. Yan, and C. G. Jørgensen, "Phase-locked, erbium-fiber-laser-based frequency comb in the near infrared," Opt. Lett. **29**, 250–252 (2004).

[33] S. Koke, C. Grebing, H. Frei, A. Anderson, A. Assion, and G. Steinmeyer, "Direct frequency comb synthesis with arbitrary offset and shot-noise-limited phase noise," Nature Photonics **4**, 462–465 (2010).

[34] T. Sizer, "Increase in laser repetition rate by spectral selection," IEEE Journal of Quantum Electronics **25**, 97–103 (1989).

[35] A. Yariv and P. Yeh, *Photonics: Optical Electronics in Modern Communications (The Oxford Series in Electrical and Computer Engineering)* (Oxford University Press, Inc., New York, NY, USA, 2006).

[36] A. Bartels, D. Heinecke, and S. A. Diddams, "10-GHz self-referenced optical frequency comb," Science **326**, 681–681 (2009).

[37] D. C. Heinecke, A. Bartels, T. M. Fortier, D. A. Braje, L. Hollberg, and S. A. Diddams, "Optical frequency stabilization of a 10 GHz Ti:sapphire frequency comb by saturated absorption spectroscopy in ^{87}Rubidium," Phys. Rev. A **80**, 053806 (2009).

[38] M. Endo, A. Ozawa, and Y. Kobayashi, "Kerr-lens mode-locked Yb:KYW laser at 4.6-GHz repetition rate," Opt. Express **20**, 12191–12197 (2012).

[39] M. Endo, A. Ozawa, and Y. Kobayashi, "6-GHz, Kerr-lens mode-locked Yb:Lu2O3 ceramic laser for comb-resolved broadband spectroscopy," Opt. Lett. **38**, 4502–4505 (2013).

[40] M. Endo, T. Sukegawa, A. Silva, and Y. Kobayashi, "Development of compact and ultra-high-resolution spectrograph with multi-GHz optical frequency comb," in "Ground-based and Airborne Instrumentation for Astronomy V," (2014), Proc. SPIE 9147, p. 91477Y.

[41] M. Endo, I. Ito, and Y. Kobayashi, "Direct 15-GHz mode-spacing optical frequency comb with a Kerr-lens mode-locked Yb:Y2O3 ceramic laser," Opt. Express **23**, 1276–1282 (2015).

[42] P. Del'Haye, O. Arcizet, A. Schliesser, R. Holzwarth, and T. J. Kippenberg, "Full stabilization of a microresonator-based optical frequency comb," Phys. Rev. Lett. **101**, 053903 (2008).

[43] P. Del'Haye, A. Coillet, T. Fortier, K. Beha, D. C. Cole, K. Y. Yang, H. Lee, K. J. Vahala, S. B. Papp, and S. A. Diddams, "Phase-coherent microwave-to-optical link with a self-referenced microcomb," Nature Photonics **10**, 516–520 (2016).

[44] A. Ishizawa, T. Nishikawa, A. Mizutori, H. Takara, A. Takada, T. Sogawa, and M. Koga, "Phase-noise characteristics of a 25-GHz-spaced optical frequency comb based on a phase- and intensity-modulated laser," Opt. Express **21**, 29186–29194 (2013).

[45] F. Wildi, B. Chazelas, and F. Pepe, "A passive cost-effective solution for the high accuracy wavelength calibration of radial velocity spectrographs," in "Ground-based and Airborne Instrumentation for Astronomy IV," (2012), Proc. SPIE 8446, p. 84468E.

[46] A. Reiners, R. K. Banyal, and R. G. Ulbrich, "A laser-lock concept to reach cms^{-1}-precision in Doppler experiments with Fabry-Pérot wavelength calibrators," Astronomy & Astrophysics **569**, A77 (2014).

[47] C. Schwab, J. Stürmer, Y. Gurevich, T. Führer, S. Lamoreaux, T. Walther, and A. Quirrenbach, "Stabilizing a Fabry-Pérot etalon peak to 3 cm s^{-1} for spectrograph calibration," Publications of the Astronomical Society of the Pacific **127**, 880–889 (2015).

[48] R. Maiolino, M. Haehnelt, M.T. Murphy, D. Queloz, L. Origlia, J. Alcala, Y. Alibert, P.J. Amado, C. Allende Prieto, M. Ammler-von Eiff, M. Asplund,

M. Barstow, G. Becker, X. Bonfils, F. Bouchy, A. Bragaglia, M.R. Burleigh, A. Chiavassa, D. A. Cimatti, M. Cirasuolo, S. Cristiani, V. D'Odorico, D. Dravins, E. Emsellem, J. Farihi, P. Figueira, J. Fynbo, B.T. Gansicke, M. Gillon, B. Gustafsson, V. Hill, G. Israelyan, A. Korn, S. Larsen, P. De Laverny, J. Liske, C. Lovis, A. Marconi, C. Martins, P. Molaro, B. Nisini, E. Oliva, P. Petitjean, M. Pettini, A. Recio Blanco, R. Rebolo, A. Reiners, C. Rodriguez-Lopez, N. Ryde, N.C. Santos, S. Savaglio, I. Snellen, K. Strassmeier, N. Tanvir, L. Testi, E. Tolstoy, A. Triaud, L. Vanzi, M. Viel, M. Volonteri, "A community science case for E-ELT HIRES," arXiv:1310.3163 [astro-ph.IM] (2013).

[49] M. Mayor and D. Queloz, "A Jupiter-mass companion to a solar-type star," Nature **378**, 355–359 (1995).

[50] G. Laughlin, M. Crismani, and F. C. Adams, "On the anomalous radii of the transiting extrasolar planets," The Astrophysical Journal Letters **729**, L7 (2011).

[51] J. F. Kasting, D. P. Whitmire, and R. T. Reynolds, "Habitable Zones around Main Sequence Stars," Icarus **101**, 108 – 128 (1993).

[52] A. Sandage, "The Change of Redshift and Apparent Luminosity of Galaxies due to the Deceleration of Selected Expanding Universes." The Astrophysical Journal **136**, 319 (1962).

[53] J. Liske, A. Grazian, E. Vanzella, M. Dessauges, M. Viel, L. Pasquini, M. Haehnelt, S. Cristiani, F. Pepe, G. Avila, P. Bonifacio, F. Bouchy, H. Dekker, B. Delabre, S. D'Odorico, V. D'Odorico, S. Levshakov, C. Lovis, M. Mayor, P. Molaro, L. Moscardini, M. T. Murphy, D. Queloz, P. Shaver, S. Udry, T. Wiklind, and S. Zucker, "Cosmic dynamics in the era of extremely large telescopes," Monthly Notices of the Royal Astronomical Society **386**, 1192–1218 (2008).

[54] A. Loeb, "Direct measurement of cosmological parameters from the cosmic

deceleration of extragalactic objects," The Astrophysical Journal Letters **499**, L111 (1998).

[55] É. Depagne, R. A. McCracken, D. T. Reid, R. B. Kuhn, N. Erasmus, and L. A. Crause, "First light of a laser frequency comb at SALT," in "Ground-based and Airborne Instrumentation for Astronomy VI," (2016), Proc. SPIE 9908, p. 99087M.

[56] R. A. McCracken, É. Depagne, R. B. Kuhn, N. Erasmus, L. A. Crause, and D. T. Reid, "Wavelength calibration of a high resolution spectrograph with a partially stabilized 15-GHz astrocomb from 550 to 890 nm," Opt. Express **25**, 6450–6460 (2017).

[57] S. T. Wong, K. L. Vodopyanov, and R. L. Byer, "Self-phase-locked divide-by-2 optical parametric oscillator as a broadband frequency comb source," J. Opt. Soc. Am. B **27**, 876–882 (2010).

[58] Y. Kobayashi, K. Torizuka, A. Marandi, R. L. Byer, R. A. McCracken, Z. Zhang, and D. T. Reid, "Femtosecond optical parametric oscillator frequency combs," Journal of Optics **17**, 094010 (2015).

[59] D. T. Reid, "Ultra-broadband pulse evolution in optical parametric oscillators," Opt. Express **19**, 17979–17984 (2011).

[60] R. A. McCracken and D. T. Reid, "Few-cycle near-infrared pulses from a degenerate 1 GHz optical parametric oscillator," Opt. Lett. **40**, 4102–4105 (2015).

[61] D. F. Phillips, A. G. Glenday, C.-H. Li, C. Cramer, G. Furesz, G. Chang, A. J. Benedick, L.-J. Chen, F. X. Kärtner, S. Korzennik, D. Sasselov, A. Szentgyor-gyi, and R. L. Walsworth, "Calibration of an astrophysical spectrograph below 1 m/s using a laser frequency comb," Opt. Express **20**, 13711–13726 (2012).

[62] D. A. Braje, M. S. Kirchner, S. Osterman, T. Fortier, and S. A. Diddams, "As-

tronomical spectrograph calibration with broad-spectrum frequency combs," The European Physical Journal D **48**, 57–66 (2008).

[63] T. Steinmetz, T. Wilken, C. Araujo-Hauck, R. Holzwarth, T. W. Hänsch, and T. Udem, "Fabry–Pérot filter cavities for wide-spaced frequency combs with large spectral bandwidth," Applied Physics B **96**, 251–256 (2009).

[64] C.-H. Li, A. G. Glenday, A. J. Benedick, G. Chang, L.-J. Chen, C. Cramer, P. Fendel, G. Furesz, F. X. Kärtner, S. Korzennik, D. F. Phillips, D. Sasselov, A. Szentgyorgyi, and R. L. Walsworth, "In-situ determination of astro-comb calibrator lines to better than 10 cm s^{-1}," Opt. Express **18**, 13239–13249 (2010).

[65] C.-H. Li, G. Chang, A. G. Glenday, N. Langellier, A. Zibrov, D. F. Phillips, F. X. Kärtner, A. Szentgyorgyi, and R. L. Walsworth, "Conjugate Fabry-Perot cavity pair for improved astro-comb accuracy," Opt. Lett. **37**, 3090–3092 (2012).

[66] G. Chang, C.-H. Li, D. F. Phillips, A. Szentgyorgyi, R. L. Walsworth, and F. X. Kärtner, "Optimization of filtering schemes for broadband astro-combs," Opt. Express **20**, 24987–25013 (2012).

[67] D. Hackett, G. Ycas, and S. Diddams, "A low-dispersion Fabry-Perot cavity for generation of a 30 GHz astrocomb spanning 140 nm," in "CLEO 2015 Conference Digest," (2015), p. SW4G.8.

[68] R. A. Probst, T. Steinmetz, T. Wilken, G. K. L. Wong, H. Hundertmark, S. P. Stark, P. S. J. Russell, T. W. Hänsch, R. Holzwarth, and T. Udem, "Spectral flattening of supercontinua with a spatial light modulator," in "Techniques and Instrumentation for Detection of Exoplanets VI," (2013), Proc. SPIE 8864, p. 88641Z.

[69] R. A. Probst, G. L. Curto, G. Avila, B. L. C. Martins, J. R. de Medeiros, M. Esposito, J. I. G. Hernández, T. W. Hänsch, R. Holzwarth, F. Kerber, I. C.

Leão, A. Manescau, L. Pasquini, R. Rebolo-López, T. Steinmetz, T. Udem, and Y. Wu, "A laser frequency comb featuring sub-cm/s precision for routine operation on HARPS," in "Ground-based and Airborne Instrumentation for Astronomy V," (2014), Proc. SPIE 9147, p. 91471C.

[70] B. C. Smith, *Fundamentals of Fourier Transform Infrared Spectroscopy* (Taylor & Francis Inc, Bosa Roca, USA, 1995).

[71] P. R. Griffiths and J. A. de Haseth, *Fourier Transform Infrared Spectrometry* (Wiley, New York, NY, USA, 2006).

[72] G. G. Ycas, F. Quinlan, S. A. Diddams, S. Osterman, S. Mahadevan, S. Redman, R. Terrien, L. Ramsey, C. F. Bender, B. Botzer, and S. Sigurdsson, "Demonstration of on-sky calibration of astronomical spectra using a 25 GHz near-IR laser frequency comb," Opt. Express **20**, 6631–6643 (2012).

[73] A. Zybin, J. Koch, H. Wizemann, J. Franzke, and K. Niemax, "Diode laser atomic absorption spectrometry," Spectrochimica Acta Part B: Atomic Spectroscopy **60**, 1 – 11 (2005).

[74] G. Galbács, "A review of applications and experimental improvements related to diode laser atomic spectroscopy," Applied Spectroscopy Reviews **41**, 259–303 (2006).

[75] V. Tsatourian, H. S. Margolis, G. Marra, D. T. Reid, and P. Gill, "Common-path self-referencing interferometer for carrier-envelope offset frequency stabilization with enhanced noise immunity," Opt. Lett. **35**, 1209–1211 (2010).

[76] D. T. Reid, M. Padgett, C. McGowan, W. E. Sleat, and W. Sibbett, "Light-emitting diodes as measurement devices for femtosecond laser pulses," Opt. Lett. **22**, 233–235 (1997).

[77] "NL-PM-750 data sheet," `https://www.newport.com/medias/sys_master/images/images/h39/h5a/8797092970526/F-NL-PM-750-Data-Sheet.pdf`. Accessed: 26 February 2018.

[78] "Taccor comb data sheet," `https://www.laserquantum.com/download-ds.cfm?id=815`. Accessed: 26 February 2018.

[79] Z. Zhang, K. Balskus, R. A. McCracken, and D. T. Reid, "Mode-resolved 10-GHz frequency comb from a femtosecond optical parametric oscillator," Opt. Lett. **40**, 2692–2695 (2015).

[80] J. Ye, S. Swartz, P. Jungner, and J. L. Hall, "Hyperfine structure and absolute frequency of the 87Rb 5P3/2 state," Opt. Lett. **21**, 1280–1282 (1996).

[81] A. G. Glenday, D. F. Phillips, M. Webber, C.-H. Li, G. Furesz, G. Chang, L.-J. Chen, F. X. Kärtner, D. D. Sasselov, A. H. Szentgyorgyi, and R. L. Walsworth, "High-resolution fourier transform spectrograph for characterization of echelle spectrograph wavelength calibrators," in "Ground-based and Airborne Instrumentation for Astronomy IV," (2012), Proc. SPIE 8446, pp. 8446 – 12.

[82] A. Glenday, C.-H. Li, N. Langellier, G. Chang, L.-J. Chen, G. Furesz, A. Zibrov, F. Kärtner, D. Phillips, D. Sasselov, A. Szentgyorgyi, and R. Walsworth, "Operation of a broadband visible-wavelength astro-comb with a high-resolution astrophysical spectrograph," Optica **2**, 250–254 (2015).